

ON THE MECHANISMS OF HEAT LOSS BENEATH CONTINENTS AND OCEANS

by

Claude Jaupart

Ingenieur Civil des Mines, Paris, France

(1976)

SUBMITTED TO THE DEPARTMENT OF
EARTH AND PLANETARY SCIENCES IN
PARTIAL FULFILLMENT OF THE
REQUIREMENTS FOR THE DEGREE OF
DOCTOR OF PHILOSOPHY

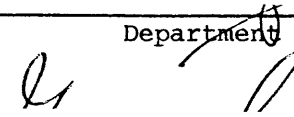
at the

MASSACHUSETTS INSTITUTE OF TECHNOLOGY

May 1981

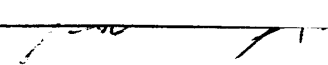
© Massachusetts Institute of Technology, 1981

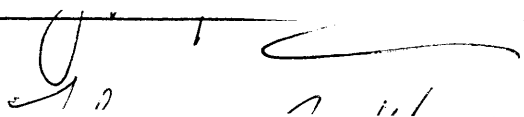
Signature of Author


Department of Earth and Planetary Sciences

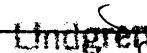
May 12, 1981

Certified by


Gene Simmons
Thesis Supervisor


John G. Sclater
Thesis Supervisor

Accepted by


Lindgren, Chairman, Departmental Committee on Graduate Students

MASSACHUSETTS INSTITUTE OF TECHNOLOGY
WITHDRAWN FROM LIBRARIES
JUL 20 1981

ON THE MECHANISMS OF HEAT LOSS BENEATH CONTINENTS AND OCEANS

by Claude Jaupart

Submitted to the Department of Earth and Planetary Sciences
on May 12, 1981 in partial fulfillment of the requirements
for the degree of Doctor of Philosophy

ABSTRACT

In the second chapter, we present a set of 35 new heat flow and radiogenic heat production determinations for many types of geological formations in the State of New Hampshire and surrounding areas. From this analysis of the distribution of heat flow and radioactivity, we conclude that the vertical distribution of the radiogenic heat production is similar in plutonic and metasedimentary rocks. Our data are compatible with the linear relationship previously established by R.F. Roy and co-workers in 1968. This suggests that, in the granitic units, the radioelements are redistributed after emplacement through the same mechanisms which have operated in the neighbouring metamorphosed sediments. Radioactive enrichment is clearly associated with the granites and plutons which do not outcrop appear as anomalies in the general heat flow versus radioactivity relationship. The lowest heat flow measured is $0.76 \mu\text{cal}/\text{cm}^2.\text{s}$ ($32 \text{ mW}/\text{m}^2$) on a poorly radioactive unit. Heat flow is high on radioactive plutons but low elsewhere. The heat flow field grades smoothly into the low heat flow regions of the Canadian Shield. The New Hampshire area is in quasi-steady conditions, with its heat flow in secular equilibrium with the heat generated by crustal sources and that supplied from the mantle. Thermal perturbations which have resulted in the generation of huge masses of granites in the State have decayed completely. The thickness of the crust and upper mantle layer which underwent significant heating is thus constrained to be less than 150-180 km. The mean heat flow value on metasedimentary formations is $1.12 \mu\text{cal}/\text{cm}^2.\text{s}$ ($47 \text{ mW}/\text{m}^2$), which is exactly the mean heat flow through continents older than 800 Ma.

In the third chapter, we analyze the various mechanisms which are likely to affect the vertical distribution of radioelements in the continental crust. The usual practice is to fit to the heat flow and radioactivity data a relationship of the form :

$$Q = Q_r + D.A$$

where Q_r and A are the observed heat flow and radiogenic heat production. Q_r is the 'reduced' heat flow and D is a depth-scale. This procedure implicitly assumes that uranium, thorium and potassium have identical distributions in the crust. We suggest that significant information may be lost as the three radioelements may in fact be affected by processes operating over different depths.

Data published for four heat flow provinces throughout the world as well as data presented in chapter two are used to estimate the distributions of uranium, thorium and potassium in the continental crust. The four provinces are the young Sierra Nevada and New England provinces, and the Archean Canadian and Western Australian Shields. The radioelements

distributions are characterized by depth-scales defined as follows :

$$D_i = \int_0^h \frac{C_i(z)}{C_i(0)} \cdot dz$$

where h is the thickness of the layer containing the bulk of radioactivity and $C_i(z)$ the concentration of element i at depth z . Three depth-scales are computed from a least-squares fit to the following relationship :

$$Q = Q_r + D_U \cdot A_U + D_T \cdot A_T + D_K \cdot A_K$$

where Q is the observed heat flow and Q_r some constant (a reduced heat flow). A_i is the heat generation due to the radioactive decay of element i and D_i is the corresponding depth-scale.

The analysis suggests that the three distributions are different and that they have the same basic features in all the provinces considered. The depth-scale for potassium is large in granitic areas, that for thorium is small and that for uranium lies between the other two. We propose a simple model according to which each radioelement essentially provides a record for one process. Potassium gives a depth-scale for the primary differentiation of the crust. Thorium gives the depth-scale of magmatic or metamorphic fluid circulation. Finally, the uranium distribution reflects the late effects of alteration due to meteoric water. We show that the heat flow and radioactivity data are compatible with this model. The analysis and the numerical results are supported by data from deep boreholes and by geochemical evidence, such as detailed investigations of plutonic series and studies of U-Th-Pb systematics.

To constrain the thickness of the layer where heat loss is conductive only in the mantle, we have investigated the influence of viscosity structure on the development of convection in a fluid cooled from above. We have also studied this simple problem as a first step towards a proper understanding of convection in fluids with large viscosity variations. A viscosity (ν) dependence with depth (z) of the form $\nu_0 + \nu_1 \cdot \exp(-\gamma z)$ was assumed. Velocity and temperature perturbations are expanded as Fourier series with time-dependent coefficients which are computed numerically. After the temperature of the top boundary is lowered the evolution of the upper thermal boundary layer is followed until convective breakdown occurs for various combinations of the parameters (ν_0, ν_1, γ). Viscosity contrasts of up to 10^7 and Rayleigh numbers of up to 10^8 were studied.

Because of the time dependent basic state, disturbances in the fluid do not grow as a simple exponential. The criteria used to determine the onset of convection is not sensitive to the initial conditions. In the uniform viscosity case, for layer Rayleigh numbers greater than about 10^5 , convection occurs when a local Rayleigh number based on the thickness of the thermal boundary layer exceeds a critical value of about 360.

In the variable viscosity case, the results are best classified according to the value of the viscosity contrast across the layer. For moderate viscosity contrasts (no higher than 10^4), convective breakdown is characterized by the almost simultaneous appearance of two modes of

instability. One has a large wavelength which can be more than 10 times bigger than that for the constant viscosity fluid with same Rayleigh number and involves the whole fluid layer. The other mode has a much smaller critical wavelength and develops below an upper mechanical boundary layer which behaves rigidly. For large viscosity contrasts, viscous dissipation in the top regions prevents the growth of the first instability mode, and the 'rigid top' mode dominates.

In the 'rigid top' mode of instability, convection develops in the lower regions of the fluid where viscosity variations are small. We propose a simple method to define the thickness of the rigid layer. Using this definition, we are able to compute several important characteristics of the flow such as its true depth extent and the effective driving temperature difference. A measure of viscosity is provided by the dissipation-weighted average of the viscosity throughout the fluid. With these effective parameters, we compute an effective Rayleigh number R_e . There is a simple relationship between the critical time and the effective Rayleigh number for all cases considered. Thus the critical time can be used to estimate the average properties of the convective system.

Viscosity contrasts in the convecting region rarely exceed a factor of 10. As a consequence, simple scaling arguments are sufficient to describe the main features of the instability. The critical wavenumber scales approximately with a suitably defined boundary layer thickness beneath the rigid lid. Using this boundary layer thickness and the local value of viscosity, a local Rayleigh number may be computed. Convective breakdown occurs when this local number exceeds a critical value of about 160-190. The actual critical value depends on the thickness of the rigid lid above the convecting fluid. The local Rayleigh number may be calculated at any depth in the fluid layer. Convection develops below depth z_R (the thickness of the rigid lid) such that this local number reaches a maximum in the layer. The calculations indicate that the effective thermal boundary condition at the top of the convecting layer is close to a fixed heat flux condition.

If the age of 70 million years which marks the flattening of the depth versus age curve on the ocean floor is the critical time for the onset of convective instability beneath the plate, the above results can be used to constrain the average value of viscosity in the thermal boundary layer. The value found is $3 \cdot 10^{16}$ m²/s which is lower than the value determined from post-glacial uplift data. This suggests that the viscosity structure of the upper mantle is complex, with maybe a low viscosity zone beneath the plate.

The comparison of heat flow data for both oceans and continents suggests that the thermal structures of continental and oceanic plates are similar. Both consist of an upper mechanical boundary layer where heat transport is mainly by conduction, and a thermal boundary layer where heat transport is essentially convective.

Thesis supervisors : Dr. Gene Simmons

Dr. John G. Sclater

Title: Professors of Geophysics

ACKNOWLEDGEMENTS

I would like to express my gratitude to Prof. Gene Simmons who welcomed me to his laboratory when I first came to MIT, and who gave me the outstanding opportunity to set up new equipment and start a new line of research in his group. His help and continued interest kept me afloat during my years at the Institute. Gene taught me the painstaking job of data acquisition (more measurements) and interpretation (more measurements).

Prof. John Sclater accepted my occasional presence in his already crowded sunny laboratory on the 8th floor and his communicative enthusiasm directed me to many different subjects of interest. I wish to thank him for moral and administrative support. John taught me how to tackle geophysical problems on the world-wide scale (more data).

Finally Barry Parsons introduced me to more theoretical aspects of geophysics and was always willing to share ideas and discuss problems. Barry showed me how to clarify thoughts and results (more calculations).

It would be impossible to acknowledge all the help I have benefited from over the years. Dorothy Frank typed the manuscript with incredible skill and speed. Debbie Gillett made sure everything was going smoothly at no small cost. Ann Harlow and Frank Miller helped me out in many instances.

The French Ministry of Foreign Affairs supported me during my first year at the Institute.

Last but not least, I thank all my friends at MIT and the Kinks (why not?) for making this hard working experience nice and easy.

TABLE OF CONTENTS

	Page
Abstract	2
Acknowledgements	5
CHAPTER ONE. INTRODUCTION	9
CHAPTER TWO. A DETAILED STUDY OF THE DISTRIBUTION OF HEAT FLOW AND RADIOACTIVITY IN NEW HAMPSHIRE (U.S.A.) AND SURROUNDING AREAS	12
2.1 Introduction	12
2.2 Geological and geophysical setting	14
2.3 Heat flow and radioactivity measurements: experimental details	16
2.3.1 Temperature measurements	17
2.3.2 Thermal conductivity measurements	18
2.3.3 Measurements of U, Th and K concentrations	20
2.4 The distribution of heat flow and radioactivity	22
2.4.1 The Winnepesaukee pluton	27
2.4.2 The Bedford anomaly in southeastern New Hampshire	28
2.5 Discussion	29
2.6 Conclusions	32
Tables 2.1-2.9	34
Figure Captions	47
Figures	49
Appendix A. Temperature logs at heat flow stations	59
Appendix B. Calibration of the gamma-ray spectrometer	84
Table 2.B1	85

CHAPTER THREE. HEAT FLOW STUDIES; CONSTRAINTS ON THE DISTRIBUTION OF	
URANIUM, THORIUM AND POTASSIUM IN THE CONTINENTAL CRUST	86
3.1 Introduction	86
3.2 The relation between heat flow and radioactivity	88
3.3 Mechanisms for the distribution of radioelements	90
3.4 Depth-scale analysis for the radioactive elements	93
3.5 Results	96
3.6 Summary and interpretation	100
3.7 Conclusions	106
Tables 3.1-3.7	108
Figure Captions	117
Figures	118
Appendix. The inverse problem	124
CHAPTER FOUR. A STUDY OF CONVECTIVE INSTABILITIES IN A VARIABLE VISCOSITY	
FLUID COOLED FROM ABOVE: THE CASE OF THE UPPER MANTLE BENEATH	
OCEANS	127
4.1 Introduction	127
4.2 Mathematical formulation	130
4.2.1 Basic equations	130
4.2.2 Boundary conditions and initial conditions	134
4.2.3 Viscosity profiles	135
4.2.4 Method of solution	136
4.3 Results for constant viscosity	139
4.4 Results for variable viscosity	141
4.4.1 The influence of the viscosity parameters λ and γ	141
4.4.2 The transition between the "whole layer" and the	143
"rigid top" modes of instability	

4.4.3	The "whole layer" mode of instability	144
4.4.4	The "rigid top" mode of instability	145
4.5	Discussion	152
	Tables 4.1-4.3	158
	Figure Captions	161
	Figures	164
	Appendix A. Expressions of the coupling coefficients	185
	Appendix B. Convergence of the numerical solutions	186
	Table	188
	Figure Captions	189
	Figures	190
	CHAPTER FIVE. SYNTHESIS AND CONCLUSION	192
	Table 5.1	197
	Figure Captions	198
	Figures	199
	REFERENCES	201-216

CHAPTER ONE

INTRODUCTION

Since the advent of the theory of plate tectonics, our understanding of the Earth has changed. Rather than regard the continents and oceans as static and unrelated, we now think that they are mobile and interconnected. In general they can be part of the same plate but their respective mechanisms of heat transfer differ markedly. In contrast with the oceans, the continents record a long geological time span. The oldest ocean floor is about 180 My old whereas the oldest continental rocks have been dated at 3900 My. A recent review of the world-wide heat flow data has been made by Sclater, Jaupart and Galson (1980) and most of the following discussion is borrowed from their conclusions.

The ocean floor is created by the intrusion of molten material which cools, solidifies and is attached to the plate as more material is intruded. The oceanic crust then increases in age, loses heat to the seawater and contracts. This explains qualitatively the observed decrease in heat flow with age and the subsidence of midoceanic ridges. The raw heat flow data is highly scattered because of the effects of hydrothermal circulation and more emphasis was placed on the analysis of the ocean floor bathymetry. The time scale of the decrease in subsidence rate and heat flow with age have permitted the calculation of lithospheric parameters through the use of simple thermal models. The most complete is that of Parsons and Sclater (1977) who estimate that the plate thickness is about 125 km. At the age of 180 My, the oceanic lithosphere is not in thermal equilibrium but both observations and theory suggest it is close. A major problem remains however which concerns the concept of plate. Although the cooling of a plate accounts for the observed decrease of heat flow and

depth with age, it cannot by itself provide an explanation for the existence of a rigid layer of approximately constant thickness over a convecting mantle.

The heat flow observed at the surface of continents is the result of many processes which are only understood in a qualitative manner. The most important and significant geologically are melting and magma intrusion during orogenic events, crustal extension, erosion and heat generation by radioactive decay in the crust. These processes have very distinct characteristics. In particular, they have time-scales which differ by one or two orders of magnitude. The continental heat flow decreases with age with a time scale which is apparently much larger than in the oceans. Steady-state conditions prevail after 800 My. The biggest problem in the interpretation of continental data is the determination of the concentration and distribution of radioactive elements in the crust. Variations in the radiogenic heat production perturb the rough relation between heat flow and tectonic age and complicate the calculation of the temperatures at depth.

This thesis is concerned with the thermal structure and the mechanisms of heat loss beneath oceans and continents. The second chapter is devoted to a detailed study of heat flow and radioactivity in a relatively young continental region, New Hampshire. Its purpose is to understand the distribution of radioactive elements in the crust and to study the thermal effects of orogenies. The third chapter deals with the same problem using data from all over the world. In the fourth chapter, we turn to the case of the oceans. We study the evolution of the oceanic mantle as it moves away from a spreading center. We investigate the thickness of the layer which behaves rigidly over the convecting mantle. In the concluding

section, we compare the thermal structure of continental and oceanic plates.

For easy comparison with earlier studies, the heat flow units employed in the second chapter are calories ($\mu\text{cal}/\text{cm}^2 \text{ s}$). The world-wide analysis of chapter 3 is written using the S.I. units (mW/m^2). Conversion is easy: $1 \mu\text{cal}/\text{cm}^2 \text{ s}$ is $41.8 \text{ mW}/\text{m}^2$.

CHAPTER TWO

A DETAILED STUDY OF THE DISTRIBUTION OF HEAT FLOW AND
RADIOACTIVITY IN NEW HAMPSHIRE (U.S.A.) AND SURROUNDING AREAS

2.1 INTRODUCTION

Although many heat flow measurements have been made on continents over the past twenty years, their interpretation is limited because we lack confidence to calculate the amount of heat produced by radioactive decay in the crust. Concentrations of uranium, thorium and potassium have been measured extensively in rocks at the surface but little is known about their vertical distribution. Direct evidence from boreholes is only available down to depths of about 4 km (Lachenbruch and Bunker, 1971; Lubimova et al., 1973). Present estimates over the whole crustal thickness rely almost entirely on an empirical relationship discovered by Birch and his coworkers (Birch et al., 1968; Roy et al., 1968a) which relates heat flow to the radiogenic heat production at the surface. The relationship is linear and is usually written as follows:

$$Q = Q_r + D \cdot A \quad (2.1)$$

where Q is the heat flow and A the radiogenic heat production. Q_r is the "reduced" heat flow and D has the dimension of length. The relationship has been observed in many parts of the world (for a summary, see Sclater et al., 1980).

There is considerable discussion about the physical significance of parameters Q_r and D and the interpretation of the linear relation remains ambiguous, relying on several models of crustal structure and crustal differentiation (Lachenbruch, 1968 and 1970; Tilling et al., 1970;

Albarede, 1975; Smithson and Decker, 1974). Since the original discovery by Birch et al. (1968), it has been found in many provinces that metasedimentary and metamorphic terrains exhibit the same relation as plutons (Jaeger, 1970; Kutas, 1977; Richardson and Oxburgh, 1978). This observation represents a constraint on the mechanism of upward segregation of radioelements but is still awaiting a complete explanation.

Heat flow and radioactivity studies have been mostly limited to plutonic environments. This is particularly true for New England where the largest formations which consist of metamorphosed sediments and volcanics have not been sampled to this date. New England has had a complicated geologic past and has been affected by several important orogenic events until recent times. Many different types of rocks outcrop in a relatively small area. This provides a unique opportunity to study in detail the relationship between heat flow and radioactivity on formations of differing origins and ages.

The region is also interesting because it was subjected to massive intrusions of magma at various periods of its history, with the last episode occurring about 100 Ma (Foland and Faul, 1977). The study of the heat flow field will enable us to determine any remaining thermal perturbations associated with these events and thus to place constraints on the depth extent of the region affected by them.

We present in this study 35 new determinations of heat flow in the State of New Hampshire and surroundings. After detailing in a first section our measurement techniques, we discuss the distribution of heat flow and radioactivity. In the last section, we analyze the different mechanisms which can be responsible for the migration of uranium, thorium and potassium.

2.2 GEOLOGICAL AND GEOPHYSICAL SETTING

New Hampshire belongs to the northern Appalachians region which has experienced a complex tectonic evolution linked with the history of the Iapetus (proto-Atlantic) Ocean. A general geological summary for the Appalachians may be found in Rodgers (1970). Schematic maps are presented in Figure 2.1a,b.

Following the opening of the Iapetus Ocean some 820 My ago (Rankin, 1976), there was volcanic activity in the Avalon chain. The Avalon basement is preserved today in the Massabessic gneiss (Aleinikoff et al., 1979). In the Ordovician, the Taconic orogeny probably saw the closure of the Ocean and resulted in the present juxtaposition of continental margin or arc-trench sedimentary rocks with oceanic lavas which is found in the Ammonoosuc volcanics on the Vermont boundary (Aleinikoff, 1977). Closure of the Ocean was not complete as there is no major unconformity and Ordovician deformation in the Merrimack Synclinorium (Moench and Zartman, 1976). In Silurian and early Devonian times, the region underwent heavy sedimentation and volcanic deposition. This led to the formation of the Littleton metasedimentary rocks which cover a large area in the State.

The major event which is recorded in the geological units is the Acadian orogeny which marked the Devonian epoch at an age of about 400 Ma (Lyons and Livingston, 1977). This episode of major deformation and metamorphism was of short duration (smaller than 30 My) and is usually interpreted as a continent-continent collision (Naylor, 1971). It is characterized in rough chronological order by high-grade metamorphism, deformation and massive intrusions of granite. These plutons, represented by the Kinsman, Bethlehem and Spaulding formations, appear tabular, and weakly foliated. They extended over a large area and outcrop in many

places (Nielson et al., 1976). There were also post-tectonic intrusions, known as the binary granites, which appear tabular too (Nielson et al., 1976). The binary granites exhibit discordant contacts with surrounding rocks and are dated at 330-360 Ma (Lyons and Livingston, 1977).

The next tectonic event was the Alleghenian orogeny which is again interpreted as a continent-continent collision (Dewey and Kidd, 1974). It left only a minor imprint in the southern part of the State (Aleinikoff et al., 1979).

A final episode of plutonism occurred between 200 Ma and 100 Ma and saw the emplacement of the White Mountain Magma Series, initially in relation with the opening of the Atlantic Ocean (Foland and Faul, 1977).

The structural units found today in the State exhibit a generally northward trend which is the obvious result of the tectonic evolution (Figure 2.1a). There are at least three sutures in New Hampshire, together with many different types of plutons. The region is therefore an ideal place to study the structure of newly formed or newly reworked continental crust.

There is an extensive body of geophysical studies concerning New Hampshire. Gravity data are summarized in Diment et al. (1972) and Kane et al. (1972). A more detailed investigation of the southeastern part of the State may be found in Nielson et al. (1976). Several plutons have been studied individually by Bothner (1974), Wetterauer and Bothner (1977) and Sharp and Simmons (1978). Aeromagnetic coverage is almost complete (Weston Geophysical Res., 1976). There are two resistivity surveys by Kasameyer (1974) and Bailey et al. (1978). Finally, the area has been investigated thoroughly using seismic data collected on the northeastern USA seismic network (Taylor, 1980).

As a result, the structure of the crust and upper mantle is fairly well constrained in this part of the North American continent. Kasameyer (1974) interpreted his data as indicating a resistive (dehydrated) lower crust which underlies a slightly conductive upper crust approximately 15 km thick. The analysis of regional travel times and Rayleigh wave velocities also reveals a well-defined upper crust about 15 km thick (Taylor, 1980). The lower crust is characterized by values of Poisson's ratio and by seismic velocities typical of pyroxene granulite rocks (Taylor, 1980). This supports the conclusions of Kasameyer (1974). The depth to the Moho discontinuity varies slightly around a mean value of 40 km (Taylor and Toksoz, 1979). The seismic structure which is deduced from the three-dimensional interpretation of P-wave residuals correlates well with the surface geological and tectonic features down to depths of about 200 km (Taylor and Toksoz, 1979).

2.3. HEAT FLOW AND RADIOACTIVITY MEASUREMENTS: EXPERIMENTAL DETAILS

Many wells are drilled each year for private water resources in the States of Vermont, New Hampshire and Maine. Their depths vary greatly but often reach 200 meters. Many of them turn out to be unproductive and can be used to make temperature logs at small cost. Industrial drillers unfortunately do not employ coring techniques and only drill cuttings are available. Ten years ago these wells could not have been used for heat flow determinations but Sass et al. (1971), Horai and Baldrige (1972) and King and Simmons (1972) have since established that reliable conductivity measurements could be made from powdered rock specimens. Using the technique of King and Simmons (1972), we have made heat flow measurements in 41 wells located in New Hampshire and surrounding areas. We have also set up a gamma-ray spectrometer to determine the concentrations in uranium,

thorium and potassium of the corresponding geological formations. These measurements are presented in Tables 2.1 and 2.2. The detailed temperature logs are given in Appendix 2.A.

In the following paragraphs, we present in detail our experimental procedure and discuss the errors in the values of heat flow and radiogenic heat production.

2.3.1 Temperature measurements

Temperatures were measured with a standard thermistor probe at 6 meter depth intervals. The thermistor was calibrated in the laboratory before each series of field expeditions. The overall precision is 0.01°C . The temperature gradient was calculated from plots of temperature versus depth. We took special care to detect any shift in the gradient which would indicate a change in lithology or water circulation. We found no such shift over the depth ranges we were able to sample and conclude that the geological units of New Hampshire are homogeneous over thicknesses of several hundred meters.

The quality of the geothermal gradient estimation varies with the depth range and the maximum depth sampled. Because surface perturbations and topographic effects are important at shallow depths, we separated the measurements in two categories according to the depth of the well. Wells deeper than 100 meters were labeled "grade A". For the depths ranges investigated in this study, the error on the actual temperature gradient does not exceed 2%.

When necessary, we applied a terrain correction to account for the effects of an irregular topography. We used the method of Lachenbruch (1969). Two corrections only were necessary, at the Jackson and Littleton sites, both amounting to about 12% of the final value. We did not apply

any correction for past climatic variations in order to compare our data with the earlier measurements of Roy et al. (1968a,b). Climatic corrections remain controversial (Sass et al., 1971; Swanberg et al., 1974), but could raise the values by as much as $0.1 - 0.2 \mu\text{cal}/\text{cm}^2 \text{ s}$ (Jessop, 1971).

2.3.2 Thermal conductivity measurements

The samples which were at our disposal consisted either of drill cuttings piled up near the well or of rock specimens taken from outcrops in the immediate vicinity of the well. We employed the technique of King and Simmons (1972).

Samples were ground and sieved to a maximum grain diameter of 0.7 mm. When drill cuttings were available, we took special care to collect only the larger chips so that the sample could be considered as representative of the whole rock composition. The powder is dried in vacuum for at least 12 hours and is then saturated with distilled water under vacuum. The average specimen weight is about 400 grams. The samples are left to rest for several days to allow for compaction.

The thermal conductivity of the water-rock mixture is determined using a needle-probe method (Von Herzen and Maxwell, 1959). The response of the apparatus is calibrated with a blue quartz standard of known conductivity and prepared in the same manner. We thus hope to eliminate any systematic error in the procedure. The rock conductivity is determined from that of the water-saturated powder using the semi-empirical model of Woodside and Messner (1961). Among all models which have been proposed for two-component mixtures, Woodside and Messner's is the most reliable over large porosity differences and the easiest to use (Goss, 1974). The biggest experimental problem is in fact due to compaction effects which

depend on the granulometry. In some cases, measured conductivities differed by more than 20% between a freshly prepared sample and the fully compacted one. To alleviate this problem, we repeat measurements every day until the conductivity values are within 5% of each other, this being the average reproducibility of our technique. A rough check is provided by the value of density which can be calculated from the specimen volume and the dry and saturated weights. An anomalously low density indicates that compaction is not complete. Densities estimated in this manner are given in Table 2.2.

The method yields conductivity values which are usually within 10% of those obtained with a divided-bar apparatus (King and Simmons, 1972). The accuracy is better for homogeneous and isotropic rocks (Horai and Baldrige, 1972) but may be worse for highly anisotropic samples. We measured thermal conductivity on two formations which had already been investigated by Roy et al. (1968b) and found an excellent agreement (Table 2.3).

In the area considered here, thermal conductivity seems to be fairly uniform over a given geological unit. We did not undertake a specific study to prove this point, but the general consistency of the values is noticeable (Table 2.2). We summarize in Table 2.4 our results for the Winnebessaukee quartz diorite where we have the largest number of sites and where we were able to get samples from three different depths. The total spread of values for 10 samples is less than 20%, and the standard deviation represents 10% of the mean (Table 4.4).

When cuttings were available, we took care to select those which came from the deeper parts of the well so that they could be considered as representative of the depth range over which the geothermal gradient was

calculated. Although this was obviously not possible for outcrop samples, the error is probably small as conductivity values are remarkably uniform in the various units studied. We estimate the sampling error to be less than 20%.

As an assessment of the general reproducibility of our technique, we list in Table 2.5 measurements which were repeated at six stations at short distances (smaller than 5 km). Note that three groups of values differ by about 15%, whereas the other three differ by less than 5%. Given this overview of the data, we estimate the error on the heat flow values to be less than 20%.

The heat flow value at Bristol (Table 2.1) is doubtful because of an unusually low thermal gradient above 100 m. The value of 9.1 °C/km for the deeper section of the well is considerably lower than the value obtained at the nearby Brayton Point station over a large depth range (200m).

2.3.3 Measurements of U, Th and K concentrations

A new gamma-ray spectrometer was set up at MIT to measure U, Th and K concentrations in samples collected at heat flow stations. Gamma-ray spectrometry techniques for geological applications have been reviewed at length by Adams and Gasparini (1970). Details about the calibration and the accuracy of the apparatus can be found in Appendix 2.B.

The spectrometer is comprised of a 3x3 inch NaI(Tl) scintillation detector which is placed inside a steel shield with 10 cm thick walls. The signal is fed through a preamplifier and recorded on a 1024 multichannel analyzer. We used the following three peaks to interpret the spectra: 1.46 MeV (K^{40}), 1.76 MeV (Bi^{214} in the U^{235} decay series) and 2.76 MeV (Th^{202} in the Th^{232} series).

The samples are ground and put in cylindrical canisters which are

placed against the surface of the detector. The canisters are 1 inch thick and self-absorption effects are small for the energy levels investigated (Hurley, 1956). The average sample weight is 380 grams, which ensures that the measured concentrations are representative of the whole rock composition. We found differences in sample weights and packing densities barely detectable. We measured the background radioactivity routinely and verified that it was constant. Counting times ranged from 5 hours to 24 hours. The precision is estimated at 7% for uranium, 5% for thorium and 3% for potassium (see Appendix 2.B). The precision in the U concentration is worse for samples with low U contents and high Th/U ratios, but is always better than 10%.

As in the case of thermal conductivity determinations, the same question arises concerning the representativeness of the analyses on the large scale required for heat flow interpretation. In samples from shallow depths, uranium may have been leached in large amounts by circulating groundwater. To investigate this problem, we carried out a limited study in two wells distant by only a few meters where we had a limited depth sampling at the Melvin Village #2 site in the Winnebepesaukee pluton. The results are plotted in Figure 2.2. The plot shows clearly that K concentrations are constant both horizontally and vertically. U concentrations also appear fairly constant except around a depth of 60 m, which may be the trace of an altered zone. In contrast with uranium and potassium, thorium is quite variable in the shallowest samples. We finally note that the deepest samples all have similar U, Th and K contents. We therefore attribute the variations in the radioelements concentrations to leaching by meteoric water in the superficial layers. Although this is expected for uranium, it is more of a surprise for thorium which is usually

considered to be immobile in low temperature mineral-water equilibria. Further evidence for Th loss in surface rocks comes from a comparison between U, Th and K concentrations determined on drill cuttings and outcrop samples at the same site (Table 2.6). The analyses show almost constant U and K values whereas the Th concentration is significantly lower in the surface samples. We also note several low Th/U ratios in outcrop specimens (Table 2.2). Th depletion near the surface has been reported by Ragland et al. (1967) in a detailed study of a plutonic complex. Langmuir and Herman (1980) have recently pointed out that Th solubility in natural waters is a strong function of the pH. These depletion effects may lead to underestimate the total heat production rate by as much as 20%.

U, Th and K concentrations do not vary greatly within a particular unit. This was stressed by Lyons (1964) for the Kinsman and Bethlehem plutons and is confirmed by our results on the Winnepesaukee quartz diorite (Table 2.2). In contrast with the granitic series, the metasedimentary formations appear highly heterogeneous, probably because they consist of rocks of different origins, as in the case of the Littleton formation. Our values for U, Th and K contents of the New Hampshire rocks compare well with the earlier determinations by Lyons (1964) and Roy et al. (1968a). We estimate at 20% the maximum sampling error on the heat production rate at a site where the Th/U ratio is "normal", i.e. comprised between 2 and 6.

2.4 THE DISTRIBUTION OF HEAT FLOW AND RADIOACTIVITY

Before going into a discussion of the heat flow field over New Hampshire and its relationship with the observed distribution of radioactivity, we study the radioelement abundances in the major geological units of the State.

As noted earlier, U, Th and K concentrations are remarkably uniform

within the plutons. We give in Table 2.7 a summary of the mean concentrations for several of them. Two observations can be made. First, concentrations are constant for one age group, for example for the Kinsman and Bethlehem formations which were both intruded in the climax of the Acadian orogeny (Lyons and Livingston, 1977). Second, concentrations seem to depend on the age of the unit, the youngest rocks being the richest (Table 2.7). The Winnepesaukee pluton is an exception with a low level of radioactivity.

The cause of the relationship of Table 2.7 is not clear. Most of the Acadian granites are probably anatectic (Thompson et al., 1968; Lyons and Livingston, 1977; Rumble, 1978). The Kinsman and Bethlehem plutons intrude the surrounding Littleton formation in numerous dikes and sills and it is sometimes impossible to distinguish between them as they are intricately entangled (Billings, 1956). Lyons and Livingston (1977) found evidence for the presence of mantle-derived material. The binary granites are different and were emplaced forcefully some 40 My after the climax of the orogeny (Lyons and Livingston, 1977). The Winnepesaukee quartz diorite pluton has not been studied in detail. Furthermore, the origin of quartz diorite formations is still debated: they could be differentiates from basaltic magmas or the product of eclogite melting in subduction zones (Arth and Hanson, 1972). Extensive differentiation is ruled out as the Winnepesaukee rocks are poor in U, Th and K. The White Mountain Magma Series probably involve mantle material contaminated by lower crustal rocks (Foland and Friedman, 1977; Loiselle, 1978). They are the result of a well-documented differentiation process (Chapman, 1976). The relationship documented in Table 2.7 may therefore be related to a variation in the degree of differentiation and also to differences in the nature of the source

material.

In contrast with the plutons, the metasedimentary units exhibit large variations in U, Th and K concentrations across the State. They are enriched in the vicinity of the highly radioactive units, for example at the Jackson site close to the White Mountain batholith and the Goffstown site close to Kinsman and Bethlehem granites.

Heat flow values at 32 stations in New Hampshire and vicinity are plotted in Figure 2.3. When measurements were repeated in neighboring wells, the values were averaged to yield the heat flow at the site. No contouring was attempted for reasons which will be clear at the end of the discussion. A detailed comparison of the heat flow distribution with the geology is made in a later section.

Several features of the heat flow field are noteworthy. In the metasedimentary formations of the northern part of the State, the heat flow is uniformly low around $1 \mu\text{cal}/\text{cm}^2 \text{ s}$. In central New Hampshire, these metasedimentary rocks are associated with slightly higher values of heat flow and with marked heat flow highs near the White Mountain batholith at the Jackson station ($1.49 \mu\text{cal}/\text{cm}^2 \text{ s}$) and at the edge of the Winnepesaukee pluton ($1.73 \mu\text{cal}/\text{cm}^2 \text{ s}$ at the Lake Wentworth station). In the south, heat flow values are again uniformly low in the metasedimentary units with local highs around plutons.

A histogram of all these measurements is given in Figure 2.4. The distribution is roughly bimodal with a large number of values centered around 1.1 and $1.6 \mu\text{cal}/\text{cm}^2 \text{ s}$. The first peak represents the metasedimentary formations and the second plutonic rocks younger than 450 My (Acadian and post-Acadian). The lowest heat flow measured is $0.76 \mu\text{cal}/\text{cm}^2 \text{ s}$, on a poorly radioactive schistose quartzite at Lebanon on

the Vermont boundary. The heat flow field may be described schematically as a rather uniform background of 1.0-1.2 $\mu\text{cal}/\text{cm}^2 \text{ s}$ on which local highs are superimposed. These local highs are observed on highly radioactive young granites. The North-East trending ridge of high heat flow indicated in the map of Diment et al. (1972) is therefore an artifact due to a bias in favor of plutonic rocks. The background heat flow value is confirmed by our measurements in Vermont and Massachusetts (Table 2.1). Towards the North, heat flow seems to grade smoothly into the low values of Canada (Diment et al., 1972; Jessop and Lewis, 1978).

Heat flow is highly variable within short distances and is essentially a function of the geological environment. We plot in Figure 2.7 heat flow vs. radiogenic heat production for the New Hampshire and Maine sites. Data from the Winnepesaukee pluton have been excluded because they appear highly variable. They are anomalous and will be discussed in a later section. The linear relationship of Roy et al. (1968a) for 12 sites in the Eastern USA province is also indicated in Figure 2.5, together with $\pm 10\%$ error domains. We have separated our data according to the presumed quality of the measurements. We take as "grade A" data pairs those who meet the following requirements:

- (a) well deeper than 100 meters, (b) Th/U ratio between 2 and 6.

Considering the errors in the data, our heat flow and radioactivity measurements agree with the relationship established by Roy et al. (1968a) with two notable exceptions: points 1 and 2 on Figure 2.5. Both these points correspond to the same area around Bedford in southern New Hampshire and will be discussed separately.

For further comparison, we interpreted our data in terms of the familiar relationship:

$$Q = Q_r + D \cdot A \quad (2.1)$$

We determined the parameters Q_r and D using a standard least-squares analysis for the different data sets at our disposal (Table 2.8). The standard deviation for heat flow data is assumed to be 0.10 and 0.15 $\mu\text{cal}/\text{cm}^2 \text{ s}$ according to the quality of the measurements. These figures are reasonable for our measurements and are compatible with the RMS residuals found (Table 2.8). The errors on the parameters Q_r and D are slightly larger than those for the Roy et al. data set, either because of the lower quality of our measurements or because of the more complex geologic environments sampled.

Several authors have suggested that heat flow and average P-wave residuals are positively correlated (Horai and Simmons, 1968; Combs and Simmons, 1973; Buschbinder and Poupinet, 1976; Poupinet, 1979), the underlying cause being differences in mantle temperatures. Although the NEUS seismic network offers a rather sparse coverage of New Hampshire, the P-wave residuals appear uniform with positive values of +0.3 and +0.4 s, except in the southeastern corner of the State (Taylor and Toksoz, 1979; Figure 2.6). The positive residuals are clearly associated with the presence of massive granitic intrusives but there is no relationship with the individual heat flow values which vary by more than a factor of 2. The highest residual in the State is obtained on the Vermont border where heat flow never exceeds 1.3 $\mu\text{cal}/\text{cm}^2 \text{ s}$, whereas the low P-wave residuals in Massachusetts are associated with heat flow values which can be as high as 1.63 $\mu\text{cal}/\text{cm}^2 \text{ s}$ (Roy et al., 1968b). P-wave residuals are essentially sensitive to the mantle structure (Taylor and Toksoz, 1979). Their lack of correlation with the surface heat flow emphasizes that heat flow variations

in New Hampshire are due to relatively superficial differences in heat production.

We have seen that most of the geological units of New Hampshire satisfy the same heat flow vs. radioactivity relationship. We study now the two exceptions to this rule.

2.4.1 The Winnepesaukee pluton.

A detailed map of the area is presented in Figure 2.7 (from Billings, 1956 and Lyons, 1978, unpublished). The Winnepesaukee quartz diorite pluton is surrounded by a Kinsman tonalite formation on its western side and by binary granite on its eastern side. Both these formations are enriched in uranium, thorium and potassium (see Table 2.7). From the structural relationships which can be tentatively deduced from the map, it appears that the Winnepesaukee pluton was emplaced after the Kinsman, and thus after the climax of the Acadian orogeny. It was later intruded by several members of the White Mountain Series, between 198 and 110 My ago (Foland and Faul, 1977).

The three plutons are flanked by the Littleton formation where heat flow is uniformly low (Figure 2.7). Heat flow is higher on the Winnepesaukee and also exhibits large variations. A very high value is measured in the East at the Lake Wentworth station and near the southern boundary of the pluton at the Alton station ($1.57 \mu\text{cal}/\text{cm}^2 \text{ s}$). These high values cannot be due to thermal refraction effects because thermal conductivity contrasts are small.

All the heat flow - radioactivity data pairs for the Winnepesaukee pluton fall unambiguously above the general relationship of Figure 2.5. We therefore suggest that the quartz diorite is underlain by more radioactive rocks, and more precisely by the Kinsman tonalite below the western part

and by the more radioactive binary granite below the eastern part. The heat flow values are compatible with the heat generation rates of these rocks (see Tables 2.2 and 2.7).

This model agrees with the model proposed by Nielson et al. (1976) on the basis of gravity anomalies. Nielson et al. (1976) estimate that the Winnepesaukee forms a cuppola of 3.5 maximum thickness which thins markedly towards its contact with the Kinsman formation. They further suggest the presence of a low density body below the Kinsman which could be the binary granite which outcrops on the East. Using our heat flow data together with the interpretation of Nielson et al. (1976) and the geological information, we have constructed a schematic cross-section of the Winnepesaukee area (Figure 2.8). The vertical extents of various units remain poorly constrained as the gravity field is influenced by a strong regional gravity gradient towards the White Mountain batholith.

2.4.2 The Bedford anomaly in southeastern New Hampshire

We now turn to an area located within the Merrimack Synclinorium in the southern part of the State (Figure 2.9).

The heat flow determined in this study on the Kinsman pluton agrees with an earlier measurement by Roy et al. (1968b) further up north (Figure 2.9). Again, thermal refraction effects are small in this region.

There is an anomaly in the heat flow vs. radioactivity relationship at the Bedford station (point 1, Figure 2.5). The heat flow is too high for the radioactive elements abundances of the Massabessic gneiss. This high value is confirmed by a less reliable measurement at the Londonderry station located on the Rye formation (point 2, Figure 2.5). We suggest again that this anomaly is due to the presence of radioactive rocks at depth. Likely candidates are binary granites from the Devonian Acadian orogeny or the

Permian Alleghenian orogeny which outcrop elsewhere in the area (Figure 9) or a member of the White Mountain Series such as the tiny Pawtuckaway pluton which intrudes the Massabessic gneiss further up north (see the map of Billings, 1956). The last hypothesis is not supported by magnetic data (Weston Geophysical Res., 1976), which do not show the large anomalies usually associated with intrusives of the White Mountain Series (Sharp and Simmons, 1978). There is unfortunately no dense gravity coverage over this part of the State to test this interpretation. It seems that the anomaly is localized as there are several stations around Bedford where heat flow and radioactivity data agree with the general relationship.

2.5 DISCUSSION

The New Hampshire region was affected by several important thermal events until recent times, the last one being dated at 110 Ma (Foland and Faul, 1977). It represents a young continental region over which the heat flow coverage is now fairly complete. It is impossible to compare the heat flow distribution to the world-wide distribution determined by Sclater et al. (1980) without some care. As the distribution is bimodal (Figure 2.4), the mean value of all measurements has no particular significance. In fact, the largest portion of the State is occupied by metasedimentary and metavolcanic formations where heat flow is generally low. The corresponding mean value is $1.12 \mu\text{cal}/\text{cm}^2 \text{ s}$ which is just the mean heat flow for old continents (Sclater et al., 1980). All the high heat flow values are obtained on relatively thin granitic intrusions which are markedly enriched in radioactive elements. Thus New Hampshire is characterized by a typical continental crust overlain by a radioactive upper layer. This layer is not homogeneous and consists of many different units which were emplaced at varying depths at various times. Some of

these do not outcrop and are revealed by anomalies in the general heat flow vs. radioactivity relationship.

The metasedimentary and plutonic rocks of New Hampshire define the same heat flow vs. radioactivity relationship. This was already observed in Australia by Jaeger (1970), in Ukraine by Kutas (1977) and in England and Wales by Richardson and Oxburgh (1978). Therefore the vertical distribution of the radiogenic heat production is characterized by the same depth scale in both plutons and metamorphosed sediments. This poses a problem concerning the nature of the mechanism responsible for the concentration of uranium, thorium and potassium in the upper layers of the crust. Although it is clear that granitic intrusions are enriched with respect to the formations they intrude, a mechanism essentially related to magma transport and crystallization such as magmatic differentiation (Lachenbruch, 1968, 1970) cannot explain the observations in the other formations. Furthermore, the vertical depth scale for radioactive enrichment is remarkably uniform not only throughout the State (Table 2.8) but also over the whole Eastern USA province, and it is surprising that it cannot be correlated with any seismic discontinuity (see Taylor, 1980) nor with any of the estimated thicknesses of the granitic intrusives. We list in Table 2.9 the vertical extents of several New Hampshire plutons determined on the basis of gravity data. These estimates may be in error because of the possible existence of vertical density gradients and because of basic uncertainties in density values. However, the general geological relationships and the extremely large area covered by most of these plutons argue strongly in favor of the conclusion of Nielson et al. (1976) that they are tabular. None of the values indicated in Table 2.9 comes close to 7 km, which is the depth scale indicated by the heat flow and radioactivity

analysis.

We suggest that the initial distribution of radioactive elements which is established when the granites are intruded is modified at later times. The circulation of aqueous solutions released during retrograde metamorphism and magma cooling is now well documented for the New Hampshire intrusions, in the White Mountain batholith by Brimhall and Adams (1964) and in the Bethlehem pluton by Rumble (1978). Such solutions can transport both uranium and thorium in significant amounts (Brimhall and Adams, 1964) and are thus likely to perturb their initial distributions in and around the granite masses. Models taking explicitly these effects into account have been proposed by Albarede (1975) and Buntebarth (1976). Finally, a late perturbation may be caused by meteoric water in the superficial layers of the crust. These processes most probably result in the depletion of uranium and maybe thorium in the surface rocks, thus leading to an underestimation of the true heat production. In consequence, the depth scale determined from the heat flow will be overestimated in compensation.

We have shown that the heat flow variations can be accounted for by the observed differences in heat production of a relatively thin upper layer. Therefore, the thermal perturbations which resulted in the generation of the huge amounts of granitic rocks observed in New Hampshire have left no detectable effects on the surface heat flow. Using an average thermal diffusivity of 10^{-2} cm²/s for lithospheric material, it is possible to calculate the maximum depth extent which was thermally affected during these events. The White Mountain batholith is roughly 200 million years old (Foland and Faul, 1977), which places an upper bound of 150 km for the thickness of the layer which underwent significant heating. Similarly, the Alleghenian orogeny which is interpreted as a continent-continent collision

has been dated at 275 Ma (Aleinikoff et al., 1979). This yields an upper bound of 180 km for the thickness of the layer which was thermally affected.

If the New Hampshire region must be classified according to its age, as is done for example in the world-wide analysis of Sclater et al. (1980), it is not clear what is the "good" age to select. If the last major event is taken, then the age is about 400 Ma. We have concluded that the representative heat flow value was $1.12 \mu\text{cal}/\text{cm}^2 \text{ s}$, close to the mean heat flow through old cratons. Thus the characteristic time-scale of the decay of continental heat flow is constrained to be less than 400 ma in this part of the world. If the subsequent events are considered, this estimate could be revised to much smaller values around 200 Ma. Thus this detailed study of heat flow and radioactivity provides no basis for supporting the arguments of Vitorello and Pollack (1980) concerning the large thickness of the continental lithosphere. Part of the long time-scale of continental heat flow decay may be due to the effects of erosion which is slow over the most radioactive crustal rocks, granites. Furthermore, part of the scatter in the heat flow values over a given province can be explained by the presence of plutons below the surface, as in the case of the Winnepesaukee area.

2.6 CONCLUSIONS

We have presented an extensive set of heat flow and radiogenic heat production measurements over the State of New Hampshire and surrounding areas. Our analysis has established that the linear relationship obtained by Roy et al. (1968a) on a suite of homogeneous plutons is also valid for many more complicated geological environments, such as the metasedimentary and metavolcanic rocks which occupy a large surface in the region. This

observation represents a strong constraint on the mechanism of radioactive enrichment in the upper layers of the crust. We also found two anomalies to this general relationship, which can be interpreted by the existence of radioactive intrusions at depth. This indicates that primary enrichment in U, Th and K is due to granite migration and that the vertical distribution of radioactivity is not homogeneous.

The relationship holds on many different plutons which have varying thicknesses. Most of them are thin, however, and their estimated thicknesses are significantly smaller than 7 km which is the depth scale revealed by the heat flow analysis. This suggests that uranium, thorium and potassium are redistributed after the emplacement of the granites, probably through the action of metamorphic and magmatic waters and of meteoric waters in a late stage.

The reduced heat flow determined by Roy et al. (1968a) is confirmed by our data. On a total of 41 measurements, the lowest heat value value is $0.76 \mu\text{cal}/\text{cm}^2 \text{ s}$ and corresponds to a very poorly radioactive formation. Heat flow is high on plutons but is low elsewhere and grades smoothly into the low heat flow regions of Canada. The thermal perturbations which have affected the region have decayed completely. This gives a constraint on the maximum thickness of the lithosphere beneath New England.

TABLES 2.1 and 2.2

HEAT FLOW AND RADIOACTIVITY DATA IN NEW HAMPSHIRE AND SURROUNDINGS

The symbols and units employed are as follows:

Depth range in meters,

k thermal conductivity in 10^{-3} cal/cm s°C,

$\Delta T/\Delta z$ geothermal gradient in °C/km,

Q heat flow in $\mu\text{cal}/\text{cm}^2$ s,

A radiogenic heat production in 10^{-13} cal/cm³ s,

ρ density of samples.

R indicates that the conductivity sample was taken from an outcrop.

C indicates that the conductivity sample consisted of drill cuttings.

* indicates that the heat flow value was corrected for topographic effects (see text).

** indicates that the heat flow value is doubtful (see text).

HEAT FLOW DATA

Locality	Lat.	Long.	Depth Range	k	$\Delta T/\Delta z$	Q	A
NORTHERN NEW HAMPSHIRE							
Colebrook	44°56'	71°32'	35-150	8.4	11.8	0.99	2.8 C
West Milan	44°38'	71°20'	45- 80	6.7	14.4	0.96	1.9 C
Lebanon	43°36'	72°20'	45- 85	5.9	12.9	0.76	0.6 C
Littleton	44°22'	71°49'	85-125	5.6	15.8	1.00*	4.1 C
Jackson	44°11'	71°12'	40-105	5.0	26.0	1.49*	9.6 C
CENTRAL NEW HAMPSHIRE							
Center Sandwich	43°47'	71°28'	90-190	5.3	20.2	1.08	1.0 C
Moultonboro #1	43°44'	71°27'	75-185	6.4	18.6	1.19	2.0 C
Moultonboro #2	43°44'	71°25'	60-260	5.2	23.8	1.23	1.2 C
Meredith #1	43°39'	71°32'	35-125	5.0	24.2	1.20	C
Meredith #2	43°38'	71°31'	120-220	6.4	21.7	1.40	3.0 C
Melvin Village #1	43°42'	71°22'	60-120	5.2	20.7	1.08	1.3 C
Melvin Village #2	43°41'	71°21'	60-150	6.8	18.6	1.27	2.2 C
Lake Wentworth	43°36'	71°12'	50-150	5.9	29.6	1.73	1.4 C
Alton	43°29'	71°16'	70-200	6.1	25.7	1.57	R
Gilford	43°32'	71°26'	20- 85	7.0	15.2	1.07	3.9 C
Gilmanton Ironworks	43°23'	71°21'	45- 95	8.1	12.6	1.02	6.6 C
Franklin	43°27'	71°44'	110-160	4.6	20.0	0.92	0.9 R
Canaan Center	43°39'	72°04'	20- 55	8.9	13.1	1.16	2.3 C
West Springfield	43°29'	72°05'	120-220	6.6	19.5	1.29	8.0 C
Goshen	43°17'	72°09'	30- 80	6.2	18.7	1.17	5.2 R

SOUTHERN NEW HAMPSHIRE

Hillsboro Upper Va.	43°07'	72°00'	40-155	7.0	20.4	1.42	4.6	R
Deering	43°03'	71°51'	40-120	6.2	25.7	1.59		R
New Ipswich	42°45'	71°51'	35-125	7.5	15.7	1.18	5.7	C
New Boston	43°00'	71°46'	50-100	6.8	13.8	0.94	2.7	R
Milford	42°50'	71°43'	65-130	5.6	20.9	1.17	6.6	R
Hopkinton	43°09'	71°41'	45-100	7.5	15.0	1.12	5.0	C
Amherst #1	42°51'	71°37'	45- 65	6.4	15.5	0.99	2.0	R
Amherst #2	42°51'	71°37'	30-240	5.7	19.4	1.11	5.6	R
Goffstown	43°01'	71°37'	105-205	8.0	20.6	1.64	9.1	R
Hollis #1	42°44'	71°36'	75-125	8.0	15.1	1.20	3.6	C
Hollis #2	42°44'	71°36'	30- 75	7.7	16.2	1.25		C
Bedford	42°56'	71°32'	60-110	6.6	26.2	1.72	3.3	C
Londonderry	42°51'	71°22'	40- 80	5.5	26.4	1.45	3.7	C

MAINE

North Berwick	43°17'	70°40'	50-150	5.8	18.8	1.08	2.7	C
West Newfield	43°39'	70°52'	45-120	4.7	24.7	1.16	5.2	C

MASSACHUSETTS

Bristol**	41°39'	71°16'	120-165	11.6	9.1	1.05	3.8	C
Brayton Point	41°42'	71°10'	100-305	9.9	14.7	1.45	3.1	C
Taunton	41°53'	71°08'	115-290	9.2	13.3	1.22	2.4	C

VERMONT

Hartford	43°40'	72°22'	130-210	9.1	12.5	1.13	1.8	C
Thetford Center #1	43°49'	72°15'	85-110	10.6	12.6	1.33	2.9	C
Thetford Center #2	43°50'	72°15'	100-185	9.2	13.9	1.28	3.3	C

URANIUM, THORIUM AND POTASSIUM CONCENTRATIONS OF SAMPLES
COLLECTED AT HEAT FLOW STATIONS

Formation and rock type	k	p	U	Th	K	Th/U	K/U	
<u>PRECAMBRIAN</u>								
MASSABESSIC Granite								
Amherst #1	6.4	2.60	0.7	2.8	5.3	4.0	7.6	R
Amherst #2	5.7	2.75	3.2	15.8	3.9	4.9	1.2	R
Bedford	6.6	2.58	2.1	9.0	2.8	4.3	1.3	C
<u>CAMBRIAN-ORDOVICIAN</u>								
ALBEE Gray Quartz Micaschist								
Littleton	5.6	2.60	3.1	10.7	2.6	3.5	0.8	C
West Milan	6.7	2.92	1.0	4.4	1.7	4.4	0.6	C
GILE MOUNTAIN Phylitte								
Colebrook	8.4	2.61	1.9	8.0	1.6	4.2	0.8	C
ORFORDVILLE Schistose Quartzite								
Lebanon	5.9	2.81	0.4	1.6	0.4	4.0	1.0	C
RYE Calcareous Sandstone								
Hollis #1	8.0	2.87	2.6	7.7	2.1	3.0	0.8	C
Londonderry	5.5	2.72	3.2	7.2	2.4	2.3	0.8	C
BERWICK Schist								
North Berwick	5.8	2.61	1.8	7.2	2.0	4.0	1.1	C
<u>ORDOVICIAN</u>								
OLIVERIAN Granite								
Canaan Center	8.9	2.59	1.9	5.3	1.5	2.8	0.8	C

ORDOVICIAN-SILURIAN

LITTLETON Micaschist, Biotite Gneiss

Franklin	4.6	2.42	0.8	2.1	0.9	2.6	1.1	R
Gilford	7.0	2.58	2.6	11.5	2.6	4.4	1.0	C
Gilmanton Ironworks	8.1	2.69	4.8	17.3	3.5	3.6	0.7	C
Goffstown	8.0	2.57	12.3	6.7	4.0	0.5	0.3	R
West Newfield	4.7	2.64	4.0	14.3	2.4	3.6	0.6	C
New Ipswich	7.5	2.78	5.9	6.6	3.6	1.1	0.6	C
Jackson	5.0	2.53	7.6	29.0	3.3	3.8	0.4	C

EARLY DEVONIAN : NEW HAMPSHIRE PLUTONIC SERIES

KINSMAN Tonalite to Granite Gneiss

Hillsboro Upper Village	7.0	2.55	2.2	17.2	2.9	7.8	1.3	R
Hopkinton	7.5	2.64	4.3	13.3	2.8	3.1	0.7	C

BETHLEHEM Tonalite to Granite Gneiss

West Springfield	6.6	2.79	8.9	9.6	3.2	1.1	0.4	C
Goshen	6.2	2.89	3.1	14.5	2.5	4.7	0.8	C

WINNEPESAUKEE Quartz Diorite

Center Sandwich	5.3	2.53	0.5	2.0	2.1	4.0	4.2	C
Moultonboro #1	6.4	2.60	1.4	4.6	2.2	3.3	1.6	C
Moultonboro #2	5.2	2.40	0.6	3.4	1.6	5.7	2.7	C
Melvin Village #1	6.8	2.78	1.8	3.0	2.3	1.7	1.3	C
Melvin Village #2	5.2	2.36	0.8	3.3	1.9	4.1	2.4	C
Meredith #2	6.5	2.65	1.9	5.8	4.2	3.1	2.2	C
Lake Wentworth	5.9	2.51	0.8	4.5	1.1	5.6	1.4	C

SPAULDING Quartz Diorite

New Boston	6.8	2.40	2.7	2.5	4.0	0.9	1.5	R
------------	-----	------	-----	-----	-----	-----	-----	---

PERMIAN

BINARY Granite

Milford	5.6	2.76	1.3	30.7	2.8	23.6	2.2	R
---------	-----	------	-----	------	-----	------	-----	---

MASSACHUSETTS

BLACK SHALE

Brayton Point	9.9	2.67	2.2	9.0	1.4	4.1	0.6	C
---------------	-----	------	-----	-----	-----	-----	-----	---

Taunton	9.2	2.84	1.3	6.9	1.6	5.3	1.2	C
---------	-----	------	-----	-----	-----	-----	-----	---

Bristol	11.6	2.57	2.3	12.4	2.1	5.4	0.9	C
---------	------	------	-----	------	-----	-----	-----	---

VERMONT

SCHIST

Hartford	9.1	2.59	1.2	5.4	1.2	4.5	1.0	C
----------	-----	------	-----	-----	-----	-----	-----	---

Thetford Center #1	10.6	2.74	1.8	7.6	2.2	4.2	1.2	C
--------------------	------	------	-----	-----	-----	-----	-----	---

Thetford Center #2	9.2	2.94	2.3	7.6	1.8	3.3	0.8	C
--------------------	-----	------	-----	-----	-----	-----	-----	---

TABLE 2.3

A COMPARISON OF THERMAL CONDUCTIVITY VALUES (in 10^{-3} cal/cm s°C)

Formation	This study	Roy et al. (1968b) mean value
Kinsman pluton (southern N.H.)	7.0	7.1
Black Shale Formation (east-central Mass.)	9.2	9.0

TABLE 2.4

THERMAL CONDUCTIVITY DETERMINATIONS ON THE WINNEPESAUKEE QUARTZ DIORITE

(Values in 10^{-3} cal/cm s°C)

Number of samples	Total range	Mean value	Standard deviation
10	5.0-6.8	5.9	0.6 (10%)

MELVIN VILLAGE #2 WELL

Depth (m)	Thermal conductivity (10^{-3} cal/cm s°C)
50	6.1
61	6.3
76	5.2

TABLE 2.5

REPRODUCIBILITY OF THE HEAT FLOW MEASUREMENTS

Heat Flow Site	Measurement 1	Measurement 2	Difference
	($\mu\text{cal}/\text{cm}^2 \text{ s}$)		(%)
Moultonboro	1.19	1.23	3
Meredith	1.20	1.40	14
Melvin Village	1.08	1.27	15
Amherst	0.99	1.11	11
Hollis	1.20	1.25	4
Thetford Center	1.33	1.28	4

TABLE 2.6

COMPARISON BETWEEN URANIUM, THORIUM AND POTASSIUM CONCENTRATIONS
IN DRILL CUTTINGS AND OUTCROP SAMPLES

Heat flow station		U (ppm)	Th (ppm)	K (%)	Th/U	K/U
<u>Melvin Village #1</u>	Outcrop	1.4	0.8	2.1	0.6	1.5
	Drill cuttings	1.8	3.0	2.3	1.7	1.3
<u>New Ipswich</u>	Outcrop	5.2	2.0	4.0	0.4	0.8
	Drill cuttings	5.9	6.6	3.6	1.1	0.6

TABLE 2.7

MEAN RADIOELEMENT CONCENTRATIONS IN THE PLUTONS OF NEW HAMPSHIRE

Formation	Age (Ma)	N*	U (ppm)	Th (ppm)	K (%)	References
Exeter pluton	440	10	2.8	8.4	2.8	Gaudette et al. (1975) Roy et al. (1968a)
Kinsman pluton	441	15	3.3	15.1	2.8 ⁺	Lyons & Livingston (1977), Lyons (1964)
Bethlehem gneiss	405	28	3.4	14.9	2.9 ⁺	Same as above
Binary granite	360	145	7.6	23.5	3.9	Lyons & Livingston (1977), Roy et al. (1968a)
White Mountain	160	557	15.8	59	4.0	Foland and Faul (1977)
	190	349	15.9	61	4.1	
		145	12.6	52	4.3	
Winnepesaukee	?	8	1.1	3.8	2.2	This study

*N is the number of samples analyzed.

⁺These K concentrations are those measured in the few samples of this study.

TABLE 2.8

VALUES OF THE REDUCED HEAT FLOW AND OF THE CHARACTERISTIC DEPTH SCALE

Data Set	N*	Q_r ($\mu\text{cal}/\text{cm}^2 \text{ s}$)	D (km)	RMS residual ($\mu\text{cal}/\text{cm}^2 \text{ s}$)
"Grade A" data	9	0.86 ± 0.07	6.0 ± 1.5	0.08
Others	12	0.82 ± 0.09	6.8 ± 2.3	0.14
All	21	0.86 ± 0.07	6.2 ± 1.3	0.16
Metasedimentary only	14	0.83 ± 0.07	6.9 ± 1.5	0.12
Roy et al. (1968a)	12	0.81 ± 0.03	7.3 ± 0.2	0.05

TABLE 2.9

THICKNESS OF THE MAJOR PLUTONIC UNITS OF NEW HAMPSHIRE
 DETERMINED FROM GRAVITY STUDIES

Pluton	Maximum thickness (km)	References
Exeter pluton	3	Bothner (1974)
Kinsman pluton	2.5	Nielson et al. (1976)
Bethlehem pluton	3	Nielson et al. (1976)
Binary granite	2.5	Nielson et al. (1976)
White Mountain batholith	4.1	Joyner (1963) Wetterauer and Bothner (1977)

FIGURE CAPTIONS

Figure 2.1. a. Schematic geological map of New England showing the major units and the axis of the Merrimack Synclinorium (adapted from King, 1969); b. Map of the State of New Hampshire, USA, showing the major granitic formations. The symbols are as follows: Sedimentary and volcanic rocks (irregular pattern), Precambrian basement (inclined dashed lines), the early Paleozoic Exeter pluton (stars), the Devonian intrusives (large dots), the late Devonian binary granites (small dots), the Mesozoic plutons of the White Mountain Magma Series (crosses). Numbers refer to plutons which are often named in the text. 1: Massabessic gneiss, 2: Kinsman pluton, 3: Bethlehem gneiss, 4: Winnepesaukee pluton, 5: White Mountain batholith. (Adapted from Billings, 1956 and Lyons, 1978).

Figure 2.2. Plot of uranium, thorium and potassium concentrations vs. depth in two neighboring wells at the Melvin Village #2 heat flow station in the Winnepesaukee pluton.

Figure 2.3. Map of New Hampshire showing heat flow values determined in this study. Values are in $\mu\text{cal}/\text{cm}^2 \text{ s}$.

Figure 2.4. Histogram of all measurements in New Hampshire and Maine.

Figure 2.5. A plot of heat flow versus radiogenic heat production for New Hampshire and Maine data. Data from the Winnepesaukee pluton have been omitted because they are anomalous. Points 1 and 2 refer to the Bedford and Londonderry stations in southern N.H. which will be discussed separately. The heavy line is the linear relationship determined by Roy et al. (1968a) and the dashed lines represent $\pm 10\%$ error domains.

Figure 2.6. Average P-wave residuals in units of 10^{-1} seconds determined on the NEUS seismic network by Taylor (1980). Note that New Hampshire is characterized by positive residuals.

Figure 2.7. Detailed map of the Winnepesaukee area (from Billings, 1956 and Lyons, 1978, unpublished). Dots indicate the heat flow stations of this study, together with values of the geothermal gradient and of the heat flow.

Figure 2.8. Schematic vertical cross-section of the Winnepesaukee area. The horizontal scale is arbitrary. The vertical scale is only indicative as the vertical extents of the plutonic units are determined with rather large errors in this part of the State (see text). Heat flow values are in $\mu\text{cal}/\text{cm}^2 \text{ s}$. Symbols are the same as in Figure 2.8.

Figure 2.9. Detailed map around Bedford (southern N.H.) in the Merrimack Synclinorium (from Billings, 1956 and Lyons, 1978, unpublished). Dots indicate the heat flow stations of this study, squares those of Roy et al. (1968a,b).

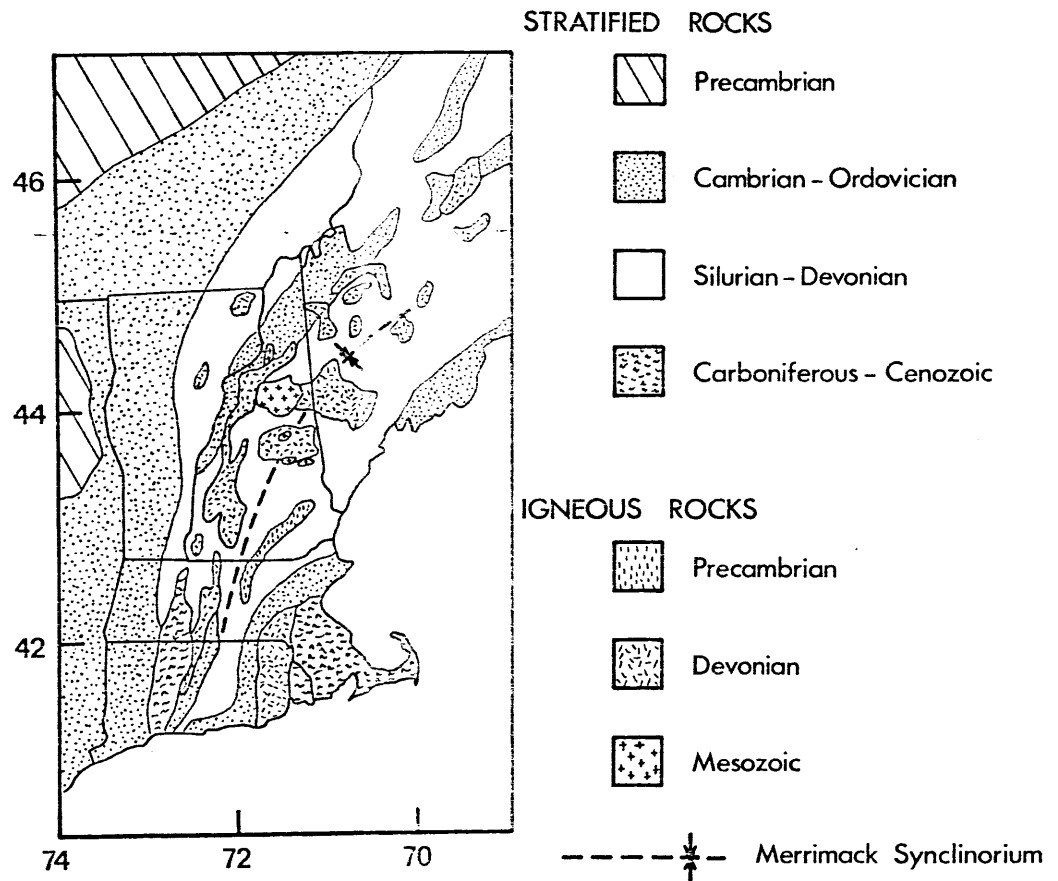


Fig. 2.1a

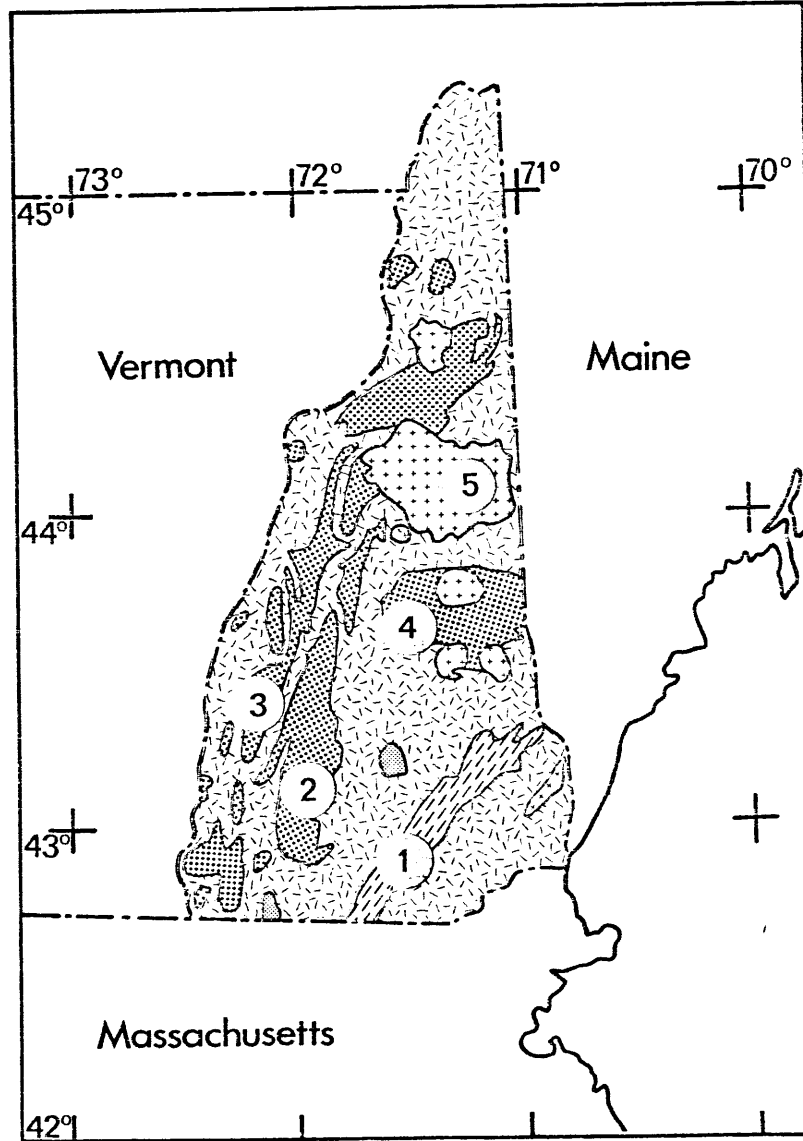


Fig. 2.1b

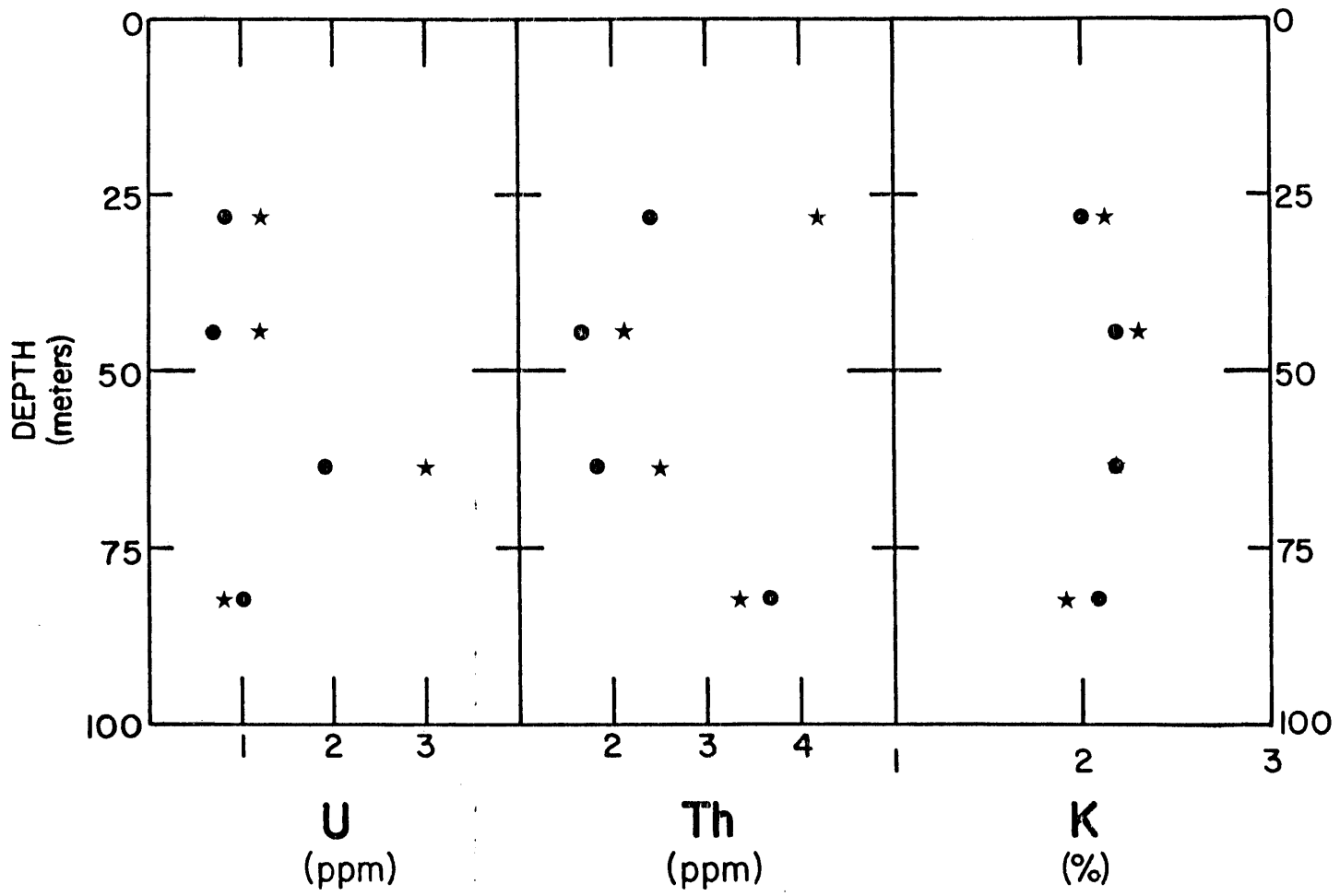


Fig. 2.2

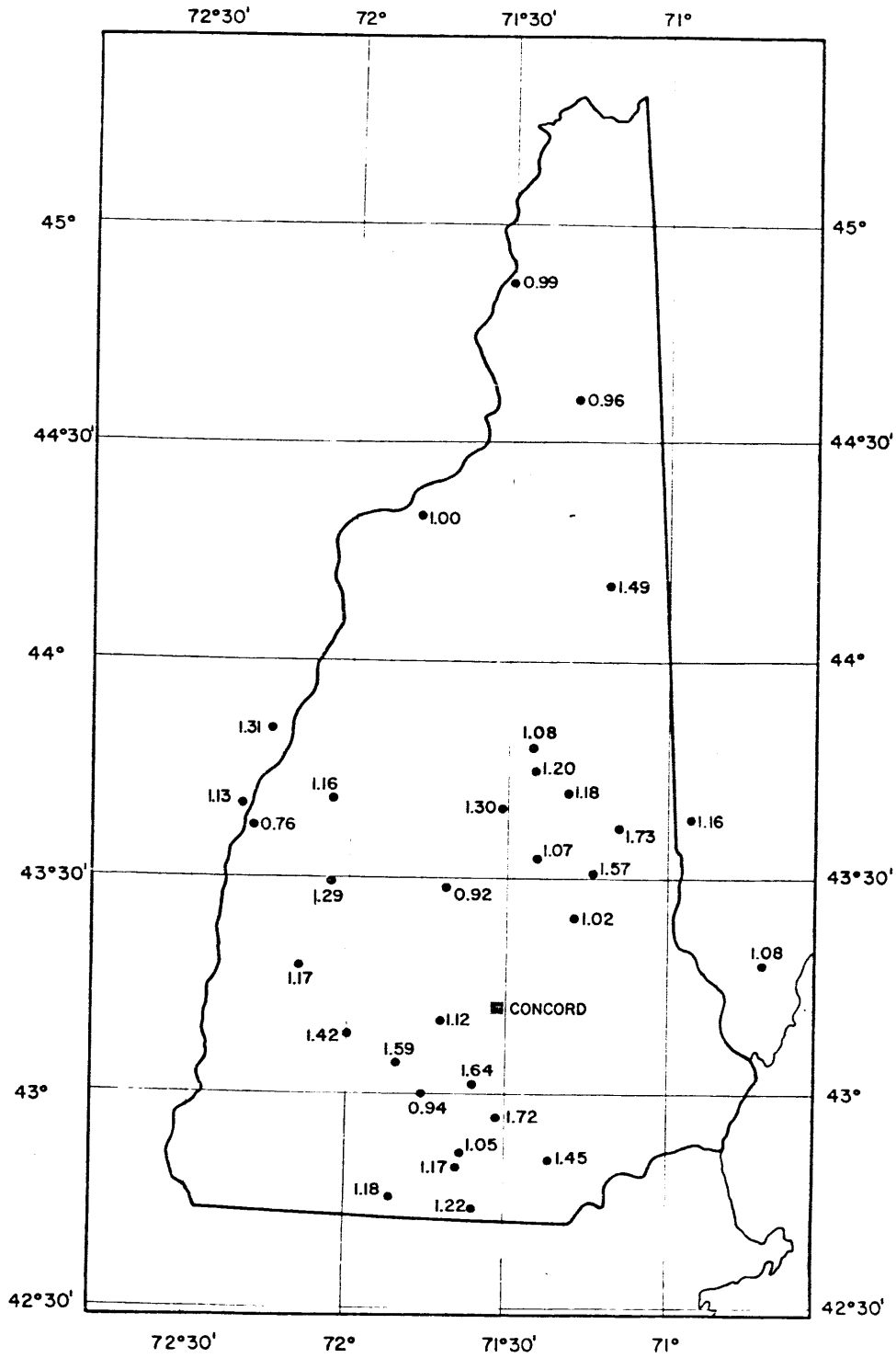


Fig. 2.3

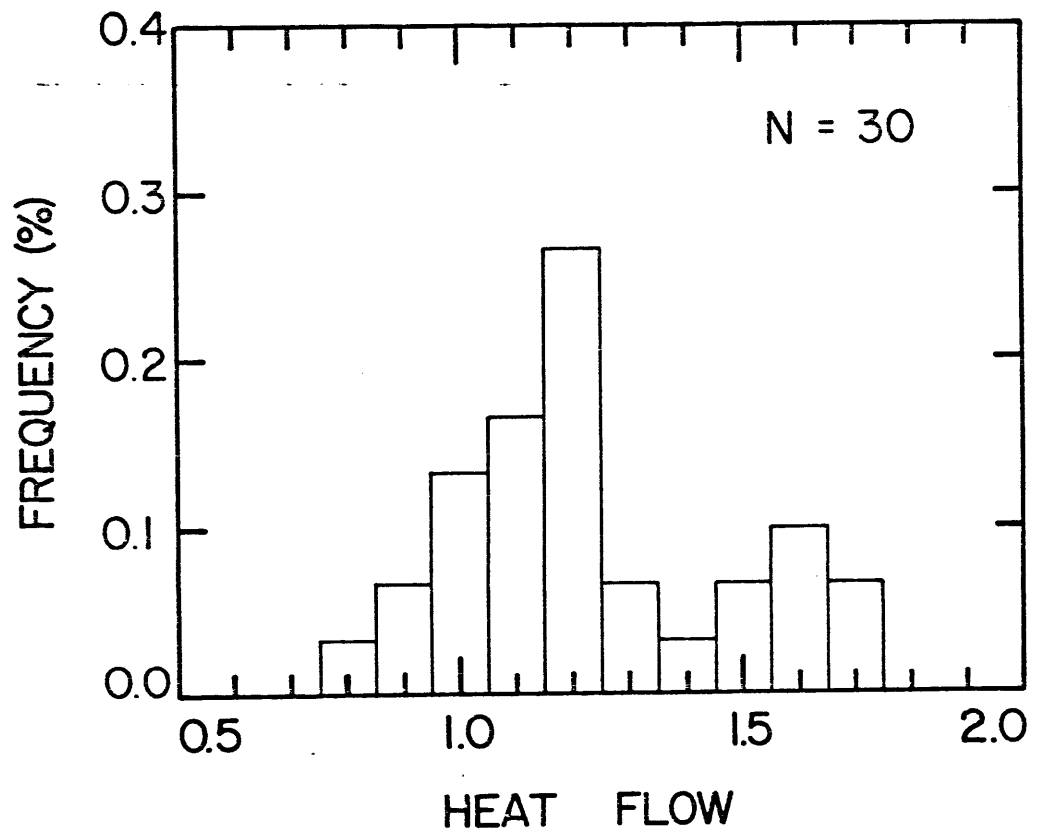


Fig. 2.4

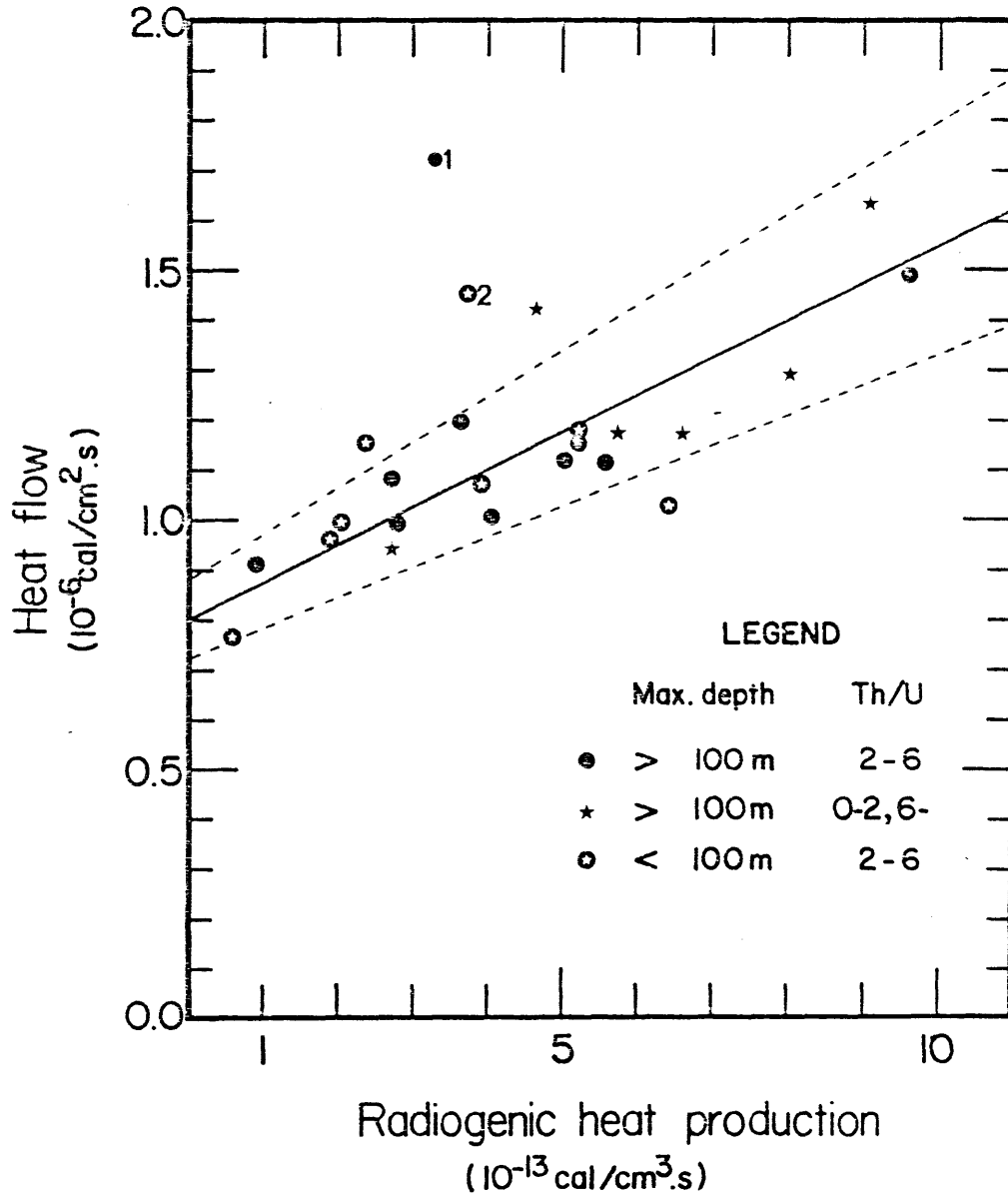


Fig. 2.5

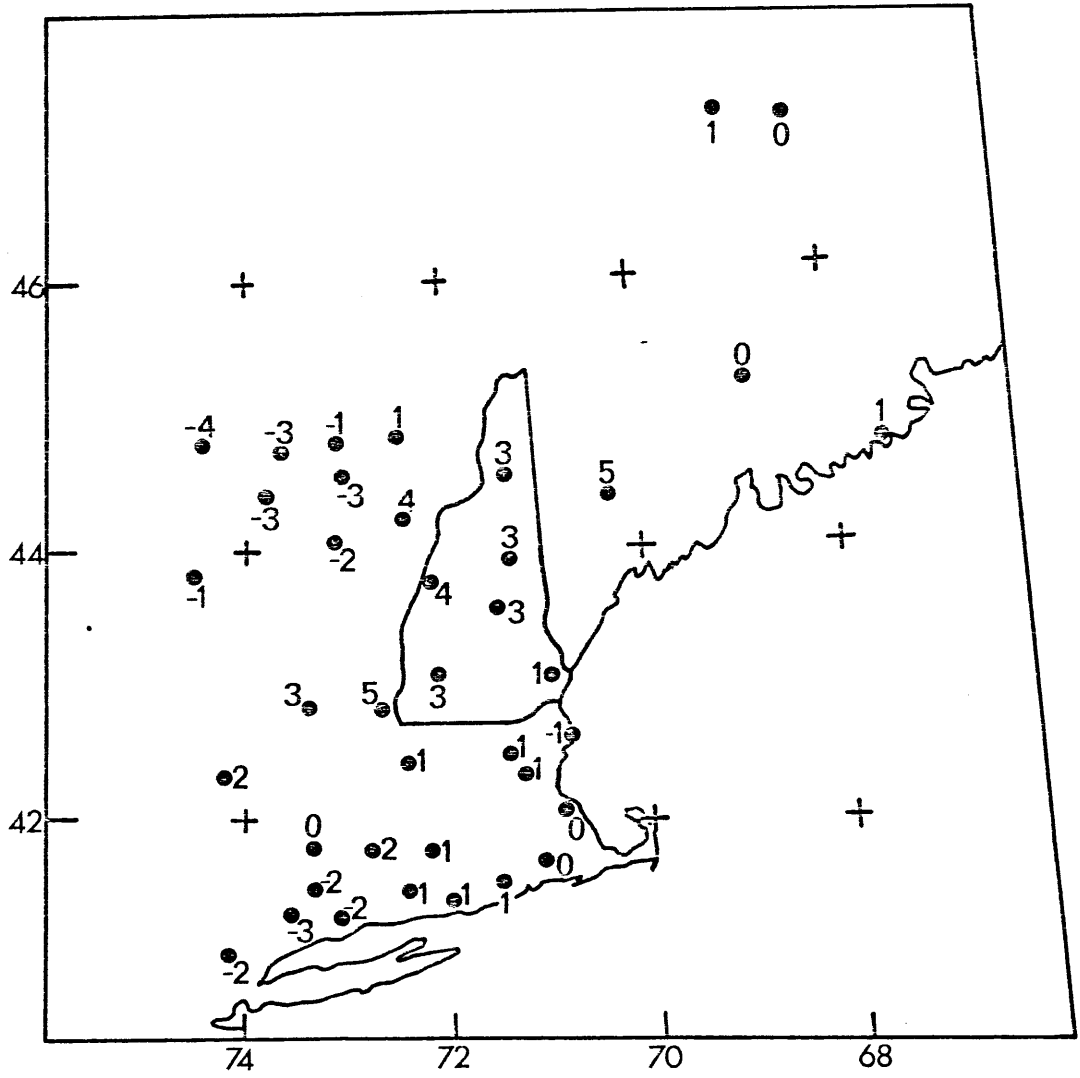


Fig. 2.6

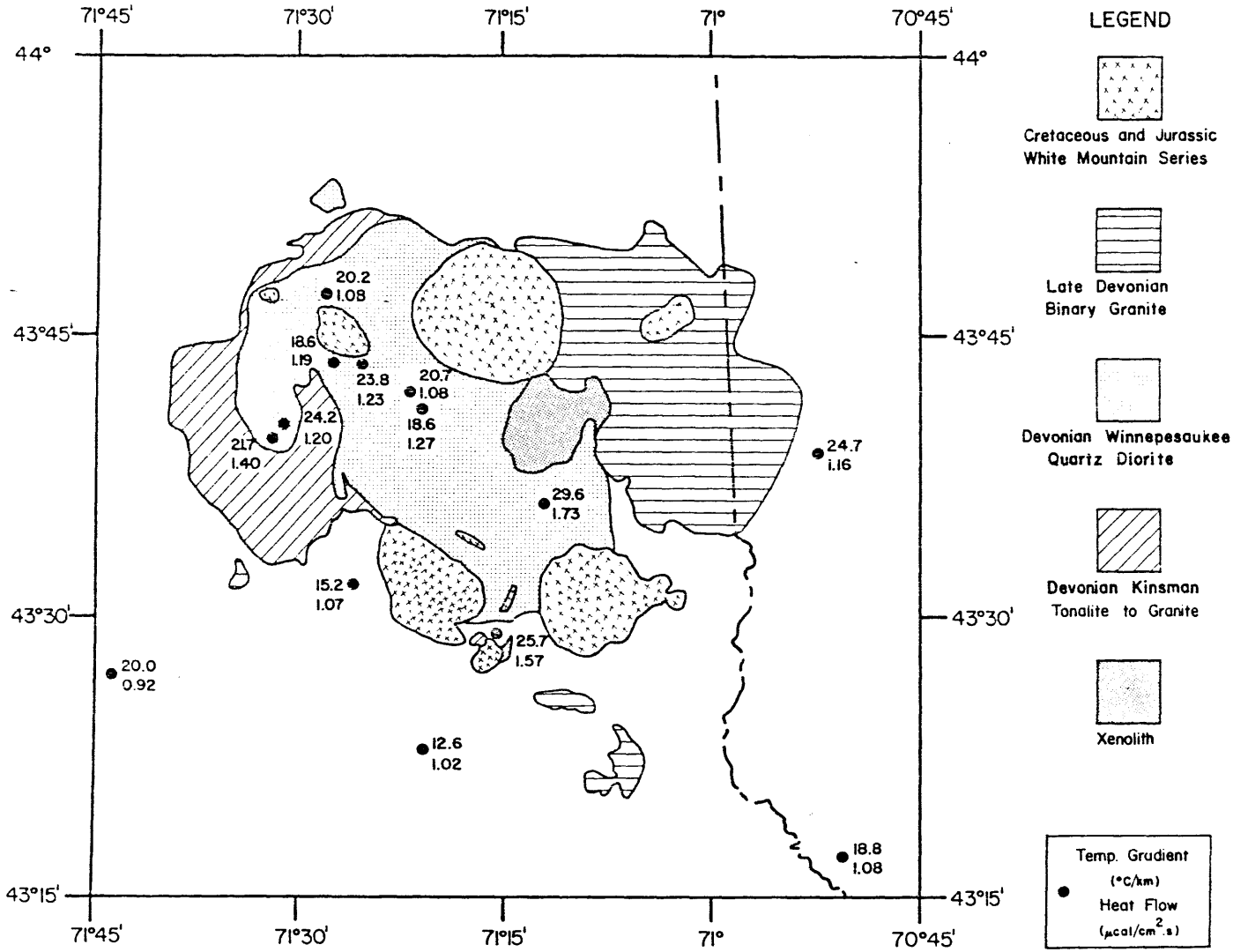


Fig. 2.7

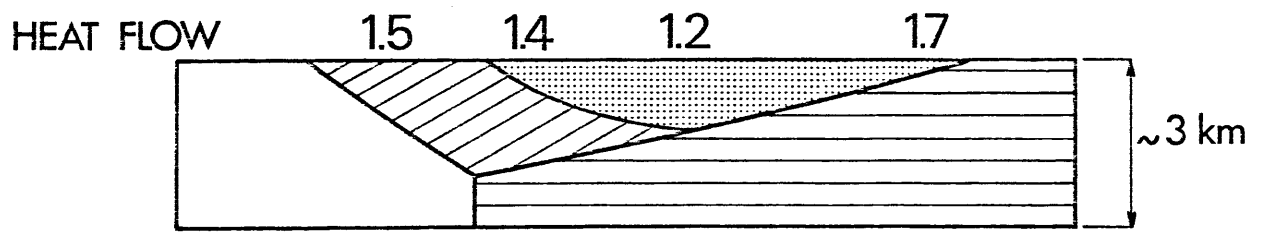
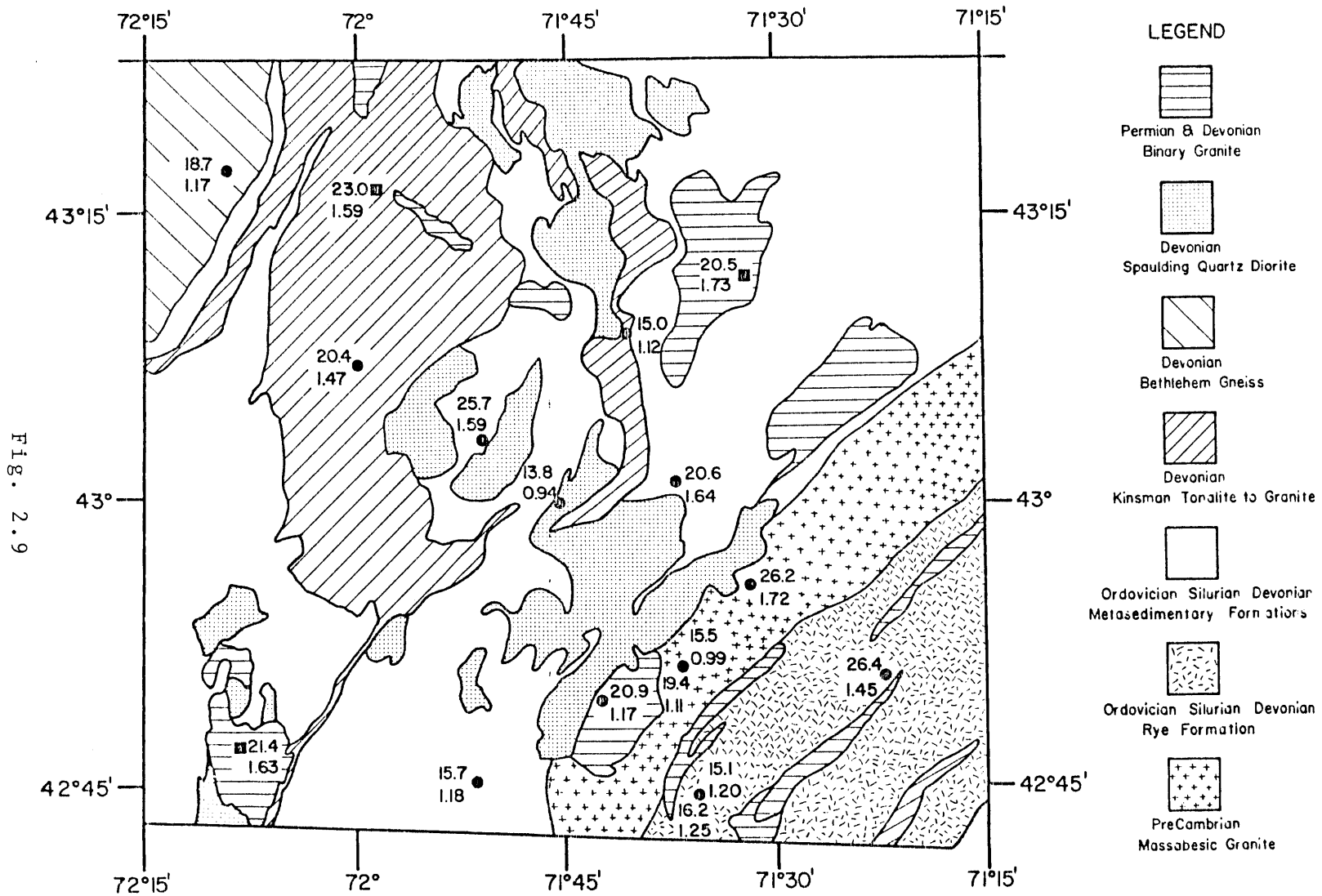


Fig. 2.8



APPENDIX A
TEMPERATURE LOGS AT HEAT FLOW STATIONS

LEBANON Station

Depth (m)	Temperature (°C)
20	9.00
26	9.02
32	9.04
38	9.08
44	9.13
50	9.20
56	9.28
62	9.37
68	9.44
74	9.51
80	9.60

THETFORD CENTER #2 Station

Depth (m)	Temperature (°C)	Depth (m)	Temperature (°C)
29	9.37	131	9.37
35	9.17	137	9.44
41	9.07	143	9.52
47	9.02	149	9.60
53	8.97	155	9.71
59	8.93	161	9.85
65	8.91	167	9.94
71	8.91	173	10.02
77	8.91	179	10.12
83	8.93	185	10.20
89	8.97		
95	9.01		
101	9.05		
107	9.11		
113	9.17		
119	9.23		
125	9.31		

COLEBROOK Station

Depth (m)	Temperature (°C)	Depth (m)	Temperature (°C)
26	7.22	127	8.34
32	7.32	133	8.41
38	7.39	139	8.58
44	7.46	145	8.65
50	7.51	151	8.70
56	7.58		
62	7.64		
68	7.70		
74	7.78		
80	7.84		
86	7.95		
92	8.03		
98	8.09		
109	8.18		
115	8.25		
121	8.34		

WEST MILAN Station

Depth (m)	Temperature (°C)
26	6.81
32	6.77
38	6.77
44	6.81
50	6.89
56	6.97
62	7.05
68	7.15
74	7.25
80	7.33

LITTLETON Station

Depth (m)	Temperature (°C)
26	7.91
32	7.92
38	7.94
44	7.97
50	8.02
56	8.07
62	8.13
68	8.19
74	8.26
80	8.34
86	8.41
92	8.50
98	8.60
104	8.69
111	8.81
117	8.90
123	9.00

JACKSON Station

Depth (m)	Temperature (°C)
29	7.29
35	7.30
41	7.32
47	7.39
53	7.51
59	7.69
65	7.87
71	7.99
77	8.22
83	8.34
89	8.51
95	8.63
101	8.86
107	8.98
113	9.13

CENTER SANDWICH Station

Depth (m)	Temperature (°C)
30	8.40
40	8.56
50	8.76
60	8.84
70	9.05
80	9.21
90	9.38
100	9.56
111	9.79
121	9.98
131	10.17
141	10.38
151	10.60
161	10.81
171	11.02
181	11.24
191	11.46

MOULTONBORO #1 Station

Depth (m)	Temperature (°C)	Depth (m)	Temperature (°C)
20	9.25	135	10.97
26	9.30	141	11.09
32	9.33	147	10.22
38	9.39	153	11.34
44	9.48	159	11.47
50	9.52	165	11.60
56	9.58	171	11.71
62	9.66	177	11.81
68	9.74	183	11.90
74	9.83		
80	9.93		
86	10.05		
92	10.15		
98	10.25		
104	10.41		
111	10.50		
117	10.60		
123	10.72		

MOULTONBORO #2 Station

Depth (m)	Temperature (°C)	Depth (m)	Temperature (°C)
20	8.10	161	11.02
30	8.14	171	11.24
40	8.29	181	11.50
50	8.47	191	11.73
60	8.63	201	11.96
70	8.86	211	12.18
80	9.10	221	12.41
90	9.32	231	12.63
100	9.56	241	12.89
111	9.83	251	13.13
121	10.07	261	13.37
131	10.31		
141	10.56		
151	10.77		

MELVIN VILLAGE #1 Station

Depth (m)	Temperature (°C)
20	8.83
30	8.99
40	9.11
50	9.25
60	9.41
70	9.60
80	9.80
86	9.93
90	9.99
96	10.15
100	10.22
111	10.43
117	10.57

GILMANTON IRONWORKS Station

Depth (m)	Temperature (°C)
20	8.62
26	8.65
32	8.64
38	8.71
44	8.77
50	8.85
56	8.92
62	9.01
68	9.08
74	9.15
80	9.25
86	9.32
92	9.39

FRANKLIN Station

Depth (m)	Temperature (°C)	Depth (m)	Temperature (°C)
20	10.44	129	11.92
26	10.32	135	12.06
32	10.32	141	12.19
38	10.35	147	12.33
44	10.40	153	12.45
50	10.46	159	12.55
56	10.53		
62	10.63		
68	10.74		
74	10.84		
80	10.94		
86	11.05		
92	11.15		
98	11.26		
104	11.40		
111	11.56		
117	11.68		
123	11.80		

CANAAN Station

Depth (m)	Temperature (°C)
16	8.55
22	8.62
28	8.70
34	8.77
40	8.86
46	8.94
52	9.02
58	9.10

HILLSBORO UPPER VILLAGE Station

Depth (m)	Temperature (°C)	Depth (m)	Temperature (°C)
20	7.51	104	8.99
26	7.55	111	9.11
32	7.60	117	9.24
38	7.67	123	9.37
44	7.78	129	9.49
50	7.89	135	9.62
56	8.01	141	9.75
62	8.13	147	9.87
68	8.26	153	9.99
74	8.37		
80	8.50		
86	8.61		
92	8.72		
98	8.86		

NEW BOSTON Station

Depth (m)	Temperature (°C)
20	9.00
26	8.98
32	8.97
38	8.97
44	8.99
50	9.02
56	9.07
62	9.18
68	9.24
74	9.30
80	9.44
86	9.51
92	9.60
98	9.68

HOPKINTON Station

Depth (m)	Temperature (°C)
20	9.12
26	9.20
32	9.23
38	9.28
44	9.34
50	9.42
56	9.52
62	9.60
68	9.69
74	9.77
80	9.89
86	9.97
92	10.05
98	10.14

NORTH BERWICK Station

Depth (m)	Temperature (°C)
20	7.79
30	7.89
40	8.04
50	8.22
60	8.40
70	8.58
80	8.77
90	8.96
100	9.15
111	9.36
121	9.54
131	9.73
141	9.92
151	10.10

WEST NEWFIELD Station

Depth (m)	Temperature (°C)
20	7.66
26	7.73
32	7.85
38	7.98
44	8.16
50	8.28
56	8.43
62	8.55
68	8.71
74	8.86
80	9.02
86	9.15
92	9.28
98	9.43
104	9.62
111	9.80
117	9.97

BRISTOL Station

Depth (m)	Temperature (°C)	Depth (m)	Temperature (°C)
20	12.30	104	11.98
26	12.27	111	12.01
32	12.19	117	12.05
38	12.10	123	12.09
44	12.05	129	12.14
50	12.00	135	12.19
56	11.96	141	12.24
62	11.94	147	12.29
68	11.92	153	12.35
74	11.91	159	12.40
80	11.90	165	12.47
86	11.91		
92	11.92		
98	11.95		

BRAYTON POINT Station

Depth (m)	Temperature (°C)	Depth (m)	Temperature (°C)
20	11.82	123	12.38
26	11.85	129	12.47
32	11.73	135	12.55
38	11.63	141	12.63
44	11.57	147	12.73
50	11.54	153	12.82
56	11.54	159	12.91
62	11.58	165	12.99
68	11.63	171	13.09
74	11.70	177	13.19
80	11.78	183	12.26
86	11.85	189	13.33
92	11.93	195	13.40
98	12.01	201	13.47
104	12.10	207	13.56
111	12.21	213	13.66
117	12.29	219	13.77

BRAYTON POINT Station (continued)

Depth (m)	Temperature (°C)
225	13.86
231	13.95
237	14.05
243	14.16
249	14.26
255	14.35
261	14.46
267	14.56
273	14.66
279	14.74
285	14.82
291	14.91
297	15.00
303	15.09

TAUNTON Station

Depth (m)	Temperature (°C)	Depth (m)	Temperature (°C)
20	10.50	147	11.01
26	10.30	153	11.09
32	10.16	159	11.15
38	9.94	165	11.23
44	9.91	171	11.31
50	9.94	177	11.40
56	9.98	183	11.48
62	10.02	189	11.56
68	10.05	195	11.64
74	10.07	201	11.72
80	10.09	207	11.81
86	10.17	213	11.89
92	10.27	219	11.98
98	10.36	225	12.03
104	10.45	231	12.12
111	10.59	237	12.21
117	10.62	243	12.30
123	10.69	249	12.38
129	10.77	255	12.46
135	10.84	261	12.54
141	10.92	267	12.60

TAUNTON Station (continued)

Depth (m)	Temperature (°C)
273	12.68
279	12.77
285	12.85
291	12.92

HARTFORD Station

Depth (m)	Temperature (°C)	Depth (m)	Temperature (°C)
20	9.08	129	9.33
26	9.05	135	9.39
32	9.00	141	9.46
38	8.94	147	9.52
44	8.90	153	9.60
50	8.89	159	9.67
56	8.89	165	9.74
62	8.90	171	9.81
68	8.91	177	9.88
74	8.94	183	9.96
80	8.97	189	10.04
86	8.99	195	10.12
92	9.03	201	10.20
98	9.07	207	10.27
104	9.11	213	10.32
111	9.17		
117	9.22		
123	9.29		

THETFORD CENTER #1

Depth (m)	Temperature (°C)
44	8.70
50	8.72
56	8.76
62	8.80
68	8.84
74	8.93
80	8.98
86	9.06
92	9.13
98	9.21

APPENDIX 2.B: CALIBRATION OF THE GAMMA-RAY SPECTROMETER

We calibrated the response of the gamma-ray spectrometer using two standards from the New Brunswick Laboratory (US Energy Research and Development Administration): samples 105 for uranium, and sample 110 for thorium.

For potassium, we used a chemically pure KCl which we blended with a low activity dunite in order to obtain a sample with density close to that of a rock. The dunite was counted separately to calculate its contribution to the counts.

Once the response of the instrument was determined with these standards, we measured samples sent from two different laboratories and obtained good agreement (Table 2.B1).*

To obtain a specified accuracy for each sample analyzed requires a counting time sufficiently long so that similar precisions in counting statistics are obtained. Repeated runs on poorly active specimens gave values within 10% of each other. The accuracy of the method was ascertained by repeating measurements on one sample D-66B and calculating the standard deviation of the measured values. We thus estimate the precision in our measurements to be:

7% for uranium,
5% for thorium,
3% for potassium.

The precision on U is worse when the uranium content is low and when the Th/U ratio is high. However, as stated before, repeated runs indicate that the precision is never worse than 10%.

*Samples were provided courtesy of Robert Roy (University of Texas at El Paso) and of John Costain (University of Virginia).

TABLE 2.B1

COMPARISON OF U, Th, K CONCENTRATIONS MEASURED AT DIFFERENT LABORATORIES

Sample #	Laboratory	U (ppm)	Th (ppm)	K (%)
S-7634	USGS, Denver, Colorado	3.8	41.0	4.4
	University of Virginia, Blacksburg	4.2	34.9	4.4
	M.I.T.	3.9	37.0	4.4
S6-89	USGS, Denver, Colorado	1.7	15.0	4.2
	University of Virginia, Blacksburg	1.8	13.8	4.1
	M.I.T.	1.9	14.7	4.1
D-66B	University of Texas at El Paso	2.4	15.0	1.6
	M.I.T.	2.2	14.4	1.6
BC-43A	University of Texas at El Paso	2.0	8.0	1.5
	M.I.T.	2.0	7.6	1.4

CHAPTER THREE

HEAT FLOW STUDIES; CONSTRAINTS ON THE DISTRIBUTION OF
URANIUM, THORIUM AND POTASSIUM IN THE CONTINENTAL CRUST

3.1 INTRODUCTION

The linear relationship between heat flow and radioactivity has been observed in many parts of the world (for a summary, see the paper by Sclater et al., 1980). Values reported for the reduced heat flow are in general agreement, with extreme values of 17 mW/m^2 and 33 mW/m^2 . On the contrary, the depth scale D appears highly variable, with about 4 km in the Western Australian Shield (Sass and Lachenbruch, 1979) to 16 km in England and Wales (Richardson and Oxburgh, 1978).

The interpretation of the relationship is not straightforward as many geologically reasonable distributions of the radiogenic heat production can satisfy the constraint it represents. Birch et al. (1968) proposed that the radioelements are concentrated uniformly in a layer of thickness D , and that Q_r is the heat flow through the bottom of this layer. Lachenbruch (1968, 1970) suggested an exponential distribution due to magmatic differentiation:

$$A(z) = A(0) \cdot \exp(-z/D) \quad (3.1)$$

where $A(z)$ is the heat generation rate at depth z . In this model, Q_r is the heat flow at a depth large compared to D and, to a first approximation, is the heat flow from the mantle. Several explanations were offered for the exponential distribution stressing the important role probably played

by fluids released during the cooling of plutons. Albarede (1975) proposed a dissolution-precipitation process, whereas Buntebarth (1976) favored diffusion effects in a migrating fluid phase.

Although the linear heat flow vs. radioactivity relationship was originally established in homogeneous plutons, it is clear now that it has a broader range of validity. The scatter about the relationship is somewhat larger when terrains other than granites are included. The fact remains that data taken on many different geological units can be globally accounted for by a single set of values for Q_r and D . Still, the use of one depth-scale to describe the crust in a large province does not seem very satisfactory. Thus Richardson and Oxburgh (1979) prefer to interpret the England and Wales data as indicating that the radiogenic heat production lies mainly in the upper crust, whose thickness is 16 km on the average. This reasoning leaves open the problem raised by the large variations of D throughout the world. An answer may be simply that the heat flow field is perturbed in many instances. For examples, several authors have recently studied the effects of erosion (Lee, 1979; Woodhouse and Birch, 1980; Clark, 1980; Singh and Negi, 1980; England and Richardson, 1980). They showed that, in transient conditions, erosion acts to reduce the apparent depth-scale D and to augment the background heat flow Q_r . On the other hand, England et al. (1980) considered the effects of radioactivity and conductivity contrasts. They demonstrated that the resulting lateral transfer of heat acts to decrease the apparent depth-scale and to increase the apparent reduced heat flow. These two types of effects must obviously be taken into account. However, most of the known heat flow provinces are old (older than 300 My) and erosion effects may be safely ignored. Also, the consideration of radioactivity

contrasts requires the a priori knowledge of the geometry of the units and, more importantly, of the vertical distribution of radioelements within them. This last piece of information is of course the heart of the matter.

In this chapter, we concentrate on the various mechanisms which are likely to determine or to perturb the distribution of uranium, thorium and potassium in the continental crust. We suggest that it may be possible to discriminate between them using heat flow and radioactivity data. This enables us to better understand the linear relationship. We conclude with a global picture of crustal evolution compatible with the heat flow data.

3.2 THE RELATION BETWEEN HEAT FLOW AND RADIOACTIVITY

The linear relation between heat flow and radiogenic heat production was initially established in New England by Birch et al. (1968). Since then, many studies have shown that this surprisingly simple relationship is not a coincidence and is of broad geological significance. We list in Table 3.1 (see also Figure 3.1) various heat flow provinces and the corresponding parameters Q_r and D . As is always the case with an empirical relationship, care must be taken in the interpretation. Typically, a heat flow versus radioactivity plot shows a majority of data points lying on a straight line defining the two parameters Q_r and D , but also a certain number of points clearly offset from the line. These anomalous points can usually be associated with geological anomalies (see for example, Jessop and Lewis, 1978, and the preceding chapter). When the number of data points is small, the validity of the relationship is doubtful and the errors in Q_r and D large. We have selected what we thought were the most reliable determinations, using a selection criterion based on the number of points which really define the regression line, and on the range of heat generation rates represented. All the information needed for this study can be found

in Table 3.1.

On examining the world-wide data (Table 3.1, Figure 3.1), two simple observations strike one. First, the reduced heat flow values are almost identical for provinces older than 300 My. Such a uniform figure must have a geological significance. Second, the values taken by D exhibit a large scatter. In particular, they differ dramatically in the two Archean Shields, the Western Australian Shield and the Superior Province of Canada. Thus D does not seem representative of the geological setting.

The same heat flow versus radioactivity relationship is observed on practically every terrain in the New Hampshire province. More specifically, the same value of 7.5 km for D fits the data on plutons which experienced totally different conditions. For example, the Exeter pluton was emplaced around 440 My ago (Gaudette et al., 1975) and was later involved in the intense metamorphism and deformation which characterizes the Acadian orogeny. The Bethlehem gneiss was formed just after the climax of the orogeny around 405 My ago (Lyons and Livingston, 1977) and grades smoothly into the surrounding formations. The binary granites at Concord and Fitzwilliam (N.H.) have discordant contacts with the metamorphosed sediments, and correspond to a distinct episode (dated 330-360 My). Finally, the plutons of the White Mountain series appear forcefully intruded and have no genetic relationships with the other units in the region. We have shown that these bodies satisfy the same relationship. This relationship fits data taken in other parts of the United States, as was shown by the data of Roy et al. (1968a) and by an independent survey in Virginia (Costain, 1977). The heat flow province covers basically the whole of the USA west of the Great Plains.

The relationship we seek to explain is therefore of a quite general

character and has a bearing on the structure of the crust as a whole. Instead of trying to model complex processes on such a large scale, it is possible to determine indirectly the vertical distribution of the radiogenic heat production. Lachenbruch (1968; 1970) presented a powerful argument to justify his exponential model. He observed that the linear relationship is certainly not an artifact of the present and must have remained valid through the past. Assuming that D does not vary with time, he showed that the only distribution which allows the linear relationship to hold with arbitrary differential erosion is given by equation (3.1). If one accepts this model, one is thus able to understand why the linear relationship is observed over large areas and why values of the reduced heat flow are similar throughout the world. One must still, however, explain why the crust appears differentiated so highly in Western Australia, and so poorly in England and Wales.

3.3 MECHANISMS FOR THE DISTRIBUTION OF RADIOELEMENTS

Considering the rather wide range of applicability of the heat flow/radioactivity relationship, it seems easier to dismiss specific mechanisms rather than to find a reasonable one which will account for all the observations. For example, hydrothermal circulation is not a good candidate: it can extend to great depths (Ward, 1972), but cannot perturb systematically the distribution of radioelements over a large area. Studies in deep boreholes reveal that hydrothermal leaching and redeposition is confined to a small number of alteration zones of limited extent (Rich et al., 1975; Stuckless et al., 1977). In fact, three basic mechanisms need to be considered. The first involves a melting event, either anatexis or transport of material from the mantle. The second involves water produced by a cooling magma or by metamorphic reactions. The third is alteration due

to groundwater circulation. Each of these processes has a geochemical signature and we expect D to be correlated with suitable indices.

One obvious geochemical index to consider is the Th/U ratio. It is often used as a differentiation index because thorium is a well-known magmatophile element (Rodgers and Adams, 1969). Indeed, there is a rough relationship between D and the mean Th/U ratio for the provinces listed in Table 3.1 (Figure 3.2). The scatter in Th and U data is large and the plot presented can only be considered as an indication of trend. But it is important to realize that there are two "poles" in a heat flow province: a metamorphic pole with a low Th/U ratio and a plutonic pole with a comparatively higher Th/U ratio. Were we to take into account the plutonic data alone, the relationship would be more striking. Nevertheless, the fact remains that the highest value of D, found in England and Wales (Richardson and Oxburgh, 1978) is associated with the lowest Th/U ratio in granites. Similarly, the highest value of the ratio is found in the Western Australian Shield where D is smallest.

This trend has an obvious interpretation, as D reflects the state of differentiation of the crust, but we cannot stop at this point in our reasoning. The general increase of Th/U ratios with differentiation is still the subject of controversy (for a summary, see Rodgers and Adams, 1969). There are large differences between ratios which are observed and ratios which are calculated to account for the Pb isotopic composition. This indicates that the radioelements are redistributed, a fact usually attributed to groundwater alteration (Sinha, 1976).

Potassium concentration is also used as a differentiation index. In ideal situations, uranium, thorium and potassium show exactly parallel trends of enrichment (Burwash and Cavell, 1978). However, in the provinces

considered here, there is no relationship between mean K-concentration and mean Th/U ratio. For example, the lowest Th/U ratio is observed in Cornwall granites which are exceptionally rich in potassium (Tammemagi and Wheildon, 1974). Further, examining again the New England data, we observe that thorium and uranium behave sympathetically whereas potassium does not follow their common trend (Figure 3.3). This indicates that whatever mechanism is responsible for the distribution of uranium and thorium did not affect potassium. This conclusion had already been reached by Ragland, Billings and Adams (1967) and Swanberg (1972) in detailed studies of several plutonic series.

We conclude that, although uranium and thorium are concentrated in plutons with respect to surrounding rocks, their distribution within a particular body is controlled by some process other than liquid/solid fractionation. Following Albarede (1975) and Buntebarth (1976), we suggest the action of aqueous solutions released during cooling and metamorphism. These distributions may then be affected by meteoric water circulation. Low temperature alteration does not have the same effect on the two elements. The frequent agreement of Th/Pb ages with other isotopic ages (for example Rosholt and Bartel, 1969; Reid, 1979) demonstrates that presently observed Th concentrations have been acquired early in the history of the rocks considered and have not been modified since. Alteration is thus likely to remove uranium selectively. It may increase significantly the Th/U ratio and alter the meaning of the trend presented in Figure 3.2.

3.4 DEPTH SCALE ANALYSIS FOR THE RADIOACTIVE ELEMENTS

From the arguments raised in the previous section, we expect potassium, uranium and thorium to record different physico-chemical processes and hence to be distributed in the continental crust with different depth-scales. To set up a framework for the following study, we go backwards a little and present a detailed analysis of the linear relationship, designed so as to identify clearly each assumption and its implications.

Let h be the thickness of the layer containing the bulk of radioactivity. h is the depth down to which U, Th and K concentrations are continuously related to their value at the surface, and below which concentrations are significantly smaller. For all practical purposes, h is smaller than the crustal thickness. We assume quasi steady-state conditions, i.e. heat flow is in secular equilibrium with the heat generated by crustal sources and that supplied from below the crust. Thermal refraction due to contrasts in conductivity and horizontal heat transfer due to contrasts in heat generation are negligible. We further assume that heat transfer is conductive only and integrate the heat flow equation between depths 0 and h :

$$Q(0) = Q(h) + \int_0^h A(z) dz \quad (3.2)$$

Comparing this equation with the linear relationship considered as a mathematical identity, we get:

$$Q(h) - Q_r = D \cdot A(0) - \int_0^h A(z) \cdot dz \quad (3.3)$$

This equation must be verified for any heat flow station in the province or, in other words, for any value of $A(0)$. $Q(h)$, the heat flow at depth h , is determined solely by heat generated at depths greater than h and, by definition of h , does not depend upon the surficial value of A . Thus, the expression on the right hand side of equation (3.3) is a constant which can be set to zero if some heat flow-values are measured very close to Q_r . We now obtain:

$$D \cdot A(0) = \int_0^h A(z) \cdot dz \quad (3.4)$$

and $Q(h) = Q_r \quad (3.5)$

Equation (3.4) may be rewritten as follows:

$$D = \int_0^h \frac{A(z)}{A(0)} \cdot dz \quad (3.6)$$

or again:

$$\frac{D}{h} = \frac{\int_0^h A(z) dz}{h \cdot A(0)} \quad (3.7)$$

Relation (3.7) can be interpreted easily. $h \cdot A(0)$ represents the heat flow contribution of a layer of constant heat generation rate $A(0)$, and D/h is therefore a measure of the departure of $A(z)$ from a constant. A small D/h , for example, would indicate a highly differentiated layer. With additional assumptions, equation (3.7) yields of course both the Roy et al. (1968a) and the Lachenbruch (1968) models.

At this stage, h is undetermined and may even vary over the heat flow

province. It is however the most important parameter for thermal calculations, because it is the depth at which heat flow is equal to Q_r . Detailed seismic scanning of the crust reveals that no single boundary can be traced throughout a region (Smithson, 1978) and thus offers no hope of identifying h . This explains why it is essential to understand the very process of radioelement migration and concentration in order to interpret correctly heat flow and radioactivity data.

Yet, we have not used all the information at our disposal and may proceed a little further in the analysis. Because rocks in a heat flow province belong to distinct series, variations of the heat production rate reflect fundamental differences and cannot be explained solely by changes in the erosion level (Tilling et al., 1970). Thus the regional value of D in relation (3.6) must be an individual property of each rock unit. Furthermore, as Th/U and K/U ratios vary laterally in a heat flow province (see for example the New England data), the same argument implies that each element must be distributed according to the same law. If this is indeed verified, then, although the radioelements have different decay constants, the linear relationship will hold through time, as required for example by Lachenbruch (1968) in his argument. Thus it is a consequence of the above analysis that each radioelement seems to be distributed according to the same law and the same depth-scale.

We have seen that there is no reason to believe that this conclusion is correct. Let $A_U(z)$, $A_T(z)$ and $A_K(z)$ denote the distributions of heat production for each radioelement. We may reexamine the data available and consider a relation of the form:

$$Q(0) = Q_r + D_U \cdot A_U(0) + D_T \cdot A_T(0) + D_K \cdot A_K(0) \quad (3.8)$$

D_U , D_T and D_K are the depth-scale we look for and are defined by the following equation for each element (j):

$$D_j = \int \frac{h C_j(z)}{C_j(0)} \cdot dz \quad (3.9)$$

$C_j(z)$ is of course the concentration of element j at depth z . Knowing the four quantities $Q(0)$, $A_U(0)$, $A_T(0)$ and $A_K(0)$ over several stations in a heat flow province, we may solve for the four parameters (Q_r , D_U , D_T , D_K). Details about the method are given in the Appendix.

3.5 RESULTS

The first province we consider is the Eastern USA heat flow province. Several data sets are at our disposal: that of Roy et al. (1968a) and our own. In the first case, two types of data were treated: one with all three concentrations of uranium, thorium and potassium, and the other with both U and Th concentrations lumped together as "equivalent uranium". In the case of the second type of data, the practical hypothesis which must be made is $D_U = D_T$: the inversion only allows us to separate the depth-scale for potassium from that of uranium and thorium. In the case of the data presented in Chapter One we separated measurements on metasedimentary formations from the rest.

The results are presented in Table 3.2a,b. We first discuss the data from Roy et al. (1968a). In their original work, two points were corrected for contrasts in heat production. These corrections remain controversial but do not change the conclusions (Table 3.2a). The 4-parameter inversion suggests that the three depth-scales D_U , D_T and D_K are different. Looking at the larger data set, and therefore fixing $D_U = D_T$, we find again that the two depth-scales resolved are not equal. The RMS residual in all these

trials is close to the presumed data variance. The uncertainty in D_K is greater than in D_U and D_T , which is not surprising as potassium contributes only about 20% of the total heat generated by radioactive decay in a rock.

The residual decreases as the number of parameters increases, a necessary condition for the procedure to be meaningful (see the Appendix). Also, the reduced data set of 9 values is consistent with the total data set of 12 values used by Roy et al. (1968a).

We give in Table 3.3 the correlation coefficients for the four parameters resolved. The correlation coefficient of D_U and D_T is high, which indicates that the data do not allow a good separation between them. This is not surprising considering the relative homogeneity of Th/U ratios in the province (Figure 3.3). In contrast, potassium shows no correlation with either uranium or thorium, in agreement with a previous discussion. Finally, we observe that Q_r has no correlation with D_U and D_T , an evidence that one can separate the background heat flux from that due to the radioactive decay of uranium and thorium.

We present in Table 3.2b the results for the data sets discussed in the preceding chapter. Consider first the metasedimentary data (Table 3.2b). The four parameter inversion yields a large error in the potassium depth-scale. By adding a damping parameter in the scheme (see Appendix), we verified that the associated eigenvalue is close to zero. This shows that the data do not allow the resolution of this depth-scale or, alternatively, that there is no consistent scale for potassium in the province. The second

hypothesis would strengthen our suggestion that potassium is not distributed by the same mechanism as uranium and thorium. If D_K is taken out of the parameter set, the singularity disappears but there is no loss of information on the remaining parameters (Table 3.2b). The thorium depth-scale is significantly smaller than the uranium depth-scale, the difference being more marked than in the preceding analysis (Table 3.2a). With the whole data set, the same phenomenon occurs for D_K ; which must be taken out of the parameter set. The results for uranium and thorium are strikingly similar to those obtained with the Roy et al. data set. The difference between results on metasedimentary formations and granites may be significant but needs further testing.

The second province is the Western Australian Shield. Heat flow and U, Th and K concentrations at seven sites are taken from Sass and Lachenbruch (1979), Bunker et al. (1975), Lambert and Heier (1967) and Hyndman et al. (1968) (Table 3.4). The four parameter inversion yields again a large error on D_K . The value of D_K is dramatically affected by the introduction of a small damping parameter in the inversion scheme. As before, D_K can be taken out of the parameter set without loss of information (Table 3.4). The thorium depth-scale is small but can be resolved by the data: taking it out of the parameter set leads to a large increase in error (Table 3.4). The striking result here is the large difference between D_U and D_T . Again, a comparison of our reduced data set (row 4, Table 3.4) with the full data set (Table 3.1) shows that the two are consistent.

In the Sierra Nevada, we found 7 stations with all the necessary information in Lachenbruch (1968) and Roy et al. (1968). Other heat flow/heat production pairs have been reported for this province but do not

include the Th, U and K concentrations which are needed. Our results can be found in Table 3.5. The residual is small and the constraints imposed by the data on the various parameters are weak. This may indicate that the data available are not independent. The uranium and potassium depth-scales are quite large, whereas that of thorium is much smaller. Removing the thorium depth-scale from the scheme leads to a marked increase in residual. Our reduced data set is compatible with that of Lachenbruch and Sass (1977).

The final data set comes from the Superior Province of the Canadian Shield. There are fifteen reliable heat flow measurements where radioelement concentrations are known (Jessop and Lewis, 1978). A few more measurements are available (Allis and Garland, 1979) but are not included here because of large errors in radioactivity data. In this province, the scatter about the linear relationship is important. The Th/U ratio is extremely variable, ranging from 0.7 to 16.0 (Jessop and Lewis, 1978), and data points with extreme values of the ratio appear as anomalies in the heat flow versus radioactivity plot. Jessop and Lewis (1978) excluded them from their analysis because they were from apparently thin structures not representative of the whole crust in the region. The data set we used is the same one and our results are given in Table 3.6. The potassium depth-scale is dramatically affected by the introduction of a damping parameter in the inversion scheme. As in previous cases, it may be taken out of the parameter set without loss of information. The errors in the parameters are still large, probably because of the small range of heat production rates in the data set.

3.6 SUMMARY AND INTERPRETATION

In summary, we conclude that the heat flow and radioactivity data do not require that the depth-scales for uranium, thorium and potassium be identical. Moreover, our analysis has revealed some interesting features. We summarize our results in Table 3.7 for clarity. With the exception of the Canadian Shield, D_U always appears larger than D_T (which takes very small values in two cases). D_K appears larger than the other two depth-scales in the two young provinces and is unresolved in the two Archean Shields.

Independent support for our numerical results comes from studies made in deep boreholes. Lachenbruch and Bunker (1975) analyzed data from a total of eight wells and saw no relation between potassium and the two other radioelements. Further, in four boreholes drilled in the Sierra Nevada, they found small depth-scales of 1-2 km for the vertical distribution of thorium. Hyndman et al. (1968) reported detailed measurements in a 300 m deep well in the Western Australian Shield, and their data give evidence of a sharp decrease in Th concentration with depth.

The systematic difference between D_U and D_T provides an explanation for the trend shown in Figure 3.2. Consider the parameter D , determined from the heat flow versus total radioactivity analysis: it is some weighted average of the three depth-scales D_U , D_T and D_K . If D_T is always smaller than D_U , we expect D to be smaller in provinces with a high Th/U ratio than in provinces with low Th/U ratios. This is only a partial explanation as there is also a variation of the depth-scales absolute values from province to province. For example, the highest value of D_T is found in the Canadian Shield which has low Th/U ratios, whereas a very low value is found in the Western Australian Shield where Th/U ratios are high on the average.

Because there are only a few measurements available in each province we studied, the errors on D_U , D_T and D_K are large and do not allow definitive statements regarding their respective values. More and better data are required. Only in the Western Australian Shield case can it be considered proven that D_U and D_T are not equal. We note however that the three depth-scales appear to be arranged in a systematic order in the four cases analyzed and that this accounts for the global D vs. Th/U trend of Figure 3.2.

We now return to our discussion on the various mechanisms likely to affect the distribution of radioelements. We momentarily set aside the case of potassium. We suggest that, within the limits of our large-scale analysis, the present distribution of uranium and thorium can be represented as some initial distribution modified either by water circulation during erosion/uplift or by quasi-permanent groundwater movements. The model is attractive because it would explain why the "bulk" parameter D holds over large areas but varies from one part of the world to another: the chemistry and dissolving power of meteoric waters are essentially a function of the climate and therefore of the latitude (Corbel, 1959).

A qualitative description is the following. As the surface layer of the crust is altered, some amount of uranium and thorium is leached and taken up in the circulation system. The control of the water chemistry takes place below the soil zone, the main process being the slight alteration of large volumes of rocks (Miller and Drever, 1977). Erosion and uplift have a dominant influence and uranium losses can be dated from a specific event (Rosholt et al., 1973; Ludwig and Stuckless, 1978). In contrast with hydrothermal activity, these low temperature effects are slow

and operate over several millions of years (Zielinski, 1978). Some amounts of uranium are eventually redeposited (Stuckless et al., 1978; Barbier, 1974; Wilson, 1977). The exact mechanism is not well defined but probably involves:

- precipitation in fractures and defect structures, usually together with Fe, Ti and Mn oxides (Barbier, 1974; Wilson, 1977);
- adsorption (Ranchin, 1968; Szalay and Samsoni, 1970).

These redistribution effects can be active over large depth ranges. In some cases, weathering has been observed down to depths of 1.5 km (Ollier, 1969, p. 121) and both seismic and microcrack studies indicate that there are non-negligible amounts of water in the first 2 or 3 km of the crust (Feves et al., 1977).

The model we propose involves a number of processes which are hard to describe quantitatively but we show next that it allows a straightforward interpretation of our results. In a sample presently recovered at the surface, the concentration in thorium or uranium can be written as follows:

$$C(0) = C_a(0) + C_i(0) - C_l(0) \quad (3.10)$$

where C_a is the concentration which has been added, C_i the original concentration present in the rock before alteration and C_l the concentration which has been leached and removed. The total amount of each radioelement in the crust is thus:

$$\int_0^h C \cdot dz = \int_0^{h_1} C_a \cdot dz + \int_0^{h_1} (C_i - C_l) \cdot dz + \int_{h_1}^h C_i \cdot dz \quad (3.11)$$

where h_1 is the depth of alteration. Taking this expression, we may divide both sides by $C(0)$ and obtain:

$$D = \int_0^h \frac{C}{C(0)} dz = \int_0^h \frac{C_i}{C(0)} dz + \int_0^{h_1} \frac{C_a - C_1}{C(0)} dz \quad (3.12)$$

In the case of superficial alteration, h_1 is small compared to h and we may write as a first approximation:

$$D \approx \int_0^h \frac{C_i}{C(0)} dz \quad (3.13)$$

or:

$$D \approx \frac{C_i(0)}{C(0)} \cdot \int_0^h \frac{C_i}{C_i(0)} dz \approx \frac{C_i(0)}{C(0)} \cdot D_i \quad (3.14)$$

where D_i is the length scale for the unperturbed distribution. Equation (3.14) is easy to understand. For example, let us assume that there has been a loss of the radioelement considered. The present concentration is therefore smaller than the original one, and it takes a greater thickness of depleted rock to account for the observed heat flow: the depth-scale obtained is larger than D_i . If, on the contrary, we assume that there has been mostly deposition surface concentrations are overestimated with respect to those at depth and it takes smaller thicknesses of those enriched rocks to account for the observed heat flow. Accordingly, we may interpret the results of Table 3.7 as indicating that uranium is more easily leached than thorium, in accordance with the known geochemistry of the two elements.

If the above concepts are correct, a comparison of D_U and D_T should

permit, through equation (3.14), an estimate of uranium loss due to alteration in a province. For example, the analysis of our results suggests major uranium losses in the Western Australian Shield. These are confirmed by lead isotope studies (Oversby, 1975, 1976) which show that, in certain places, up to 80% of the uranium has been removed.

We propose a general model of the crust as follows. First, during the initial formation of crustal material, the radioelements are concentrated towards the surface and the crust acquires a primary and gross vertical zoning. The corresponding depth-scale is given by D_K . Subsequently, the cooling material interacts with magmatic and metamorphic fluids which redistribute uranium and thorium (for example, see the model of Albarede, 1975). The depth-scale for this process is given by D_T because thorium then becomes immobile. Finally, the upper crustal layers are subjected to low temperature alteration which is somehow recorded by uranium. Therefore D_T is smaller than D_K because magmatic or metamorphic fluid flow follows primary differentiation, and is smaller than D_U because alteration has removed some amount of uranium near the surface. Although a given crustal segment probably experiences several melting and reworking events, the basic features of the model should remain preserved. The model is illustrated schematically in Figure 3.6, together with the corresponding distributions of U, Th and K. Their exact form remains undetermined, although the argument of Lachenbruch (1968, 1970) can be applied to the individual distributions of thorium and potassium. The case of uranium is more complicated because of the effects of alteration.

The sequence of events we have described above may be somewhat artificial in the sense that primary differentiation and interactions with magmatic or metamorphic fluids may occur simultaneously. Differences in

partition coefficients and solubilities could result in a variation of the characteristic depth scale among radioelements. However, alteration must be considered separately and has most probably a measurable effect on the apparent depth-scale of uranium in cases where the Th/U ratio is anomalously high.

The disparate results obtained in the two Archean provinces are worthy of some discussion. In both cases, it is impossible to resolve the potassium depth-scale. The two provinces are old and deeply eroded, and the result is hardly surprising as it is well-known that the lower crust is depleted in that element (for a summary, see (Heier and Billings, 1970)). The same agreement is not found for uranium and thorium, whose depth-scales are not consistent (Table 3.7). This apparent discrepancy arises because different geological terrains have been sampled in the two shields. In the Canadian Shield, the areas studied are low in both potassium and Th/U ratio, whereas the Western Australia Shield samples have higher potassium contents and generally high Th/U ratios (Figure 3.5). These represent mostly late and quite thin K-rich granites (Glikson and Lambert, 1976). The same type of plutons also exists in the superior Province of the Canadian Shield (points 1, 2, 3, Figure 3.5) but were not included in their analysis by Jessop and Lewis (1978) because they fell far from the main data set. These units are apparently more widespread in Western Australia and probably indicate a peculiar style of erosion. Geophysical and geological data indicate that the Yilgarn craton experienced an eastward tilt which allowed the preservation of lower grade rocks in its eastern part (Glikson and Lambert, 1976).

We also note that the average level of radioactivity is higher in Australia than in other parts of the world which have similar ages. This

can be shown by comparing U, Th and K concentrations but also, more demonstrably, by means of an average heat generation rate defined as follows in a heat flow province:

$$\bar{A} = \frac{\bar{Q} - Q_r}{D} \quad (3.15)$$

where \bar{Q} is the mean heat flow. Excepting the Australian provinces, the data show that the average radioactivity is lowest in the oldest provinces (Figure 3.6). This can be attributed partly to erosion. The Australian points are not compatible with the others, which suggests again some anomaly in the nature of erosion over this continent. The above discussion illustrates how important it is to consider the geological information when interpreting heat flow and radioactivity data.

3.7 CONCLUSIONS

We have shown in this paper that there is no reason to believe that the distributions of uranium, thorium and potassium in the continental crust are identical. On the contrary, they seem to differ in a systematic way from province to province. We suggest that this new information yields important clues for the various mechanism which determine these distributions. We have proposed a model which stresses the importance of interactions with magmatic and metamorphic fluids, and meteoric water. We have also shown that most of the observed variations of parameter D can be explained by shallow effects.

The reasonable success of our analysis suggests that it is profitable to examine the variations of heat flow and of each radioelement. In all future studies, care should be taken to measure the U, Th and K concentrations individually. These, when compared with heat flow data,

have shown the major uranium loss experienced by the Western Australian Shield, and may prove useful elsewhere to determine the extent of uranium leaching and hence to provide an estimate of the uranium "potential" of an area.

Finally, we point out that, of the four parameters considered in this study, Q_r is such that its value is least affected by the several hypotheses tried out because it is poorly correlated with the other three. This enhances the validity of the concept of reduced heat flow. It should also be noted that the value of Q_r in the Canadian Shield must be raised by about 10% when allowance is made for different distributions of uranium, thorium and potassium. Considerations about "absolute" values of the reduced heat flow should therefore be made with care.

TABLE 3.1
PARAMETERS FOR SEVERAL HEAT FLOW PROVINCES

Province	Age (M.y.)	\bar{Q}	Q_r	D	Average Th/U ratio	References
SN Sierra Nevada (N. America)	125-0	37 (13)	18 (3)	10.1 (0.1)	3.1 (0.7)	Roy et al. (1968a) Lachenbruch and Sass (1977)
EUS Eastern USA (N. America)	400-100	57 (170)	33 (4)	7.5 (0.2)	4.2 (1.1)	Roy et al. (1968a)
EW England and Wales (Eurasia)	600-300	59 (23)	23 (3)	16.0 (1.6)	1.5 ⁺	Richardson and Oxburgh (1978)
CAS Central Australian Shield (Australia)	2000-900	83 (21)	27 (6)	11.1 (2.0)	4.6 (2.0)	Sass and Lachenbruch (1979) Bunker et al. (1975)
BS Baltic Shield (Eurasia)	2000-900	36 (8)	22 (6)	8.5 (0.4)	5.1 (1.4)	Swanberg et al. (1974)
US Ukrainian Shield (Eurasia)	2600-600	37	25	7.1	-	Kutas (1977)
CS Superior Province of the Canadian Shield (N. America)	3400-2400	34 (8)	21 (1)	14.4 (0.5)	3.3 (1.1)	Jessop and Lewis (1978)
WAS Western Australian Shield (Australia)	3400-2400	39 (8)	26 (6)	4.5 (1.0)	6.7 ⁺⁺ (1.7)	Sass and Lachenbruch (1977) Lambert and Heier (1967)

Q and Q_r are the mean and reduced heat flow, in mW/m^2 . D is the length-scale from relationship (1), in km. Error estimates (1 standard deviation) are in parentheses.

⁺The Th/U ratio corresponds to only three heat flow stations in granites, studied by Tammemagi & Wheildon (1974) and Tammemagi & Smith (1975). This low value is representative of the whole SW England area (Tammemagi and Smith, 1975).

⁺⁺The Th/U ratio is taken from Lambert & Heier (1967), and is the mean value for all granites in Western Australia.

TABLE 3.2a

THE EASTERN USA HEAT FLOW PROVINCE: DATA FROM ROY ET AL. (1968A)

Method	N*	Q_r (mW/m ²)	D_U (km)	D_T (km)	D_K (km)	RMS residual (mW/m ²)
Least-squares (2 uncorrected)	9	34±2	8.6±1.5	4.0±2.0	16.4±5.7	3.2
Least-squares	9	34±2	8.9±2.0	5.5±2.0	12.5±6.3	2.0
Least-squares with $D_U = D_T$	9	34±2		7.2±0.3	11.7±6.3	2.1
Least-squares with $D_U = D_T$	12	32±2		7.3±0.3	14.5±5.5	2.2
Least-squares with $D_U = D_T = D_K$	9	34±1		7.3±0.2		2.2

*N is the number of data points used in the inversion

The error estimates indicated correspond to 1 standard deviation.

TABLE 3.2b

THE EASTERN USA HEAT FLOW PROVINCE: DATA FROM NEW HAMPSHIRE

Method	N	Q_r	D_U	D_T	D_K	RMS residual
METASEDIMENTARY						
Least Squares	14	38 ± 5	12.1 ± 4.1	3.3 ± 4.5	-23.2 ± 37.8	4.1
K taken out						
Least Squares	14	36 ± 3	10.1 ± 2.4	2.2 ± 4.1	/	4.1
ALL DATA						
Least Squares	21	37 ± 4	8.7 ± 2.6	5.6 ± 2.9	-8.8 ± 23.3	4.8
K taken out						
Least Squares	21	36 ± 3	8.1 ± 1.9	5.1 ± 2.6	/	4.8

TABLE 3.3

CORRELATION COEFFICIENTS FOR THE EASTERN U.S.A CASE

	Q_r	D_U	D_T	D_K
Q_r	1	+0.01	-0.03	-0.75
D_U		1	-0.97	-0.08
D_T			1	1
D_K				

TABLE 3.4

THE WESTERN AUSTRALIAN SHIELD HEAT FLOW PROVINCE

Method	N	Q_r (mW/m ²)	D_U (km)	D_T (km)	D_K (km)	RMS residual (mW/m ²)
Least-squares	7	27±5	11.4±5.5	-2.2±3.7	13.3±21.0	3.2
K Taken out of scheme						
Least-squares	7	30±1	7.2±1.0	0.9±0.4	/	2.9
Th taken out of scheme						
Least-squares	7	29±3	8.2±1.2	/	3.9±13.9	3.3
Least-squares with						
$D_U = D_T = D_K$	7	30±1			2.6±0.3	3.1

TABLE 3.5

THE SIERRA NEVADA HEAT FLOW PROVINCE

Method	N	Q_r	D_U	D_T	D_K	RMS residual
Least-squares	7	15 ± 2	17.9 ± 7.3	0.2 ± 9.5	21.6 ± 13.4	0.7
Th out of scheme						
Least-squares	7	14 ± 2	15.3 ± 3.5	/	43.7 ± 23.7	1.1
Least-squares with						
$D_U = D_T = D_K$	7	16 ± 1		10.3 ± 0.7		1.1

TABLE 3.6

THE SUPERIOR PROVINCE OF THE CANADIAN SHIELD

Method	N	Q_r	D_U	D_T	D_K	RMS residual
Least-squares	12	24 ± 2	24.1 ± 12.8	17.1 ± 10.3	-23.6 ± 18.5	2.8
K taken out of inversion scheme						
Least-squares	12	23 ± 2	16.9 ± 11.0	18.4 ± 10.3	/	3.0
Least-squares with	12	21 ± 1		14.7 ± 1.1		3.1
$D_U = D_T = D_K$						

TABLE 3.7
SUMMARY OF RESULTS

Province	Q_r (mW/m ²)	D_U (km)	D_T (km)	D_K (km)
Sierra Nevada	14 ± 2	15.3 ± 3.5	0.2 ± 9.5	21.6 ± 13.4
Eastern USA				
Plutons	34 ± 2	8.6 ± 1.5	4.0 ± 2.0	16.4 ± 5.7
Metased.	36 ± 3	10.1 ± 2.4	2.2 ± 4.1	/
Western Australia	29 ± 2	7.2 ± 1.0	0.9 ± 0.4	/
Canadian Shield	23 ± 2	16.9 ± 11.0	18.4 ± 10.3	/

A bar indicates that the depth-scale is not resolved by the data and has been taken out of the parameter set.

FIGURE CAPTIONS

Figure 3.1. Values of the reduced heat flow Q_R in mW/m^2 (top value) and of depth-scale D in km (lower value) for the last flow provinces of the world. Shaded areas are Archean Shields.

Figure 3.2. Depth scale D as a function of mean Th/U ratio for all heat flow provinces. Vertical and horizontal bars represent error estimates. There are not enough detailed data for the England and Wales province to allow the calculation of errors.

Figure 3.3. Thorium versus uranium, and potassium versus uranium for the plutons of New England (data from Roy et al., 1968a).

Figure 3.4a. Schematic representation of the various processes controlling the distribution of radioelements in the continental crust.

3.4b. Possible vertical distributions of U, Th, and K. The potassium distribution is uncertain because it is poorly constrained by heat flow data. There is practically no information concerning the lower crust. Note the distribution of uranium in the superficial altered zone.

Figure. 3.5. Th/U ratio as a function of K concentration in the Canadian and Western Australian Shields (data from Jessop and Lewis, 1978; Bunker et al., 1975; Lambert and Heier, 1967; Hyndman et al., 1968). Points 1, 2 and 3 in the Canadian Shield are considered as anomalous (see text). Note that in the Western Australian Shield a majority of data points have Th/U ratios greater than 5.

Figure 3.6. Mean heat generation rate as a function of age for the heat flow provinces of Table 3.1 (Symbols are explained in Table 3.1).

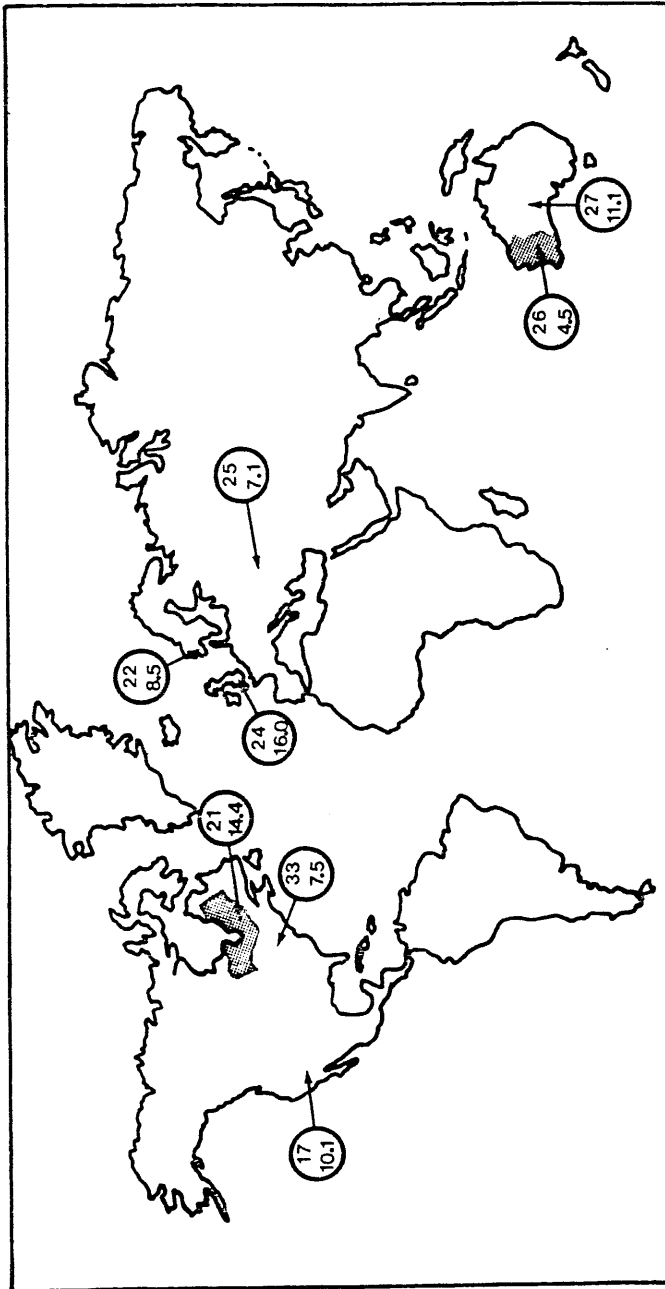


Fig. 3.1

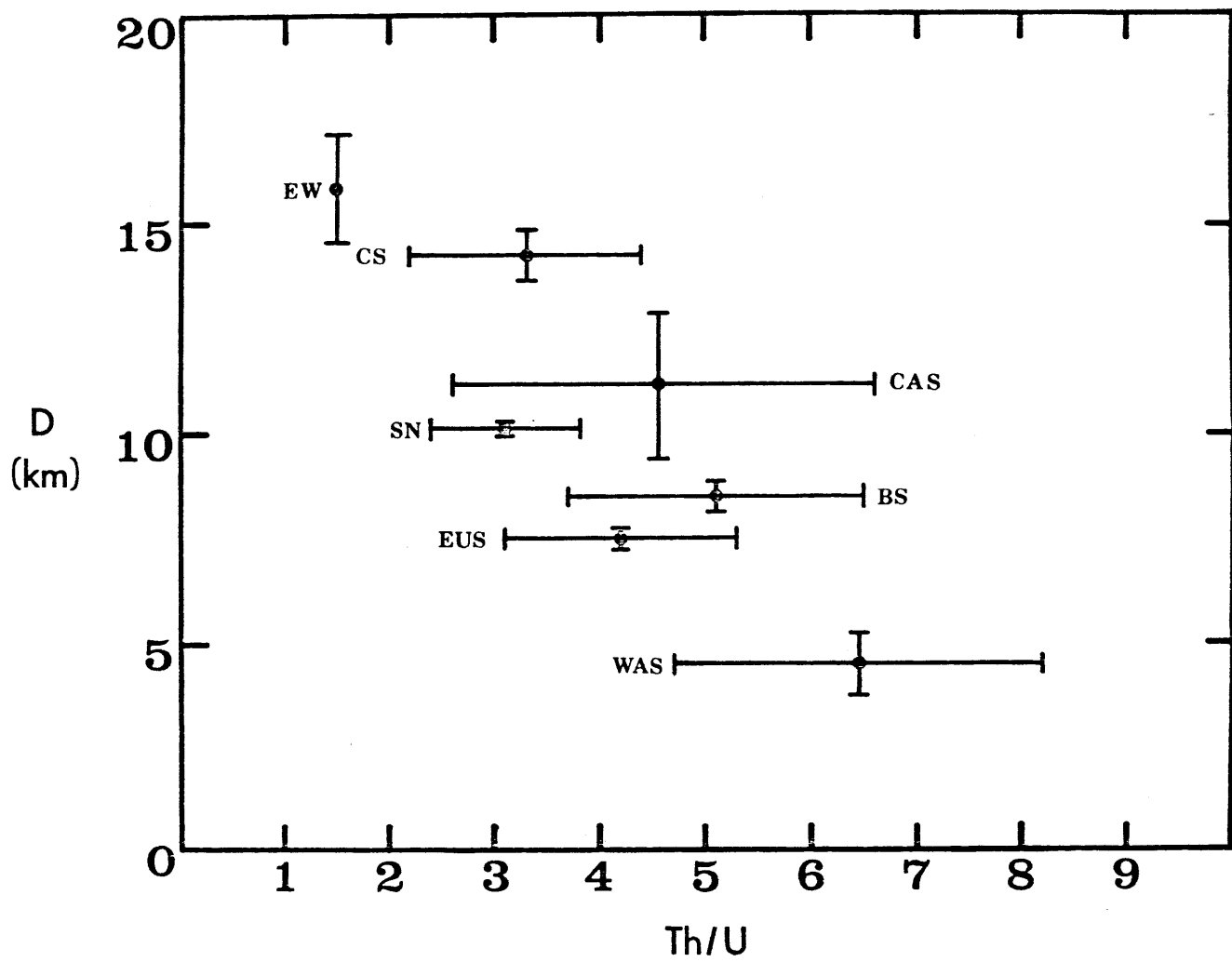
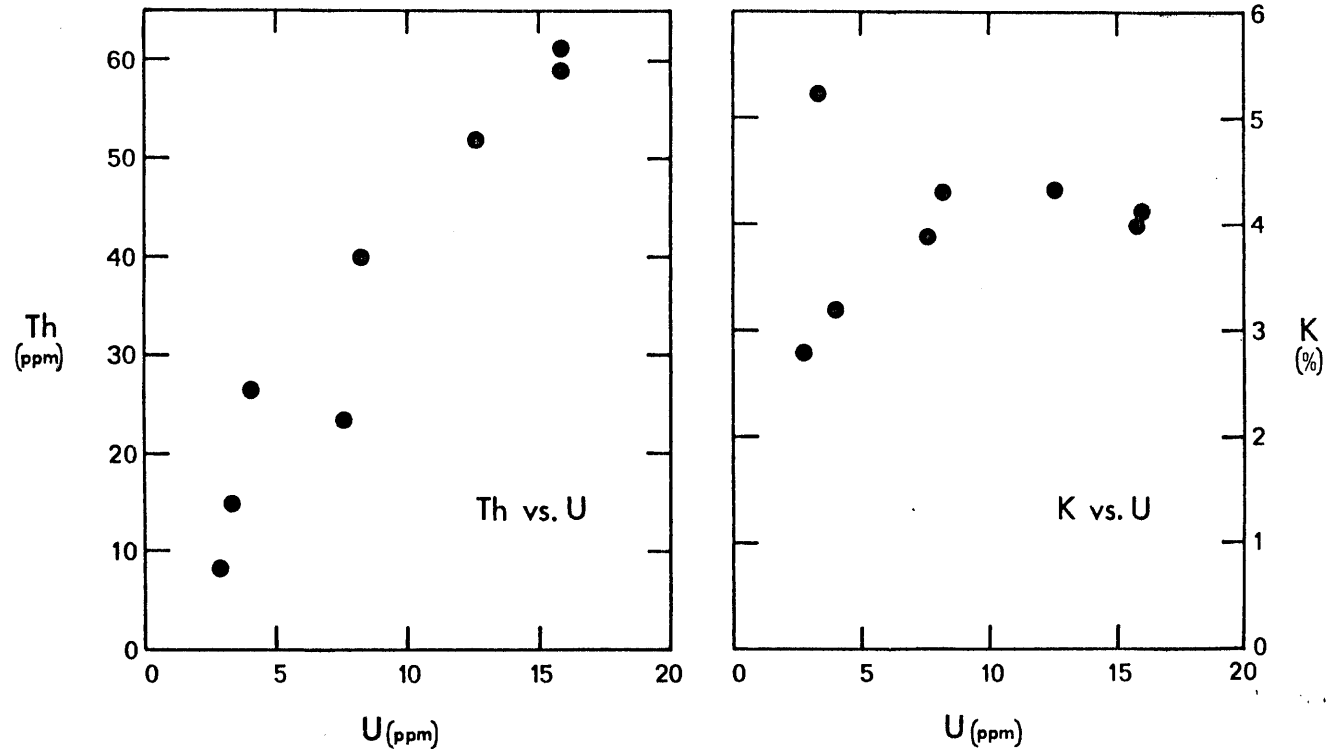


Fig. 3.2

Fig. 3.3



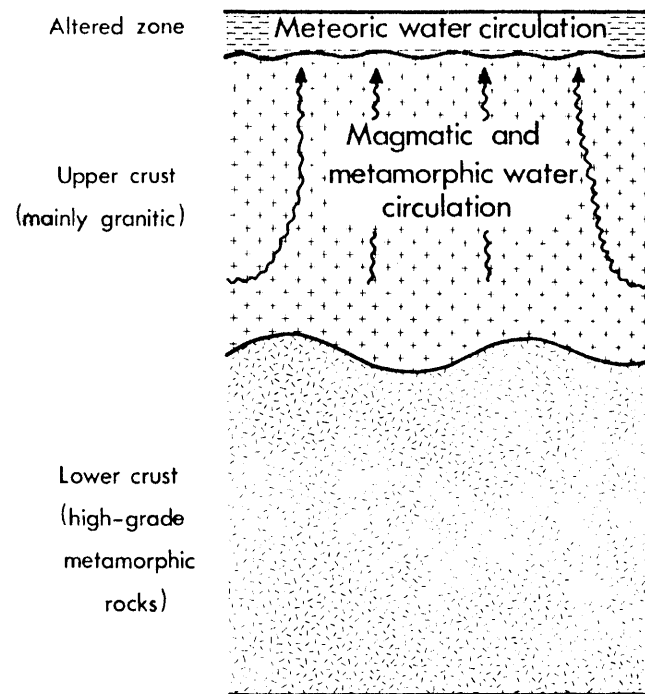


Fig. 3.4a

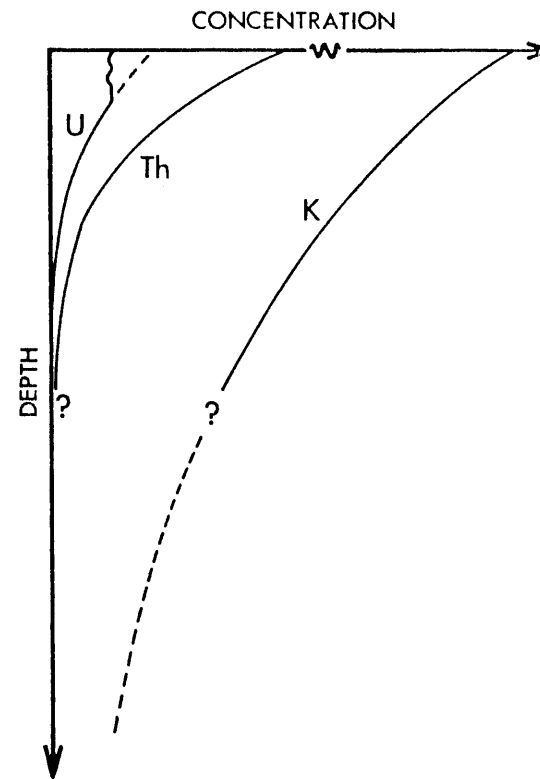
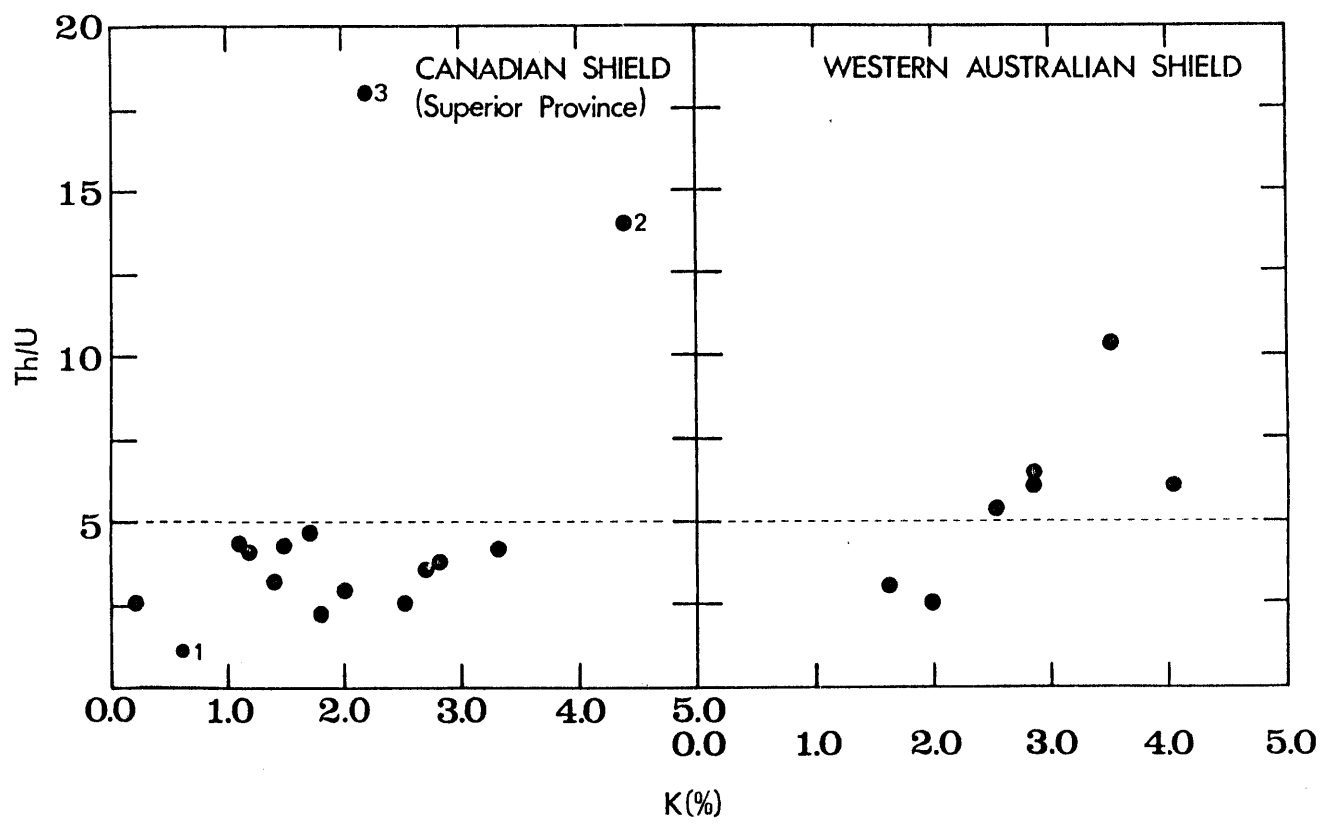


Fig. 3.4b

Fig. 3.5



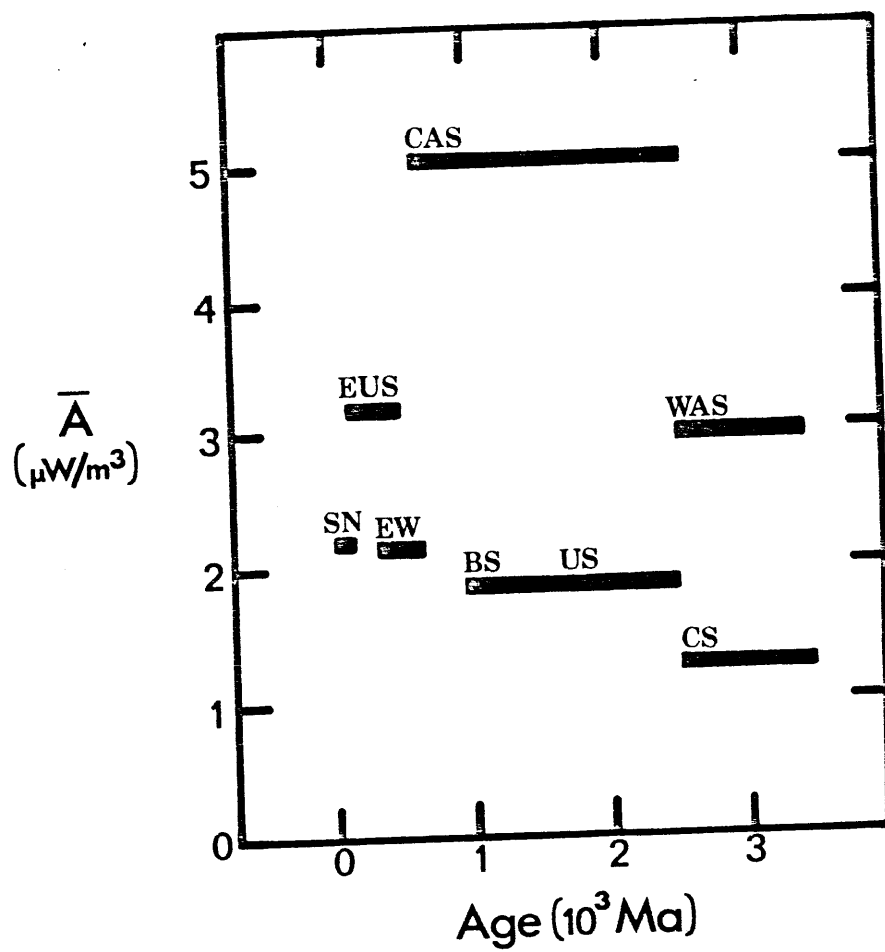


Fig. 3.6

APPENDIX: THE INVERSE PROBLEM

Heat flow and radiogenic heat production are characteristically inaccurate variables with errors inherent in the measuring techniques and in the sampling. The data sets are not of constant quality and may not contain the information requested. To treat such a typical geophysical inverse problem, we have followed the usual procedure. The problem is set up in matrix form as follows:

$$Q = A \cdot P \quad (3.A1)$$

where Q is a $n \times 1$ column matrix containing the heat flow values, and P is a 4×1 column matrix containing the unknowns:

$$\tilde{P} = (Q_r, D_U, D_T, D_K) \quad (3.A2)$$

The coefficients of matrix A are measured quantities and an exhaustive study would require the consideration of the statistical characteristics of each one. Measurements of U , Th and K concentrations vary greatly in character and accuracy. For example, they may be obtained from a set of rock samples collected at the surface, or from certain parts of a cored sample. A detailed data analysis would be space-consuming and out of the scope of this introductory paper.

We use a least square method which minimizes errors on the observed heat flow. This yields the following solution:

$$P_{LS} = (A \cdot A)^{-1} A \cdot Q \quad (3.A3)$$

The parameters have the covariance matrix C:

$$C = \sigma_{\alpha}^2 \cdot (\tilde{A} \cdot \tilde{A})^{-1} \cdot \tilde{A} \cdot Q \quad (3.A4)$$

where σ_{α}^2 is the data variance. We take a value of 2.0 (mW/m²) throughout the following. This figure is reasonable for heat flow measurements and is consistent with the data we had at our disposal, being comparable with the RMS residuals found. For our own data set, we took a higher value of 6 mW/m² which is more appropriate for our type of measurement technique.

The least-squares approach may fail for different reasons:

- first, there may not be a unique solution to the problem. This will usually happen because one of the parameters is badly resolved by the data: D_K in this study (because potassium only accounts for less than 20% of the heat generated by radioactive decay in the crust). To check that potassium was really responsible for the non-uniqueness of the solution, we used the "damped" least-squares technique which yields the following solution:

$$P_{DLS} = (\tilde{A} \cdot \tilde{A} + \varepsilon^2 \cdot I)^{-1} \cdot \tilde{A} \cdot Q \quad (3.A5)$$

This method allows us to estimate which eigenvalue is close to zero as the addition of a small damping parameter (ε^2) will change significantly the corresponding eigenvector. If this was the case, we simply took the relevant depth-scale out of the set of parameters. This procedure is justified in the sense that no error is propagated on the two other depth-scales because they are independent. The potassium contribution is then included in the reduced heat flow.

- second, the least-squares solution may fit the data better or worse than it should. In this case, it is difficult to estimate the constraints placed on the model parameters. Let E_{LS} denote the root-mean-square of the residuals and m the number of parameters to be estimated from n observations. $(n-m)$ is thus the degree of redundancy. A criterion to be verified is:

$$E_{LS} \approx \sqrt{\frac{n-m}{n}} \cdot \sigma_{\alpha} \quad (3.A6)$$

If (3.A6) is not verified, the results cannot be used, either because the available data are not truly independent or because the model does not agree with the observations.

In any case, (3.A6) provides a check on the consistency of the method as it indicates how E_{LS} must vary when m , the number of parameters to be found, is changed.

CHAPTER FOUR

A STUDY OF CONVECTIVE INSTABILITIES IN A VARIABLE VISCOSITY FLUID COOLED
FROM ABOVE: THE CASE OF THE MANTLE BENEATH OCEANS

4.1 INTRODUCTION

The study of convective instabilities in a fluid subjected to transient thermal conditions is of considerable interest in geophysics and geology. Examples where the problem is directly raised include cooling magma chambers and the upper mantle beneath oceans. The latter has been the cause of many discussions in the recent past because of its obvious importance regarding the temperature structure at depth in the Earth (see for example Sclater et al., 1980).

A number of laboratory experiments have been made concerning the onset of instabilities in the particular case of transient cooling from above or heating from below. The earliest was probably that of Thomson (1882), which was in fact the first scientific account of convective motions in a fluid. Much later, Spangenberg and Rowland (1961), Foster (1965a), Elder (1968), Blair and Quinn (1969), Whitehead and Chen (1970) and Sparrow, Husar and Goldstein (1970) published detailed accounts of the appearance and the form taken by the instability. These authors showed that convection occurs initially as the breakdown of a thermal boundary layer, characterized by the release of buoyant "jets" and "thermals". Blair and Quinn (1969) and Sparrow et al. (1970) also observed that the onset of convection could be determined as the time at which a Rayleigh number defined locally (using the thermal boundary layer thickness as a length-scale) exceeds a critical value, in agreement with ideas put forward

by Howard (1966).

Theoretical studies of the same problem belong to two categories: quasi-static analyses and transient analyses. Quasi-static or "frozen time" analyses (Morton, 1957; Lick, 1965; Currie, 1967; Nield, 1975) consider the intrinsic stability of specific density profiles under the assumption that the growth rate of disturbances is large compared to that of the mean temperature. On the contrary, transient analyses take into account the time-dependent terms explicitly. Following the initial approach of Foster (1965b), these were developed by Robinson (1967), Malher et al. (1968), Foster (1968) and Gresho and Sani (1971). The most detailed study is that of Elder (1968) who used a slightly different method and who concentrated on the physics of the instability. For large times, the frozen-time analysis is valid and compares well with transient analyses (Gresho and Sani, 1971). However, the onset of instability occurs before the quasi-static approximation begins to apply (Gresho and Sani, 1971). The results of transient analysis agree with laboratory observations (Foster, 1965a; Blair and Quinn, 1969). Although these studies provide a basic insight into the physics of instability phenomena, they must be adapted with caution to geological problems because of the large variations of viscosity involved.

The particular model which prompted this work was proposed by Parsons and McKenzie (1978) when they studied the evolution of the oceanic mantle. The basic concept is illustrated in Figure 4.1. Hot material is intruded at a spreading center and cools as the plate moves away from the ridge. A one-dimensional conductive solution of the heat equation in a semi-infinite fluid gives predictions which match both the bathymetry and the reliable heat flow data up to an age of about 70 Ma (Parsons and Sclater, 1977). At

that age, the depth vs. age relationship indicates a supply of heat at some depth. This provided one of the justifications for the widely used plate model of the oceans where the bottom of the plate is at a fixed temperature. Because they felt that this bottom boundary condition was somewhat artificial, Parsons and McKenzie (1978) suggested that the temperature structure was not stable and that the age of 70 Ma marked the onset of convective instabilities in the upper mantle. Convective overturn then essentially maintains the plate lower boundary at a constant temperature. The argument of Parsons and McKenzie (1978) was based on an idealized representation of the problem (see Figure 4.1) but was in reasonable agreement with the known properties of the mantle.

This reasoning was criticized by Yuen et al. (1981), who argued that the rheology of mantle material was not modelled in a realistic way. They suggested instead that the upper mantle structure is stable for all ages smaller than 200 Ma if the mantle viscosity is around 10^{17} m²/s, the value determined from post-glacial uplift data by Cathles (1975) and Peltier and Andrews (1976). Their conclusions remain doubtful because they ignored time-dependent effects. We will show in this paper that these totally control the form and the type of instabilities which develop. Because the detailed viscosity profile of the upper mantle beneath oceans remains poorly constrained, we prefer to concentrate on the basic phenomena involved and to evaluate precisely the constraints imposed by the hypothesis of Parsons and McKenzie (1978).

In this paper, we take an alternative approach to the same problem, in which we concentrate on a parametric study in order to understand the effects of various quantities which remain poorly determined. We hope to provide a set of results for a simple experiment which may be useful for

studies of convection in variable viscosity fluids. We consider a fluid whose viscosity varies with depth only, this being a reasonable approximation for a stability analysis of a 1-D conductive temperature profile. The first section is devoted to the method of solution employed. The second section contains results obtained in the limiting case of constant viscosity. In the third section, we present our analysis of the variable viscosity case. Finally, we discuss the implications of our findings for the structure of the upper mantle beneath oceans.

4.2 MATHEMATICAL FORMULATION

We consider an incompressible fluid which is initially at rest at a uniform temperature ΔT . At time $t=0$, the upper surface temperature is fixed at 0 and is maintained at that value. We study the evolution of temperature and velocity perturbations until the onset of instability.

4.2.1 Basic equations

We restrict our analysis to two dimensional perturbations. The z -axis is vertical and oriented positively in the downward direction (see Figure 4.2 for a sketch of the system considered). The equations of motion are, in the Boussinesq approximation:

$$\nabla \cdot \underline{u} = 0 \quad (4.1a)$$

$$\frac{\partial \underline{u}}{\partial t} + (\underline{u} \cdot \nabla) \underline{u} = - \frac{1}{P} \nabla P - \nabla \sigma - \alpha \rho T \underline{g} \quad (4.1b)$$

where \underline{u} is the 2-D velocity vector with components (u, w) , ν is the viscous stress tensor and P a modified pressure. \underline{g} denotes the acceleration of gravity, α the coefficient of thermal expansion and ρ is the fluid density at the reference temperature $T = 0$. The fluid is Newtonian with a

viscosity ν . The heat equation is:

$$\frac{\partial T}{\partial t} + (\underline{u} \cdot \nabla) T = \kappa \nabla^2 T \quad (4.2)$$

where T is temperature and κ thermal diffusivity.

In cases of geological interest, viscosity is not constant and depends strongly on temperature. Temperature may be written as the sum of its horizontal mean \bar{T} and a fluctuating part θ (the perturbation):

$$T = \bar{T}(z,t) + \theta(x,z,t) \quad (4.3)$$

with $\bar{\theta} = 0$, where the overbar indicates a horizontal average. Viscosity may thus be approximated to the first order in the perturbation amplitude by a function of depth and time:

$$\nu(T) \approx \nu(\bar{T}) = \nu(z,t) \quad (4.4)$$

In this paper, we consider a depth-dependent viscosity. The equations for the perturbation velocities are then, to the second order in the perturbation amplitude:

$$\nabla \cdot \underline{u} = 0 \quad (4.5a)$$

$$-\frac{1}{\rho} \nabla P^2 + \nu \nabla^2 \underline{u} + \frac{d\nu}{dz} \cdot \underline{Lu} - \alpha g \theta = \frac{\partial \underline{u}}{\partial t} \quad (4.5b)$$

$$\underline{Lu} = \left(\frac{\partial u}{\partial z} + \frac{\partial w}{\partial x}, 2 \frac{\partial w}{\partial z} \right) \quad (4.5c)$$

The heat equation (4.2) may be averaged horizontally and separated into:

$$\frac{\partial \bar{T}}{\partial t} + \frac{\partial \bar{w}\theta}{\partial z} = \kappa \frac{\partial^2 \bar{T}}{\partial z^2} \quad (4.6a)$$

$$\frac{\partial \theta}{\partial t} + w \frac{\partial \bar{T}}{\partial z} + \underline{u} \nabla \cdot \theta - \frac{\partial \bar{w}\theta}{\partial z} = \kappa \nabla^2 \theta \quad (4.6b)$$

These may be simplified by neglecting higher-order terms:

$$\frac{\partial \bar{T}}{\partial t} = \kappa \frac{\partial^2 \bar{T}}{\partial z^2} \quad (4.7a)$$

$$\frac{\partial \theta}{\partial t} = \kappa \nabla^2 \theta - w \frac{\partial \bar{T}}{\partial z} \quad (4.7b)$$

We non-dimensionalize equations (4.5) and (4.7) using the following scales:

$$(x, z) = (x', z') \cdot d \quad (4.8a)$$

$$t = t' \frac{d^2}{\kappa} \quad (4.8b)$$

$$(\bar{T}, \theta) = (\bar{T}', \theta') \Delta T \quad (4.8c)$$

$$v = v' \cdot \nu(d) \quad (4.8d)$$

In equation (4.8a), we have normalized the viscosities with respect to the viscosity at the bottom. Dropping the primes, we obtain the following equations:

$$\nabla \cdot \underline{u} = 0 \quad (4.9a)$$

$$\frac{1}{Pr} \frac{\partial \underline{u}}{\partial t} = -\nabla P + \nu \nabla^2 \underline{u} + \frac{d\nu}{dz} L \underline{u} - R\theta \quad (4.9b)$$

$$\frac{\partial \bar{T}}{\partial t} = \frac{\partial^2 \bar{T}}{\partial z^2} \quad (4.9c)$$

$$\frac{\partial \theta}{\partial t} = \nabla^2 \theta - w \frac{\partial \bar{T}}{\partial z} \quad (4.9d)$$

where Pr and R are Prandtl and Rayleigh numbers based on the value of viscosity at the bottom of the fluid:

$$Pr = \frac{\nu(1)}{\kappa} \quad (4.10a)$$

$$R = \frac{g\alpha\Delta T d^3}{\kappa\nu(1)} \quad (4.10b)$$

For the cases considered here, the Prandtl number may be taken as infinite. Typical values for the mantle and molten silicate rocks are 10^{24} and 10^4 . Hence the inertial terms can be neglected in equation (4.9b). Taking the curl of (4.9b), we obtain after a few simplifications:

$$0 = \nu \left(\frac{\partial^2}{\partial x^2} + \frac{\partial^2}{\partial z^2} \right) \left(\frac{\partial u}{\partial z} - \frac{\partial w}{\partial x} \right) + \frac{d\nu}{dz} \left(\frac{\partial^2 u}{\partial x^2} + 2 \frac{\partial^2 u}{\partial z^2} - \frac{\partial^2 w}{\partial x \partial z} \right) + \frac{d^2 \nu}{dz^2} \left(\frac{\partial u}{\partial z} - \frac{\partial w}{\partial x} \right) + R \frac{\partial \theta}{\partial x} \quad (4.11)$$

Differentiating (4.11) with respect to x yields:

$$R \frac{\partial^2 \theta}{\partial x^2} = \{v \nabla^4 + 2 \frac{dv}{dz} \cdot \nabla^2 - \frac{\partial}{\partial z} - \frac{d^2 v}{dz^2} \left(\frac{\partial^2}{\partial x^2} - \frac{\partial^2}{\partial z^2} \right)\} w \quad (4.12)$$

Equations (4.12), (4.9c) and (4.9d) are the equations which are to be solved.

4.2.2 Boundary conditions and initial conditions

Temperature is fixed at the top and bottom boundaries:

$$\bar{T} = 0 \quad \text{at} \quad z = 0 \quad (4.13a)$$

$$\bar{T} = 1 \quad \text{at} \quad z = 1 \quad (4.13b)$$

The initial condition for the mean temperature is:

$$T(z, 0) = 1 \quad (4.13c)$$

With these conditions, equation (9c) may be solved:

$$\bar{T}(z, t) = z + \frac{2}{\pi} \sum_{n=1}^{\infty} \frac{\exp(-n^2 \pi^2 t)}{n} \sin(n \pi z) \quad (4.14)$$

We assume further that the temperature perturbations vanish at the boundaries. This may represent a severe limitation on the physics of the development of instabilities, but Foster (1965b) used the same assumption in his study and obtained results equivalent to those of Elder (1968) who took the perturbations to be some specified noise at the upper boundary. Furthermore, Foster (1968) and Gresho and Sani (1971) investigated the effects of widely different boundary and initial conditions and concluded

that they were small provided that a proper criterion for the onset of instability is used.

The top and bottom boundaries are assumed to be stress-free. The upper boundary condition is realistic for the problem considered here but the bottom one may not be. This is however of little importance as we will see that the instability develops in the upper parts of the layer for most cases studied. These boundary conditions may be expressed as:

$$w = \frac{\partial^2 w}{\partial z^2} = 0 \quad \text{at } z = 0, 1 \quad (4.15)$$

With the boundary conditions on, equation (4.12) yields:

$$\frac{\partial^4 w}{\partial z^4} = 0 \quad \text{at } z = 0, 1 \quad (4.16)$$

Because viscosity is only depth-dependent, it is possible to separate the horizontal wavelengths. We thus consider the Fourier transforms of both temperature and velocity perturbations in the x-coordinate and examine the behavior of each mode separately:

$$w(x, z, t) = w_1(z, t) \exp(iax) \quad (4.17a)$$

$$\theta(x, z, t) = \theta_1(z, t) \exp(iax) \quad (4.17b)$$

4.2.3 Viscosity profiles

We chose viscosity functions of the form

$$\nu(z) = \nu_0 + \nu_1 \exp(-\gamma z) \quad (4.18)$$

Two parameters characterize the viscosity profile: γ , the decrement ($1/\gamma$ is a measure of the thickness of the viscous layer located at the top of the fluid), and λ , the viscosity contrast between the top and the bottom surface. For fixed λ , the viscosity function tends to a linear function as γ goes to zero.

4.2.4 Method of solution

The method we use is essentially the one developed by Foster (1965b, 1969). The velocity perturbations may be expanded in Fourier sine series, so that boundary conditions (4.15) and (4.16) are automatically satisfied:

$$w_1(z,t) = \sum_{n=1}^{\infty} A_n(t) \sin(n\pi z) \quad (4.19a)$$

Similarly, we write:

$$\theta_1(z,t) = \sum_{n=1}^{\infty} C_n(t) \sin(n\pi z) \quad (4.19b)$$

We considered two different types of initial conditions for the perturbations: a white noise for either velocity or temperature. These give the highest growth-rates (Foster, 1965b) and the latter is the most realistic.

The series are truncated after N terms. Equation (4.12) provides a direct coupling between the coefficients of w_1 and θ_1 which may be written in matrix form:

$$C_n = Q_{nm} A_m \quad (4.20a)$$

or

$$A_m = Q_{nm}^{-1} C_n \quad (4.20b)$$

The expressions for coefficients Q_{nm} may be found in Appendix 4.A.

They can be computed analytically for the viscosity function chosen. The interest of the method lies in the fact that the coupling matrix Q_{nm} and its inverse must be evaluated only once for a given set of parameters. Using equations (4.12) and (4.20a), we integrate equation (4.9d) using a 4-th order Runge-Kutta method. Details about the performance of the numerical scheme and about the convergence criteria used can be found in Appendix 4.B.

In a standard procedure for stability analysis, we determine which mode grows the fastest for each viscosity profile and each value of the Rayleigh number. The corresponding wavenumber will be called the critical wavenumber and will be denoted a_c .

In order to study quantitatively the evolution of disturbance in the fluid, we define an average growth factor as:

$$\sigma(t) = \left\{ \frac{\int_0^1 f(z,t)^2 dz}{\int_0^1 f(z,0)^2 dz} \right\}^{1/2} \quad (4.21)$$

where $f(z,t)$ is some which will be either the temperature perturbation, the velocity perturbation or the convective heat flux. At time $t = 0$, σ is equal to 1, so that $\sigma(t)$ is a measure of the amplification of disturbances throughout the fluid. We determine the times t_i at which the growth factor reaches prescribed values. When these correspond to the critical wavenumber, they are called characteristic times. We also determine the characteristic time for which the time-derivative of $\sigma(t)$ is zero, i.e. the time at which disturbances start to grow. We show in Figure 4.3 the evolution of the average velocity perturbation in a constant viscosity case. After an initial period of decay, disturbances grow

superexponentially (Figure 4.3). In fact, the growth curve can never be identified with an exponential. The growth rate always increases with time even up to amplification ratios of 10^8 (Malher et al., 1968).

The question now is to define the critical time which marks the onset of instability. The method used here does not allow an unequivocal determination of it. The critical time must somehow correspond to the time at which disturbances first become detectable physically, either in a carefully controlled laboratory experiment or, more naturally, in a real situation. From an other point of view, the critical time may be defined as the time at which the perturbations reach the finite amplitude level. This obviously depends on the initial amplitude and the form of the starting disturbance. The dilemma concerning the proper criterion cannot be resolved by a comparison with experimental data as the observations of Spangenberg and Rowland (1962), Foster (1965a), Blair and Quinn (1969) are compatible with growth factors lying between 50 and 10^6 .

In this study, we arbitrarily define the critical time t_c as the time at which the growth factor reaches the value of 100. By this time, the growth rate is very large and the growth curve becomes steeper and steeper as the instabilities blow up (Figure 4.3). Therefore the onset of instability depends weakly on the specific critical value selected. For example, characteristic times for factors of 10^2 and 10^3 differ by less than 5%. As will be shown in the next section, the above definition does not depend on which initial condition is chosen, nor on which variable is used to compute the growth factor. In marked contrast, a definition using the time at which $\dot{\sigma}$ is zero, i.e. the time at which the disturbances start to grow, is extremely sensitive to the initial conditions and the particular variable focussed upon.

The above study of convective instabilities differs from the usual marginal stability analysis. Whereas the latter determines whether or not a given density profile is intrinsically unstable, we are concerned here with the precise time at which a growing thermal boundary layer breaks down. The criterion chosen agrees with some laboratory experiments (Spangenberg and Rowland, 1962; Foster, 1965a), as stated above, and also with the recent numerical results of Houseman and McKenzie (1980). We finally remark that experimentally determined onset times do not appear sensitive to the form of the starting perturbation. Blair and Quinn (1969) found that widely variable conditions shifted critical times by no more than 10%.

4.3 RESULTS FOR CONSTANT VISCOSITY

We determined the critical wavenumber and the corresponding critical time for a wide range of Rayleigh numbers, using the two types of initial conditions defined above and different definitions of the growth rate. The characteristic times are plotted as a function of the Rayleigh number in Figure 4.4a,b. For all cases such that R is greater than 10^5 , the results satisfy a relationship of the form:

$$R \cdot t_C^{3/2} = A \quad (4.22a)$$

which may be recast as:

$$\frac{g \alpha \Delta T (\sqrt{K t_C})^3}{\kappa \nu} = A \quad (4.22b)$$

where A is some constant (Figure 4.4a,b). Considering how the variables have been non-dimensionalized, the relationship is evidence that d , the total depth of the fluid layer, does not enter the problem as a relevant length-scale. This property was emphasized by Foster (1965b). The proper length-scale is the thickness of the thermal boundary layer, which grows as \sqrt{t} for small values of t (such that $\sqrt{t} \ll 1$). This scaling was in fact used explicitly by Robinson (1967) who reproduced the results of Foster (1965b) in the high Rayleigh number limit.

The critical wavenumber is plotted as a function of the Rayleigh number in Figure 4.5. The values can be fit to a relationship of the form:

$$a_c \cdot R^{-1/3} = B \quad (4.23)$$

where B is some constant. This shows again that the proper length-scale is proportional to \sqrt{t} . Scaling the critical wavenumber with a length-scale equal to \sqrt{t} , we find:

$$a_c \cdot \sqrt{t}_c = \text{constant} = 0.47,$$

in excellent agreement with the results of Robinson (1967).

Relationship (4.22) and (4.23) break down for Rayleigh numbers lower than about 10^5 because the effect of the lower boundary cannot be neglected anymore.

We define the critical time as the time at which the growth rate is equal to 100. As can be seen in Figure (4.4a,b), this definition is not sensitive to which variable is used to compute the growth rate nor to which type of initial condition is chosen. Note that a criterion using $\sigma = 0$

would yield widely different onset times depending on the initial conditions and the growth variable selected.

Relationship (4.22b) shows that the onset of instability occurs when a Rayleigh number based on the thickness δ of the thermal boundary exceeds a critical value:

$$R_{\ell} = \frac{g\alpha\Delta T\delta^3}{\kappa\nu} = R_C$$

For $\delta(t) = 2\sqrt{t_C}$, the critical value R_C is approximately 560.

4.4 RESULTS FOR VARIABLE VISCOSITY

4.4.1 The influence of the viscosity parameters λ and γ

We now investigate cases for which viscosity varies with depth according to law (4.18). Each case is therefore defined by the following set of three parameters: R , γ , λ . To clarify the effect of each of them, we study first a number of calculations obtained with R fixed at a value of 10^6 .

We show in Figure 4.6 the variation of the critical time with $1/\gamma$, the thickness of the upper viscous layer, for fixed λ . For viscosity contrasts smaller than 10^3 , the values converge to a finite limit as $1/\gamma$ increases (as γ goes to zero). This limit is of course the critical time for a fluid whose viscosity is a linear function of depth. In contrast, when λ is larger than 10^3 , critical times do not converge to any finite value. This is because a Rayleigh number based on the value of viscosity at the top is sub-critical: the fluid is stable at all times if the thickness of the viscous layer is large enough. The critical time depends only weakly on λ when the viscosity variation is confined to a thin layer ($1/\gamma$ small).

The existence of high viscosities at the top has a marked effect on

the eigenfunctions. Vertical velocity profiles are shown in Figure 4.7 for a fixed λ of 10^3 and various values of γ . As γ decreases, and therefore as the thickness of the viscous upper layer increases, the instability is confined to deeper and deeper parts of the fluid. As could be predicted intuitively, convective flow develops preferentially in the low viscosity regions. However, when γ is small, the viscosity profile is close to linear and the viscosity variation is distributed somewhat uniformly in the layer. Thus the marked difference between a very viscous top and a lower region no longer exists. When γ decreases below about 10, the instability develops at the expense of progressively larger portions of the fluid.

The inspection of velocity profiles (Figure 4.7) reveals that there is a layer near the top where velocities are negligible. This layer behaves rigidly. We observed the existence of a rigid layer for viscosity contrasts higher than 10^2 and γ larger than 5. As γ decreases, rigid behavior becomes less pronounced and eventually disappears. The transition to rigid behavior as γ increases may be observed in Figure 4.8 where horizontal velocity eigenfunctions have been drawn for a constant γ (equal to 20).

We show in Figure 4.9a how the critical wavenumber varies with λ for fixed γ . a_c steadily decreases as λ increases and jumps to higher values for some particular value of λ . This marks the transition to rigid behavior and depends on γ (Figure 4.9a). Figure 4.9a must be compared to Figure 4.8. a_c decreases as the thickness of the upper region where horizontal velocities are positive increases.

We study in the next paragraphs the two distinct behaviors observed, as well as the transition between them for three values of R : 10^6 , 10^7 and 10^8 .

4.4.2 The transition between the "whole layer" and the "rigid top" modes of instability

As stated above, the transition to rigid behavior is best characterized using the critical wavenumber. That this transition is sharp may be appreciated in Figure 4.9b, where it appears clearly as a discontinuity. This is somewhat of an artifact as the convective instability does not "switch" to a rigid behavior mode for some particular combination of parameters. Rather, there is an intermediate stage where both the "whole layer" and the "rigid top" mode coexist. This may be seen in Figure 4.10 where the characteristic time $t(\sigma = 100)$ has been plotted as a function of the wavenumber for $R = 10^7$ and $\gamma = 20$. For small viscosity contrasts ($\lambda = 10^2$), there is only one mode of instability: the "whole layer" mode, with a small critical wavenumber. As λ increases, the characteristic time vs. wavenumber curve becomes more and more distorted until a second mode of instability appears. This second mode is the "rigid top" instability. It is the first to appear for λ between 8×10^2 and 10^3 . As λ increases further, this mode totally dominates (Figure 4.10). Throughout the following, the transition viscosity contrast will be denoted by λ_t .

The transition to the "rigid top" mode is also marked in a t_c vs. λ plot (Figure 4.11). There, it appears as an inflexion point: for λ greater than λ_t , the critical time increases less rapidly with increasing λ . This is because the instability develops in the low viscosity regions and is not affected strongly by the actual value of viscosity in the rigid layer above. The critical time is thus a weak function of λ .

The transition is a dynamic effect as shown in Figure 4.12 where the growth factor σ is plotted as a function of time. At the beginning, potential energy is available only in the top layers of the fluid. However

viscous dissipation is large and dampens the instability growth. The "whole layer" mode initially develops first but is overtaken by the "rigid top" mode as time increases. The transition is such that both modes develop with similar growth rates. Whether this happens at a particular value λ_c is thus quite sensitive to the criterion chosen to define the onset of instability: were it taken for example as the time at which σ is equal to 10, λ_c would be larger than the present value.

Evaluating the transition viscosity contrast requires a lot of computer runs and only a limited number of cases could be considered. Nevertheless, it is clear that λ_c varies as a function of both R and λ in a straightforward manner (Figure 4.13).

4.4.3 The "whole layer" mode of instability

In this case, the critical wavenumber decreases sharply as λ increases (Figures 4.9a,b,c) and takes values which cannot be identified with any constant viscosity case. This mode of instability is characterized by an upper layer which moves coherently and where velocity gradients are small (Figure 4.8a). This upper layer gets thicker as the viscosity contrast increases. Eventually, when λ is larger than λ_c , the lower parts of the fluid become unstable before this layer.

The dominant wavelength for the "whole layer" mode of instability can be larger than that for the corresponding constant viscosity calculation by as much as an order of magnitude. It is essentially a function of the viscosity contrast and depends weakly on R and γ .

Cases with similar critical wavelengths differ markedly by their critical times. For a given value of the critical time, the higher the Rayleigh number, the higher the critical wavelength.

4.4.4 The "rigid top" mode of instability

This mode is characterized by critical wavenumbers which are significantly higher than for the "whole layer" mode (Figure 4.9a,b,c). The reason is that the bulk of the highly viscous region has been isolated from the convecting layer.

Looking back at Figure 4.6, it is apparent that different viscosity structures are associated with the same critical times. A natural question arises whether there is a single parameter which describes the system in terms of which the critical time is a single-valued function. We need to define the depth extent of the flow and therefore the thickness of the layer which can be considered as rigid. Rigid behavior is characterized by zero velocity gradients and the rigid boundary condition on a horizontal surface is written as:

$$w = \frac{dw}{dz} = 0 \quad (4.25)$$

The tangents to the vertical velocity profile all intersect the axis $w=0$ at some point. We arbitrarily define the bottom of the rigid layer (at a depth denoted z_R) as the lowest of these intersections, i.e. using the tangent through the inflexion point (Figure 4.14). This definition is self-consistent in the sense that it yields $z_R = 0$ when there is no rigid behavior at the top (see for example case $\gamma = 5$, Figure 4.7). In all our calculations, z_R is close to the depth at which both the vertical velocity and the convective heat flux are one-tenth of their maximum value. z_R is of course most sensitive to γ . The higher γ , the thinner the rigid layer.

The effective depth-extent of convective flow is thus defined as:

$$h = d - z_R \quad (4.26)$$

and the corresponding temperature difference:

$$\Delta T_e = \Delta T(z_R) = T(1) - T(z_R) \quad (4.27)$$

The last quantity to be defined must be a measure of viscosity. Chandrasekhar (1961) showed that instability occurs when the energy released by buoyancy forces balances the kinetic energy dissipated by viscous forces. This last term may be written as:

$$\nu \int_0^1 e_{ij} dz \quad (4.28)$$

where e_{ij}^2 stands for the irreversible dissipation of kinetic energy in the fluid:

$$e_{ij}^2 = 2 \left(\frac{\partial u}{\partial x} \right)^2 + \left(\frac{\partial w}{\partial z} \right)^2 + \left(\frac{\partial w}{\partial x} + \frac{\partial u}{\partial z} \right)^2 \quad (4.29)$$

We define an "effective" viscosity as follows:

$$\bar{\nu} = \frac{\int_0^1 \nu e_{ij} dz}{\int_0^1 e_{ij} dz} \quad (4.30)$$

For all calculations reported here, the effective viscosity thus calculated lies between $\nu(z_R)$, the viscosity at the top of the convecting layer, and $\nu(1)$, the viscosity at the bottom. $\bar{\nu}$ is simply the dissipation-weighted average of viscosity in the layer, already used by Parmentier et al. (1976) in a study of free convection in a fluid with temperature and stress dependent viscosity. Parmentier et al. (1976) showed in particular that a

Rayleigh number based on this value of viscosity was sufficient to characterize the steady state flow in all the cases they considered.

Using the three quantities defined by equations (4.26), (4.27) and (4.30), we compute an effective Rayleigh number as follows:

$$R_e = \frac{g\alpha\Delta T_e h^3}{\bar{\nu}} \quad (4.31)$$

R_e is given as a function of t_c in Figure 4.15. Note that cases for which the computed t_c are close to each other are associated with almost equal values of R_e . All the results define a simple relationship.

An obvious drawback is that the determination of R_e requires a detailed knowledge of the flow structure. However, when the high viscosity region is thin, the instability occurs below it and $\bar{\nu}$ is close to $\nu(1)$. This may be seen in Figure 4.16, where $\nu(z_R)$ is plotted against λ . In most cases, replacing $\bar{\nu}$ by $\nu(z_R)$ or by $\nu(1)$ in expression (4.31) will not change the value of R_e by more than a factor of 2.

The regularity of the R_e vs. t_c relationship as well as the reduced range of viscosities in the convecting region suggest that simple scaling laws may be useful in describing the results. For that purpose, we need a length-scale for the instability, which we identify with the thickness of the thermal boundary layer below z_R . Parsons and McKenzie (1978) and Houseman and McKenzie (1980) used an isotherm to define the bottom of this boundary layer. This is not possible in the present analysis because ΔT_e decreases continuously as R increases and no specific isotherm may be used throughout. A more natural definition is the following (see Figure 4.17):

$$\delta = \frac{\Delta T(z_R)}{\frac{\partial T}{\partial z}(z_R)} \quad (4.32)$$

For large z , δ behaves as $\frac{2\kappa t}{z}$ and therefore goes to zero as z goes to infinity.

The critical wavenumber scales approximately with this length-scale. For all runs reported here, the quantity $a_c \cdot \delta$ is found between 0.5 and 1.0, with most values grouped around a mean value of 0.7 (Figure 4.18).

In the constant viscosity limit, $\delta = \sqrt{\pi\kappa t}$ and the corresponding critical value of the local Rayleigh number is about 360. In the variable viscosity calculations, the equivalent local Rayleigh number is:

$$R_l = \frac{g\alpha\Delta T_e \delta^3}{\kappa\nu} \quad (4.33)$$

For the majority of cases, R_l remains between values of 160 and 210 (Figure 4.19). This regular behavior accounts for the R_e vs. t_c relationship of Figure (4.15).

When γ is equal to 20, in contrast with the other cases, R_l increases significantly with λ . This is because the perturbations are affected by the bottom boundary. In this case, the curvature of the mean temperature profile changes rapidly with time and a simple scaling law is not sufficient. An exhaustive study would require the consideration of the shape of the profile as was done by Sparrow et al. (1964) and Whitehead and Chen (1970).

R_l is a weak function only of R and λ , and thus depends essentially on γ (Figure 4.19): values for $\gamma = 40$ are centered around 165 while those for $\gamma = 80$ are higher, around 190. As γ influences strongly the value of z_R , these differences are associated with variations in the thickness of the rigid lid where heat transport is conductive. The thermal boundary condition at the top of the convecting layer is no longer of the fixed

temperature type and is of the "mixed" type:

$$\frac{\partial T}{\partial z} - BT = \text{constant} \quad (4.34)$$

where B is a Biot number (Sparrow et al., 1964). As $B \rightarrow \infty$, this boundary condition approaches the fixed temperature condition, while $B=0$ obviously reduces (34) to the constant heat flux boundary condition. In general, B depends on the horizontal variation of temperature and cannot be defined a priori. For a temperature varying as $\cos(ax)$ at the bottom boundary of the rigid layer, Hewitt et al. (1980) showed that the thermal boundary condition can be reduced to:

$$\frac{\partial T}{\partial z}(z_R) = \ell a \coth(az_R) \cdot T(z_R) \quad (4.35)$$

where ℓ is a length-scale.

$$\text{Hence:} \quad B = \ell a \coth(az_R) \quad (4.36)$$

The proper length-scale in the convecting layer is δ . As the quantity $a \cdot \delta$ remains approximately constant at a value A (equal to 0.7), equation (4.36) may be rewritten as:

$$B = A \coth\left(A \frac{z_R}{\delta}\right) \quad (4.37)$$

Therefore B tends to ∞ as $\frac{z_R}{\delta}$ goes to zero, which indicates indeed that the boundary condition approaches the fixed temperature condition. On the other hand, B tends to the constant A as $\frac{z_R}{\delta}$ goes to infinity. It is clear that $\frac{z_R}{\delta}$ is an adequate measure of the effect of conduction in the rigid lid which overlies the convecting fluid. Although there is some scatter in the

data, B increases with Rl in agreement with the analysis of Sparrow et al. (1964). For Rl around 160, B is found close to 0.8, while its value is 1.0 for Rl equal to 190. Considering the low values obtained for B , the thermal boundary condition is closer to a fixed heat flux condition.

Hence the effective boundary conditions resulting from the presence of a rigid lid are somewhat complex. Furthermore, they concern a case of penetrative convection as the thermal boundary layer is bounded below by a nearly neutrally stratified layer. In such a situation, Soberman (1959) and Currie (1967) have shown that the critical Rayleigh number is lower than in the corresponding Rayleigh-Benard experiment. In a standard marginal stability analysis with fixed flux boundary conditions, Hurle et al. (1967) found critical Rayleigh numbers of 720 and 120 for the rigid-rigid and free-free cases. These values bound those reported above for R_g .

A local Rayleigh number may also be computed using $\nu(z_R)$ as the reference viscosity. This number, denoted by R_r , has the same general behavior as R_g , but the range of values is greater, with bounds of 40 and 200. This suggests a procedure to estimate both the critical time and the transition depth z_R . R_r can be computed at any depth z using definitions (4.27) and (4.32):

$$R_r(z) = \frac{g\alpha\Delta T(z) \delta(z)^3}{\kappa \nu(z)} \quad (38)$$

$R_r(z)$ is also a function of time. We plot in Figure 4.20, R_r as a function of depth for various times for the case ($R=10^7$, $\lambda = 10^4$, $\gamma = 40$). As depth increases, viscosity decreases sharply with R_r first increases. However, when the bottom of the thermal boundary layer is reached, the

temperature difference $\Delta T(z)$ and length-scale $\delta(z)$ drop to zero. Thus R_T has a maximum in the layer, whose value increases with time (Figure 4.20).

For the case considered here, the critical time is 8.18×10^{-3} , the transition depth $z_R = 0.205$ and the critical value for $R_T(z_R)$ 72. Note that the maximum of $R_T(z)$ reaches the critical value 72 at time t_C at a depth z equal to 0.205. A simple procedure is thus to compute R_T as a function of depth and time. The critical time is such that the maximum of R_T in the layer exceeds a critical value and the transition depth is simply the depth of the maximum. Although the actual critical value is poorly constrained, R_T grows rapidly with time and errors in the critical parameters t_C and z_R will be small. Considering the extreme values of 40 and 200, the resulting spread of values for t_C and z_R are less than 30% and 15% respectively.

The instability can thus be characterized by the curve $R_T(z)$ alone: convection develops below depth z_R such that the local Rayleigh number is maximum and exceeds a critical value. This observation reinforces the validity of the method chosen to determine z_R .

We conclude that the methods which were developed for constant viscosity fluids can be adapted to high viscosity contrast situations because the highly viscous regions have been isolated from the flow in the rigid lid. This is stressed in Figure 4.16 where it appears that viscosity contrasts allowed in the convecting layer rarely exceed 10.

4.5 DISCUSSION

In a real fluid, viscosity varies as a function of temperature instead of depth. For the transient cooling experiment considered in this study, the true viscosity profile is therefore characterized by a fixed viscosity contrast λ , equal to $\nu(0)/\nu(\Delta T)$, and by a γ value which increases with time as the cold thermal boundary layer thickens (under the restriction of course that the profile may be approximated by an exponential). The choice of γ is of particular importance as it determines the thickness of the rigid upper layer. The simplest method is to evaluate it from the true viscosity profile at the critical time t_c . But it may be that velocity perturbations have a "memory" and that their growth also reflects earlier viscosity profiles. If this is the case, the value of γ calculated at t_c is a lower bound to the true γ and the rigid layer thickness is overestimated in consequence.

The transition between the two modes of instability occurs for rather large viscosity contrasts. For Rayleigh numbers representative of mantle conditions, values would be around 10^2 . This makes both laboratory experiments and numerical calculations difficult to implement. We have shown however that many results which apply in the constant viscosity limit can be used for variable viscosity fluids, provided care is taken to consider the relevant boundary conditions.

The thermal boundary condition at the top of the convecting region is close to a fixed heat flux condition. Chapman and Proctor (1980), Chapman et al. (1980) and Hewitt et al. (1980) have recently investigated the effect of this boundary condition in some detail. They showed that the cells which develop fastest at the onset of instability are not stable to perturbations of longer wavelengths and that the dominant wavelength

increases with time. Houseman and McKenzie (1980) studied a problem closer to ours (with a "mixed" thermal boundary condition) and observed a similar behavior. For the case of the mantle, the dominant wavelength increase occurs over a large time span which is of the same order of magnitude as the age of the Earth (Hewitt et al., 1980). Values of the critical wavelength are likely to be around 500 km. This would make convective instabilities beneath the plate difficult to detect, if they exist, because of the masking effect of the plate.

We now apply our numerical results to the case of the upper mantle beneath the oceans. Values for the different parameters of interest are given in Table 4.1 (see McKenzie et al., 1974; Parsons and McKenzie, 1978). We shall assume here for the sake of argument that the flattening of the depth vs. age curve occurs at the age of 70 Ma and that it marks the onset of convection beneath the plate. Other explanations for the flattening have been proposed (Forsyth, 1977; Schubert et al., 1976; Jarvis and Peltier, 1980) but remain controversial (Sclater et al., 1980; Houseman and McKenzie, 1980). The viscosity profile of the upper mantle remains poorly determined, especially in the vicinity of ocean ridges, and we find it more useful to evaluate the constraints imposed by the hypothesis of Parsons and McKenzie rather than to analyze some pre-conceived mantle structure.

We assume further that the results obtained in this study apply not only to exponential viscosity functions but also to the general class of monotonically decreasing functions. We consider first the effective Rayleigh number vs. critical time relationship, and second the local Rayleigh number criterion.

With the parameters given in Table 4.1, the age of 70 Ma corresponds to a non-dimensional time of 6.8×10^{-3} . Using the R_e vs. t_c relationship of

Figure 4.15, we find an effective Rayleigh number of approximately 3×10^5 . Further interpretation requires values for z_R , ΔT_e and $\bar{\nu}$. z_R must be less than the plate thickness of 125 km determined by Parsons and Sclater (1977) and greater than 30 km, the thickness of the elastic portion of the plate (Watts, 1978). The value of the oceanic heat flux at large ages provides the only constraint on ΔT_e and z_R , for steady-state convection. The method is detailed in Parsons and McKenzie (1978). We consider the estimate of 34 mW/m^2 given by Parsons and Sclater (1977). This predicts a temperature difference of 291°C which itself yields a thickness of 93 km for the rigid layer. Using the numerical estimates and the above value for R_e , we obtain the following estimate for the effective viscosity of the upper mantle:

$$\bar{\nu} = 3 \times 10^{16} \text{ m}^2/\text{s}$$

Although the value inferred for ΔT_e may be somewhat in error because it makes use of results derived for a constant viscosity fluid heated from within in steady-state conditions, the order of magnitude is certainly correct. Variations in ΔT_e do not alter significantly the results (Table 4.2).

We now consider the behavior of the local Rayleigh number R_r when depth increases. As shown before, the transition depth z_R depends mostly on γ and therefore on how viscosity varies with temperature. Unfortunately, presently available experimental data do not allow precise statements concerning the rheology of the mantle and its variation with depth. It is not the purpose of the present paper to review the relevant literature and we simply remark that recent studies have stressed the importance of grain boundary processes (Goetze, 1978; Chopra and Paterson,

1980; Poirier, 1981, personal communication). Critical parameters such as the grain size and the water content remain poorly known in mantle conditions, although it seems that the grain size profile is rather complex (Ave Lallemant et al., 1980; Mercier, 1980). As a first step, we consider a Newtonian creep law with an apparent activation energy E which is appropriate for grain-boundary processes (Ashby and Verrall, 1978):

$$\gamma = AT \exp(E/RT) \quad (4.39)$$

where A is some constant which depends on the grain size, the grain boundary thickness and the volume diffusion coefficient (Ashby and Verrall, 1978). We neglect the pressure dependence of E as we restrict ourselves to a relatively small depth range. Values for E determined experimentally on single crystals or polycrystalline aggregates of olivine range from about 355 kJ/mole (Schwenn and Goetze, 1978) to 565 kJ/mole (Relandeau, in press). Finally, it must be noted that E decreases with the grain size (Chopra and Paterson, 1980).

Instead of determining a "best fit" γ with a viscosity profile computed with a law of the type (4.39), we assume again that the local Rayleigh number criterion developed previously does not depend on the exact form of the viscosity function. We estimate both z_R and $v(z_R)$ using the mean temperature profile at time $t = 6.8 \times 10^{-3}$ and the viscosity law (4.39) for various values of E (Table 4.3). The critical value chosen for R_γ is the upper bound of 200. Taking into account the uncertainty in this estimate, viscosity values may be higher than those indicated in Table 4.3 by a factor of $200/40 = 5$.

Remembering the constraints on z_R stated at the beginning of the

discussion, we conclude that activation energies allowed by this analysis cannot be greater than 200 kJ/mole. The results of Table 4.3 call for two observations. First, estimates for the local values of viscosity agree with those derived above using the effective Rayleigh number. This is not surprising as the two approaches are related. Second, the activation energy values are significantly lower than those which have been measured in the laboratory. This implies a relatively flat viscosity profile in the upper mantle and probably indicates that this profile cannot be represented by a law of the form (4.39) with a constant apparent activation energy. Sharp variations in the grain size, as reported by Ave Lallemant et al. (1980), could provide an explanation.

The results of this study do not constrain the actual viscosity profile in the upper mantle as we have shown that the instability was essentially characterized by local parameters. Thus the viscosity values found in Tables 4.2 and 4.3 are local estimates which are valid only for the thermal boundary layer. The true viscosity profile may be more complicated than those represented by equations (4.18) and (4.39), with for example a low viscosity layer at some depth. Richter and McKenzie (1978) suggested the existence of such a layer in a study of forces which act on the plates.

Our estimate for the mean viscosity in the thermal boundary layer beneath the plate is 3×10^{16} m²/s, which agrees with values calculated by Parsons and McKenzie (1978) and Houseman and McKenzie (1980). This is the value required for the onset of convective instabilities to occur beneath the plate at an age of about 70 Ma. It is smaller than the estimate of 3×10^{17} m²/s calculated from post-glacial uplift data by Cathles (1975) and Peltier and Andrews (1976). This may be due to assumptions regarding the uncertain behavior of the lithosphere which constrain heavily the

interpretation of uplift rates. Alternatively, the difference may simply indicate that viscosity structures beneath oceans and continents are not similar. We note however that Ave Lallemand et al. (1980) and Mercier (1980) infer viscosity values of about $10^{16} \text{ m}^2/\text{s}$ for the asthenosphere beneath the Southern African craton using geological thermobarometers and grain size piezometers on a series of peridotite xenoliths.

TABLE 4.1

Quantity	Symbol	Value
Layer depth	d	700 km
Temperature difference	ΔT	1300°K
Gravity	g	10 m/s ²
Thermal expansion	α	2 x 10 ⁻⁵ /°K
Specific heat	C _p	1.2 x 10 ³ J/kg/°K
Density Asthenosphere	ρ	3.7 x 10 ³ kg/m ³
Thermal diffusivity	k	1.5 x 10 ⁻⁶ m ² /s
Density Lithosphere	ρ	3.3 x 10 ³ kg/m ³
Thermal diffusivity	k	8 x 10 ⁷ m ² /s
Asymptotic heat flux	Q	34 mW/m ²

TABLE 4.2

VALUES OF THE RIGID LAYER THICKNESS AND OF THE EFFECTIVE VISCOSITY
DEDUCED FROM THE VALUE OF R_e

ΔT_e ($^{\circ}K$)	z_R (km)	$\bar{\nu}$ (m^2/s)
400	83	4.2×10^{16}
300	92	3.0×10^{16}
200	101	1.9×10^{16}

TABLE 4.3

VALUES OF THE RIGID LAYER THICKNESS AND OF THE LOCAL VISCOSITY INFERRED
FROM THE LOCAL RAYLEIGH NUMBER CRITERION

E (kJ/mole)(kcal/mole)	50 (12)	100 (24)	200 (48)	400 (96)	500(120)
z_R (km)	67	100	125	148	160
$\nu(z_R)$ (m ² /s)	6.5×10^{16}	1.7×10^{16}	8.6×10^{15}	2.1×10^{15}	9.7×10^{14}

FIGURE CAPTIONS

- Figure 4.1. Schematic evolution of the upper mantle beneath oceans as it moves away from a spreading center. Adapted from Parsons and McKenzie (1978).
- Figure 4.2. General presentation of the problem to be solved. For the infinite Prandtl number fluid considered here, three non-dimensional parameters define the problem: λ , γ , R .
- Figure 4.3. Growth of the average velocity disturbance. Constant viscosity case, Rayleigh number of 10^6 . The dashed line is the tangent to the growth curve at the time $t(\sigma=10)$. Note that the growth curve is not a straight line, which indicates that growth is superexponential.
- Figure 4.4. Constant viscosity calculations. Characteristic times against Rayleigh number for $\sigma=0$, $\sigma=10$ and $\sigma=100$.
- a. Dots represent calculations with white noise in temperature as initial conditions and the temperature perturbation as the growth variable. Triangles are for the same initial conditions and with the convective heat flux as the growth variable.
 - b. Same as a. Stars: white noise in temperature as initial conditions and velocity perturbation as growth variable. Dotted stars: white noise in velocity as initial conditions and velocity perturbation as growth variable.
- Figure 4.5. Constant viscosity case. Critical number vs. Rayleigh number.
- Figure 4.6. Critical time as a function of $1/\gamma$ for various values of the viscosity contrast λ .
- Figure 4.7. Vertical velocity profiles for $R=10^6$ and $\lambda=10^3$. Numbers on the curves are values of γ . Note that the case $\gamma=5$ does not exhibit rigid behavior near the top of the layer.

Figure 4.8a,b. Horizontal velocity profiles for $R=10^6$ and $\gamma=20$. Numbers on the curves are values of λ .

Figure 4.9. Critical wavenumber as a function of the viscosity contrast for various values of γ . a,b,c for Rayleigh numbers of 10^6 , 10^7 , 10^8 .

Figure 4.10. Characteristic time $t(100)$ as a function of wavenumber for $R=10^7$, $\gamma=20$. Numbers on the curves are values of λ . Every curve is drawn using the same time-scale but has been translated up or down to appear on a single figure. Note that there are two minimums for $\lambda=7.94 \times 10^2$ and $\lambda=10^3$.

Figure 4.11. Critical time as a function of λ for $\gamma=40$. Small arrows indicate the inflexion points, i.e. the transition between the "whole layer" mode and the "rigid top" mode.

Figure 4.12. Growth factor as a function of time for $R=10^7$, $\lambda=10^3$ and $\gamma=20$. Numbers on the curves are values of the wavenumber which correspond to the two minimums of Figure 4.11. The "whole layer" mode corresponds to $a=0.8$ and the "rigid top" mode to $a=6.5$.

Figure 4.13. The transition viscosity contrast as a function of R . Numbers on the curves are values of γ .

Figure 4.14. Definition of the transition depth z_R . The region between depths 0 and z_R behaves rigidly. The Rayleigh number is 10^6 .

Figure 4.15. The effective Rayleigh number as a function of the critical time. Also drawn is the curve for the constant viscosity case.

Figure 4.16. Viscosity at the bottom of the rigid layer as a function of λ for various values of γ . Dashed lines indicate that velocity perturbations have reached the bottom of the layer and that simple local similarity concepts are not applicable.

Figure 4.17. Definition of the thermal boundary layer thickness below the rigid layer.

Figure 4.18. Critical wavenumber as a function of length-scale δ . The heavy line represents relation $a.\delta = 0.83$ valid for the constant viscosity case ($\delta = \sqrt{\pi\kappa t}$).

Figure 4.19. Local Rayleigh number R_ℓ as a function of λ for various values of γ . Note the consistency of values for a given γ . Calculations for $R = 10^8$ yield the same results and were not included for clarity.

Figure 4.20. Local Rayleigh number R_r as a function of depth for various times. Calculation for $R=10^7$, $\lambda=10^4$ and $\gamma=40$. The critical value and the transition depth determined independently for this case are 72 and 0.205 respectively.

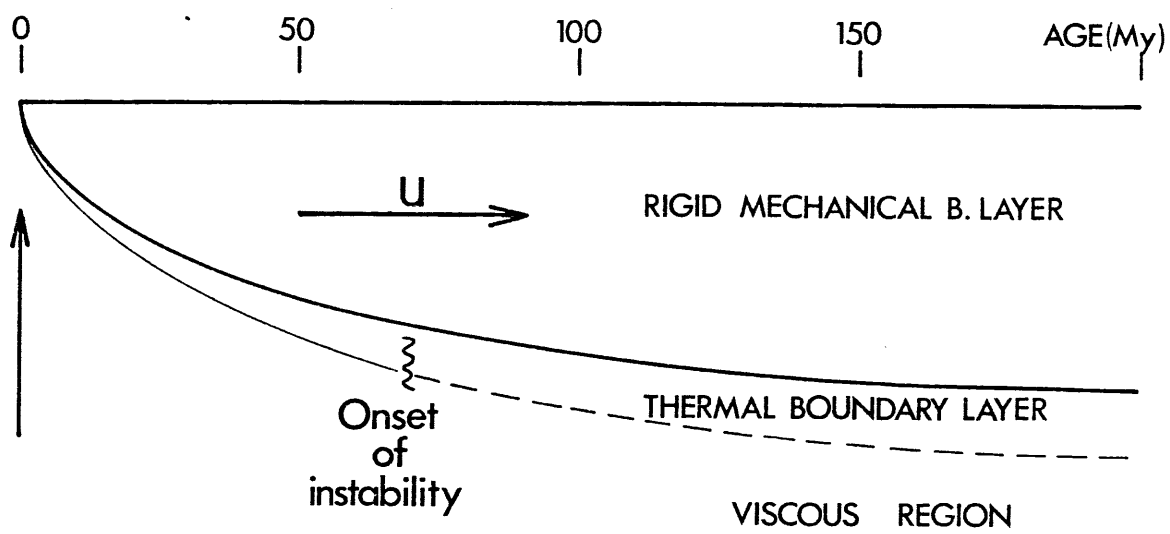
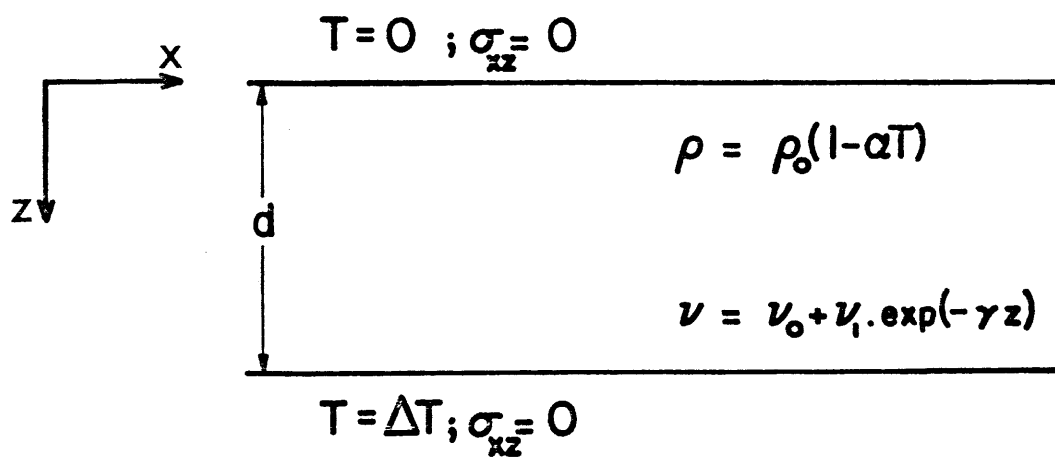


Fig. 4.1



viscosity structure

$$\left\{ \begin{array}{l} \lambda = \frac{\nu(0)}{\nu(1)} \\ \gamma \end{array} \right.$$

$$R = \frac{g \alpha \Delta T d^3}{\kappa \nu(1)}$$

Fig. 4.2

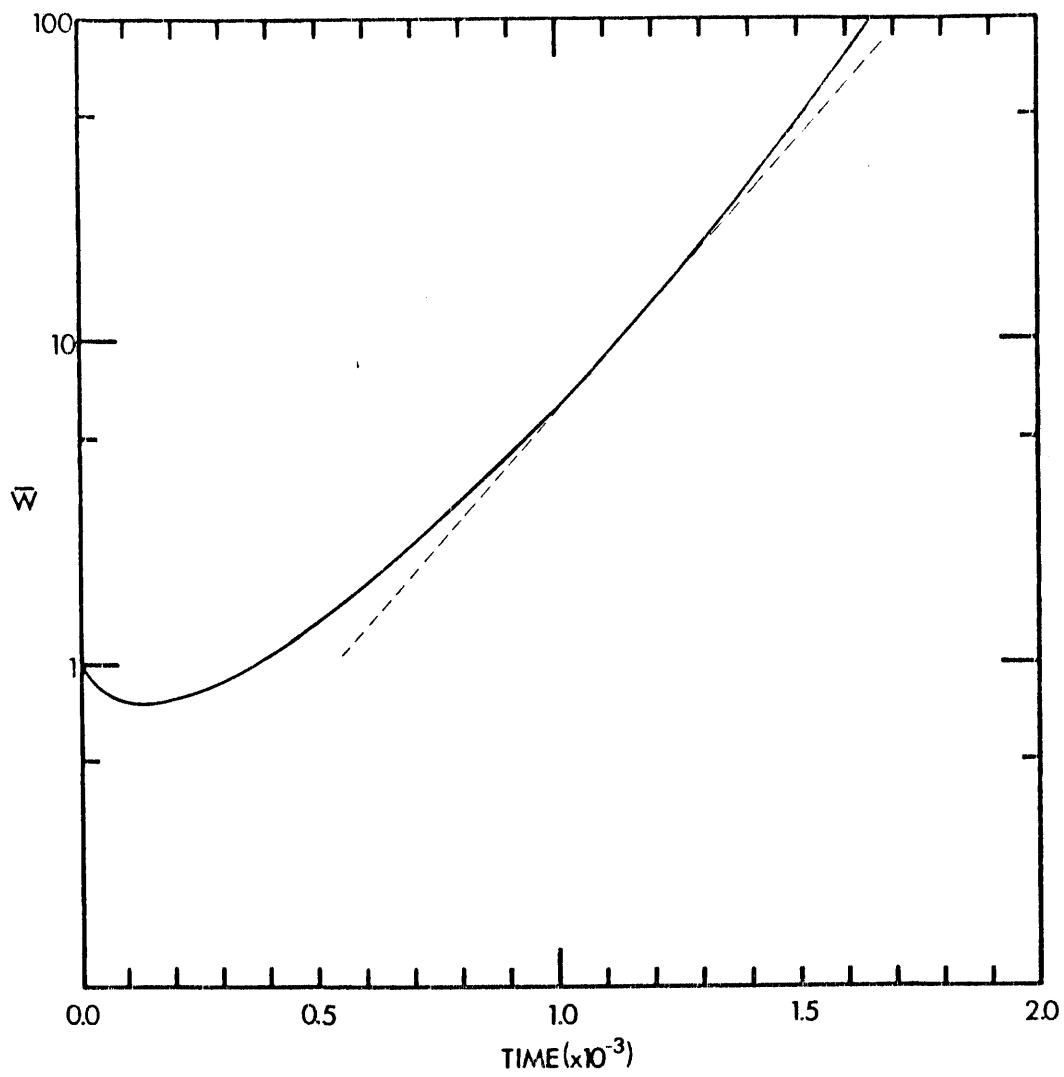


Fig. 4.3

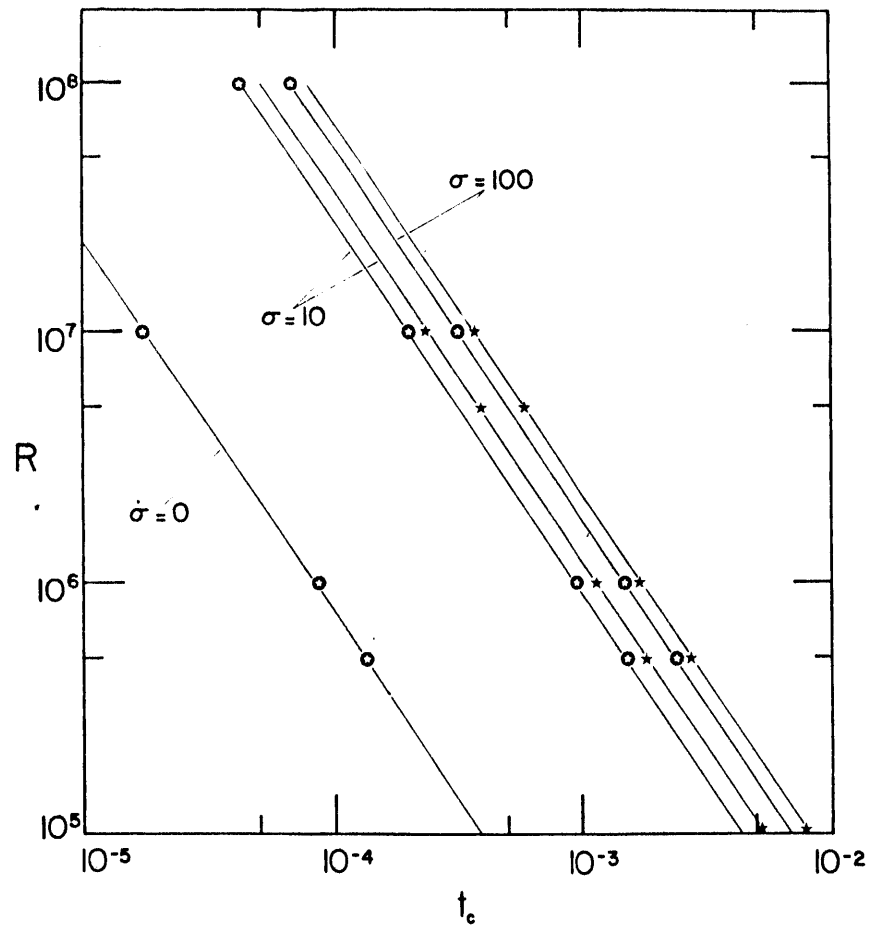


Fig. 4.4a

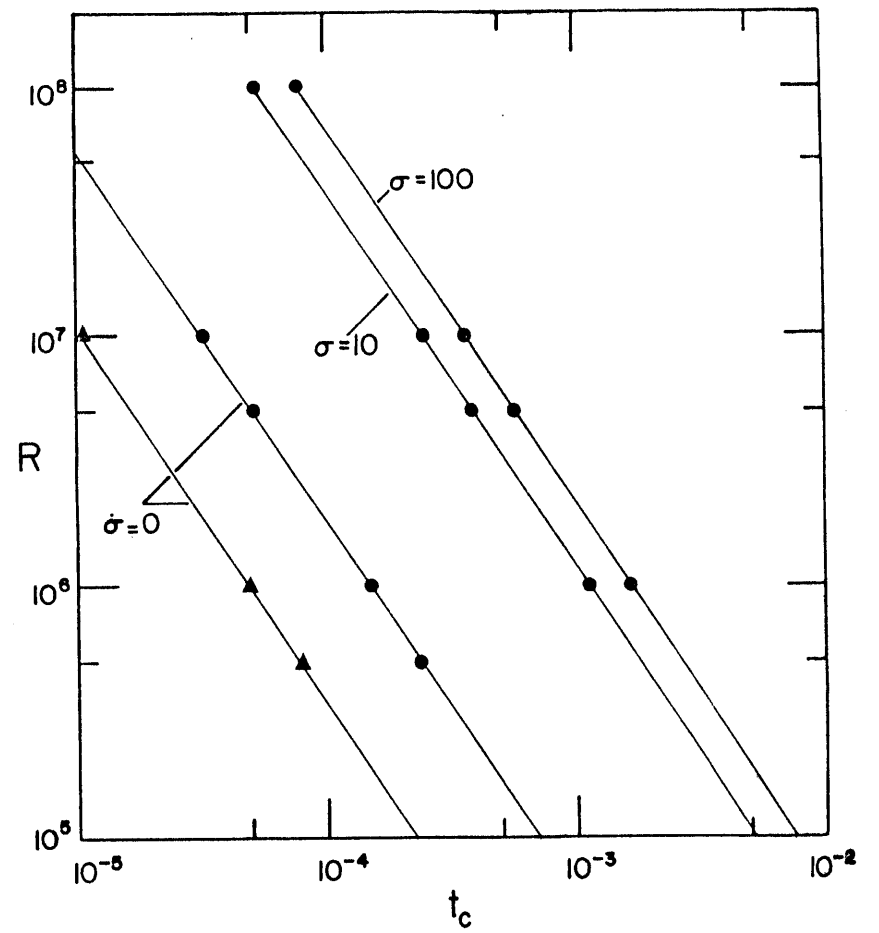


Fig. 4.4b

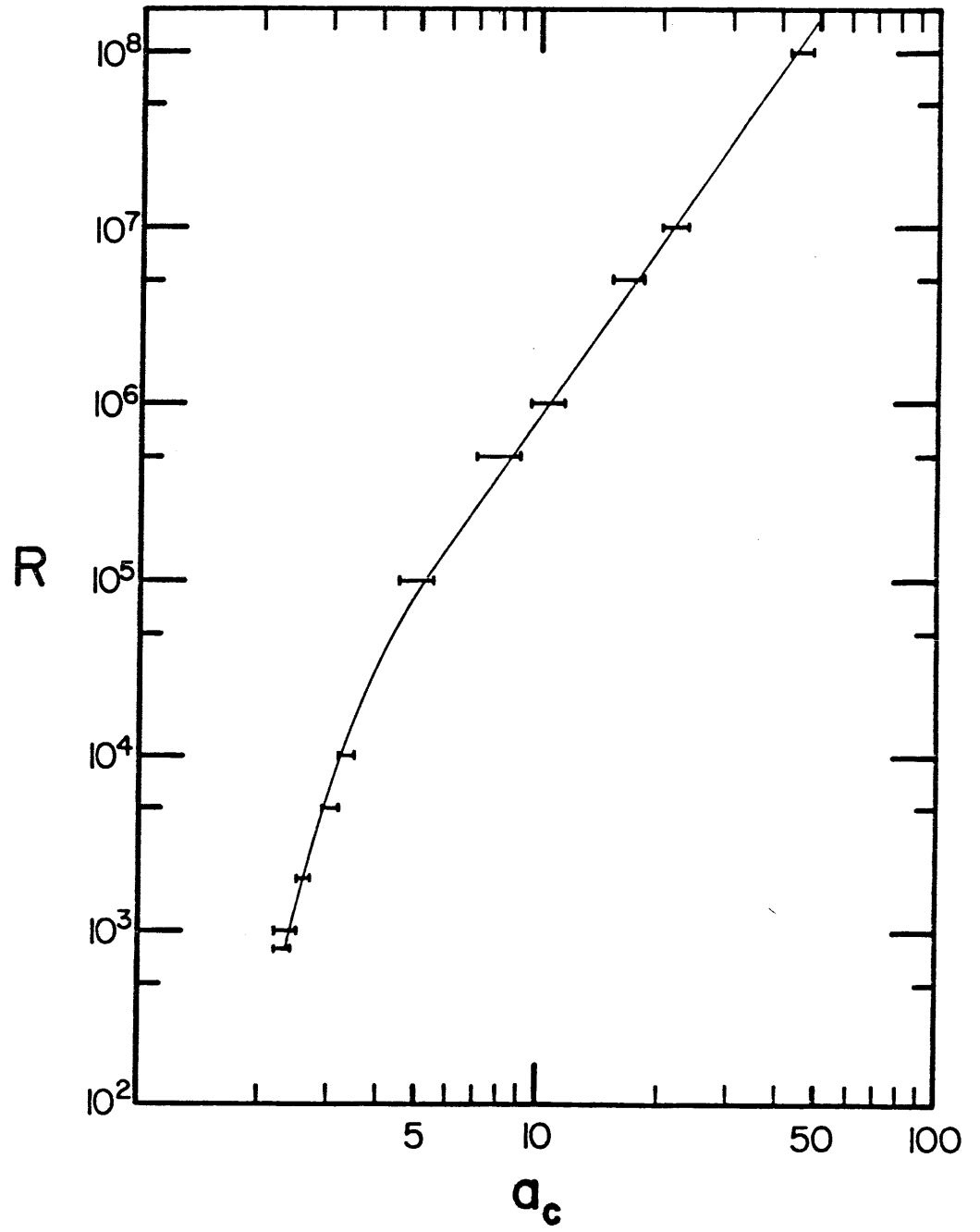


Fig. 4.5

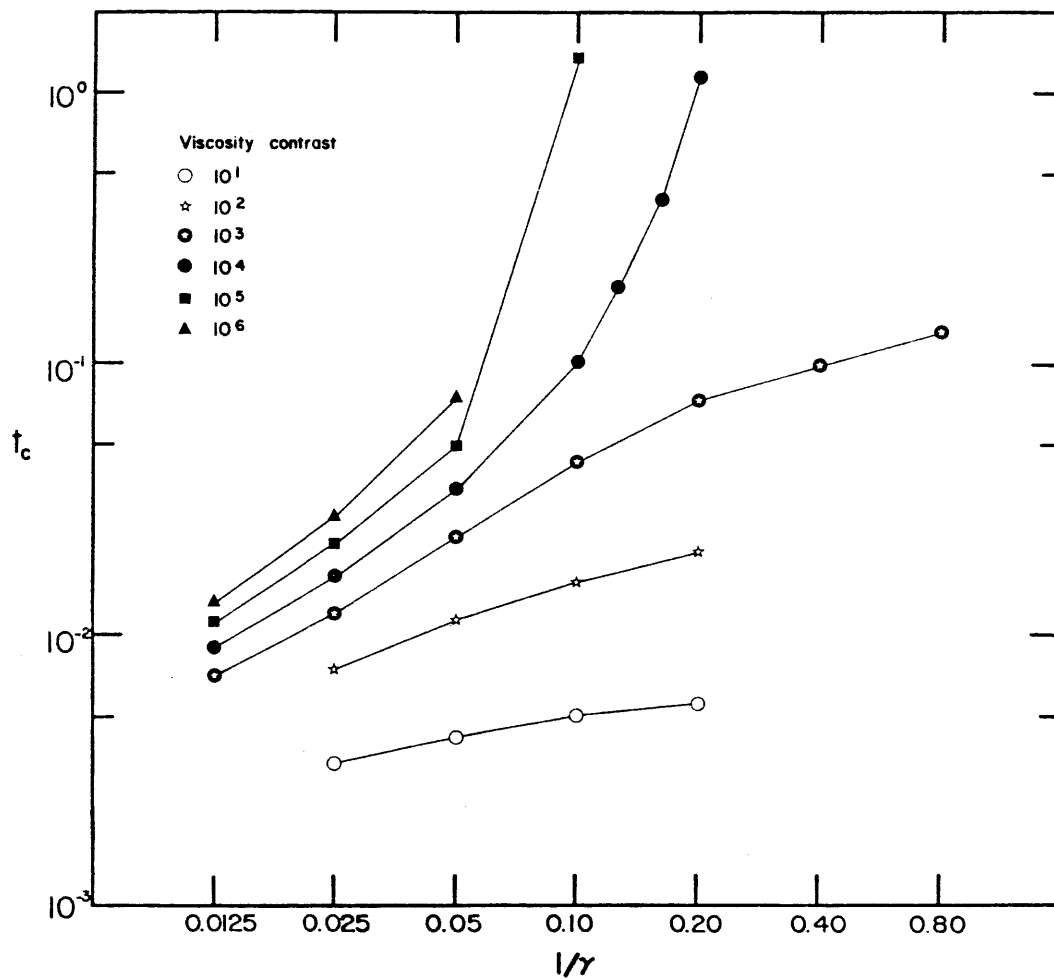


Fig. 4.6

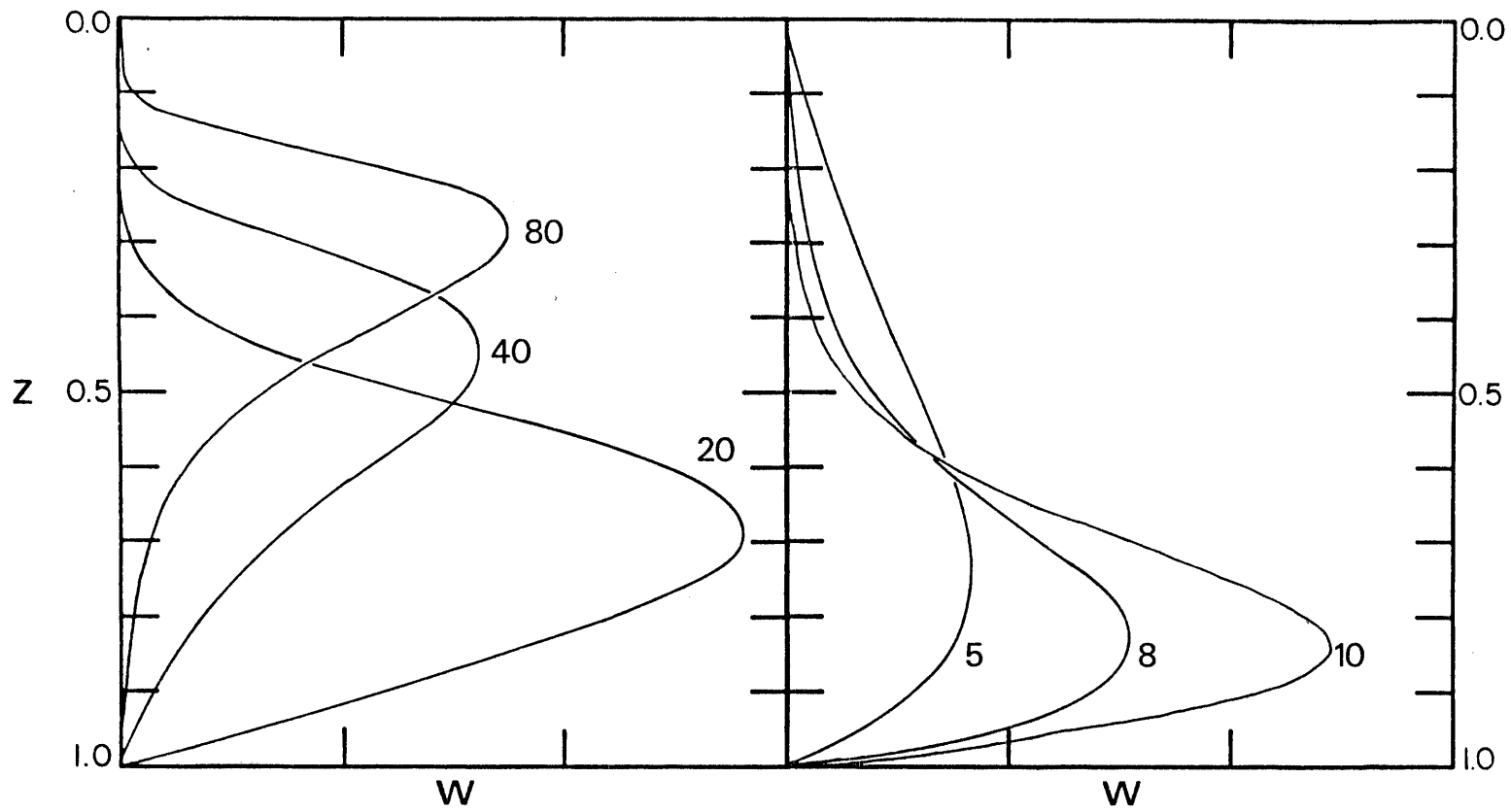


Fig. 4.7

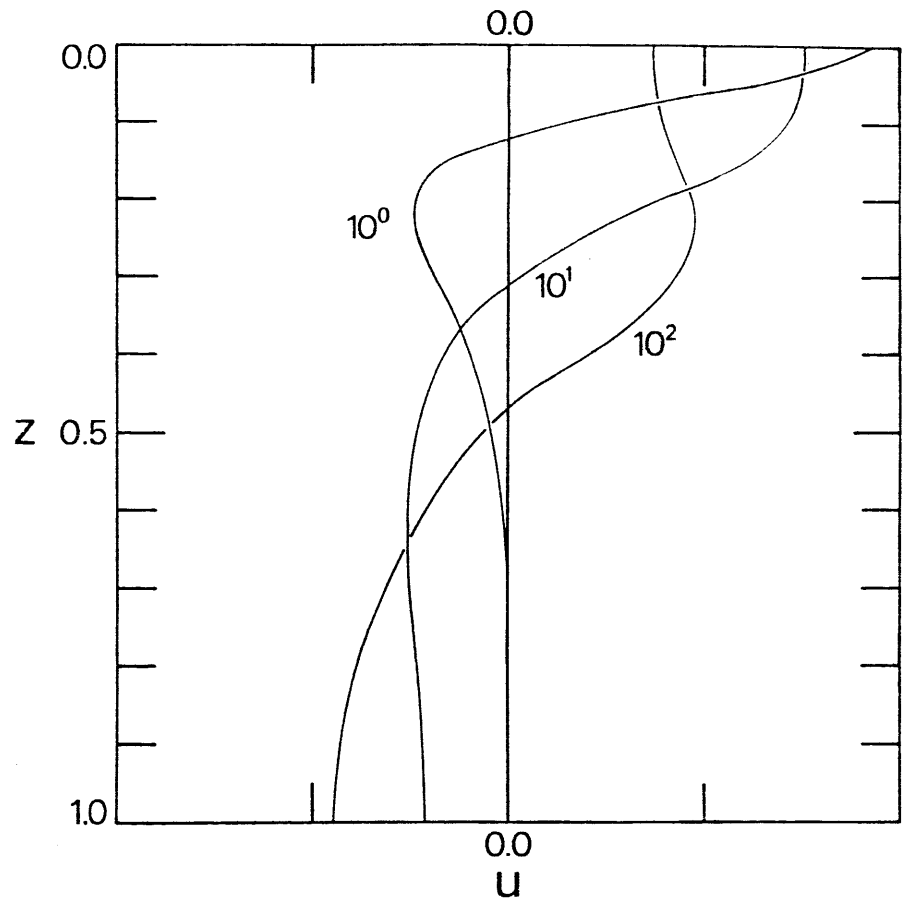


Fig.4.8a

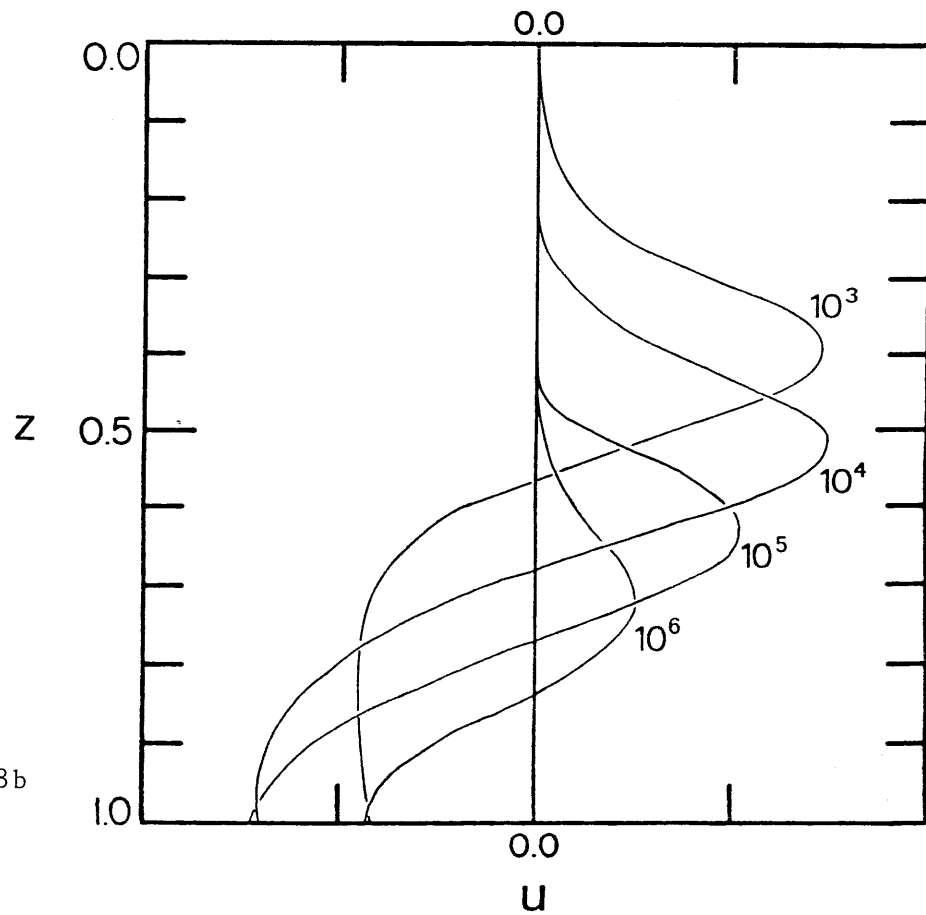


Fig. 4.8b

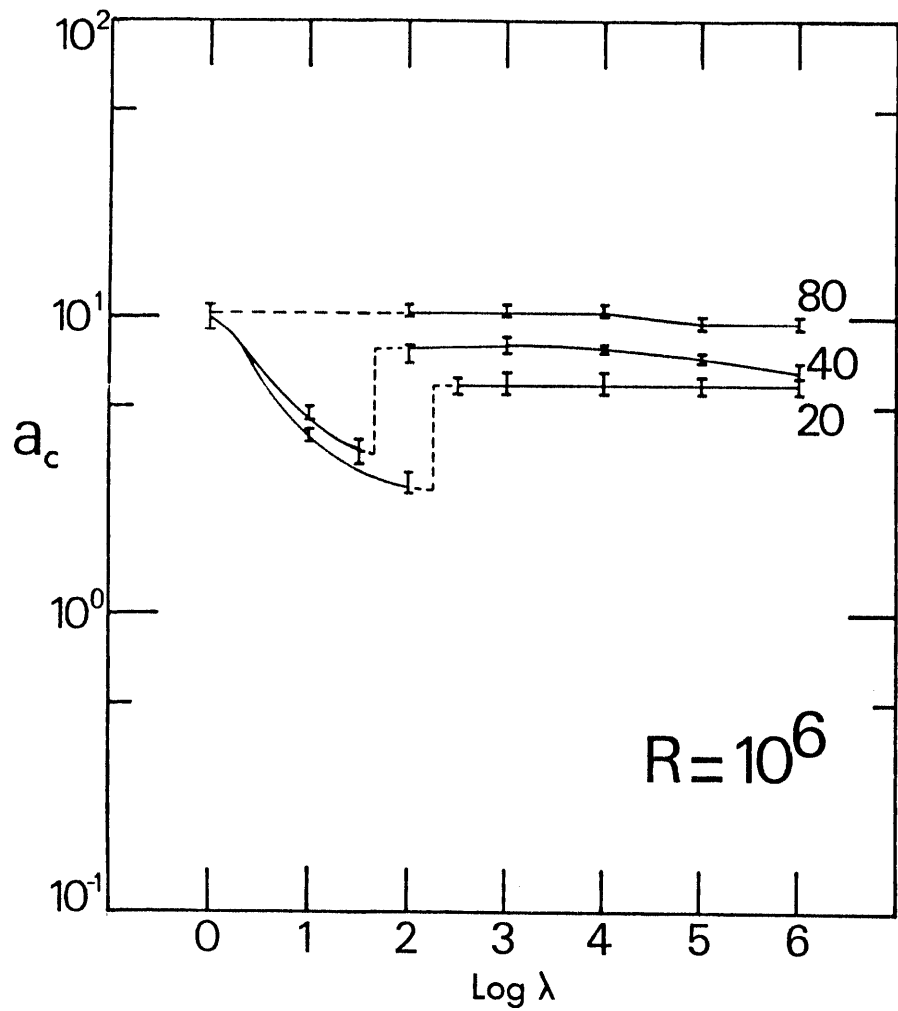


Fig. 4.9a

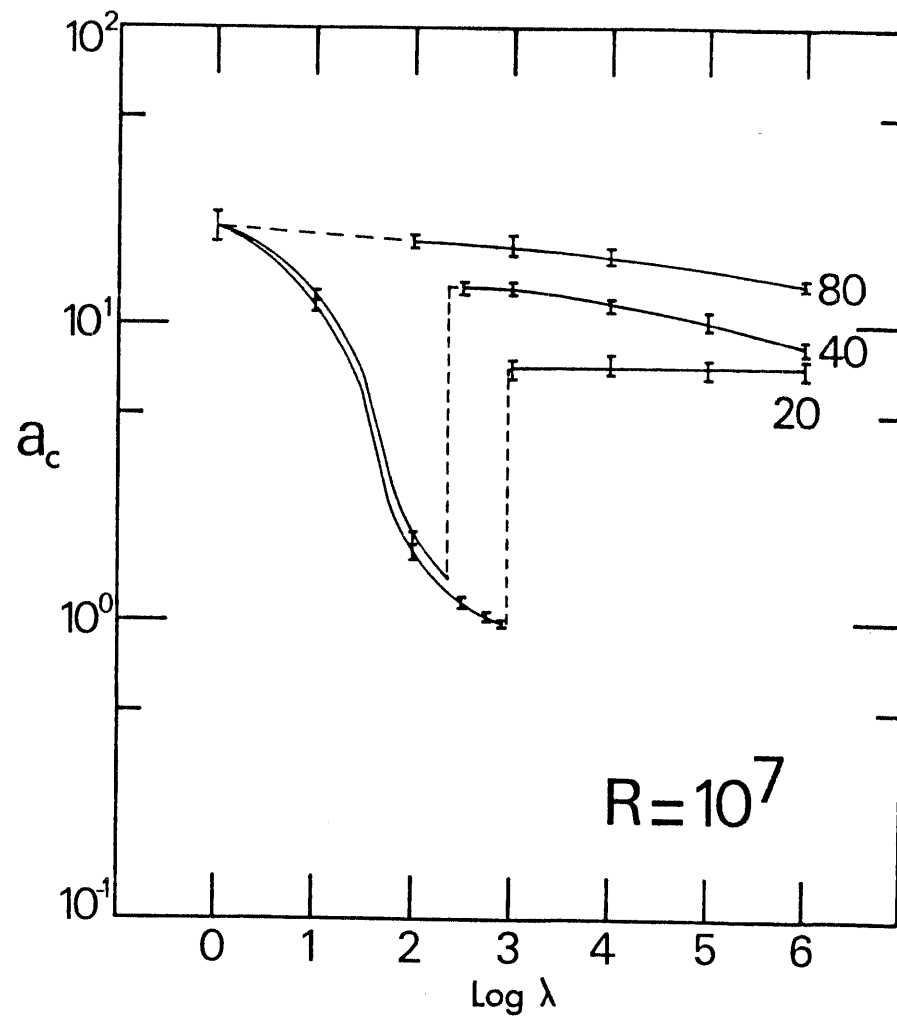


Fig. 4.9b

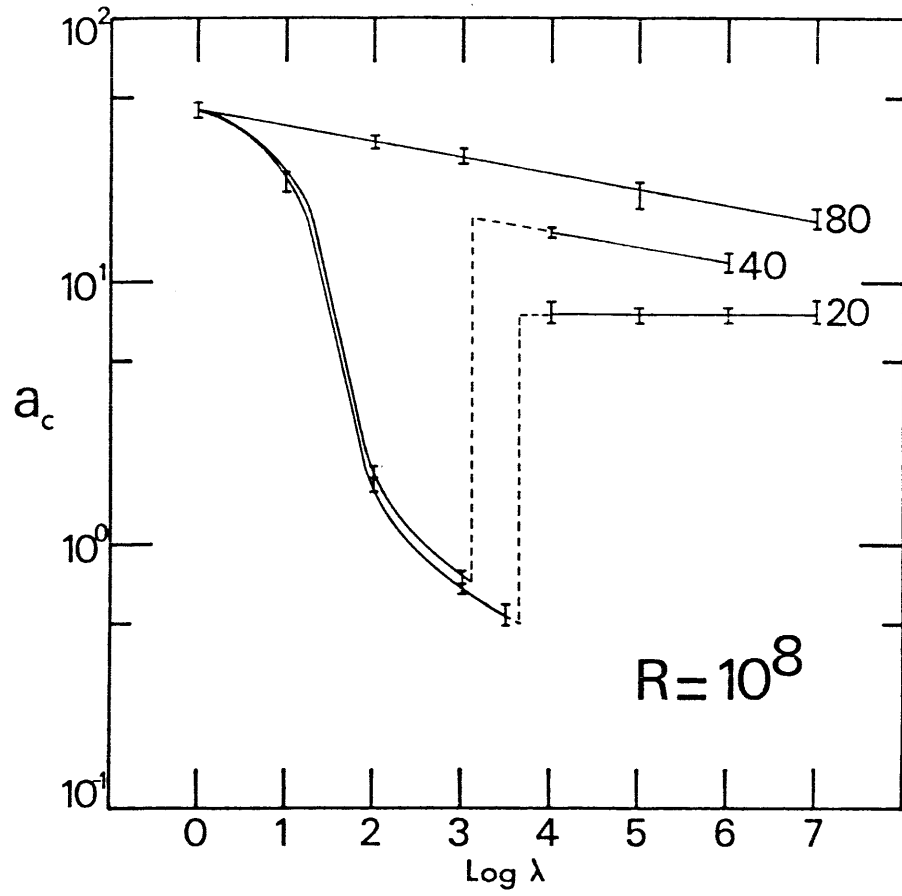


Fig. 4.9c

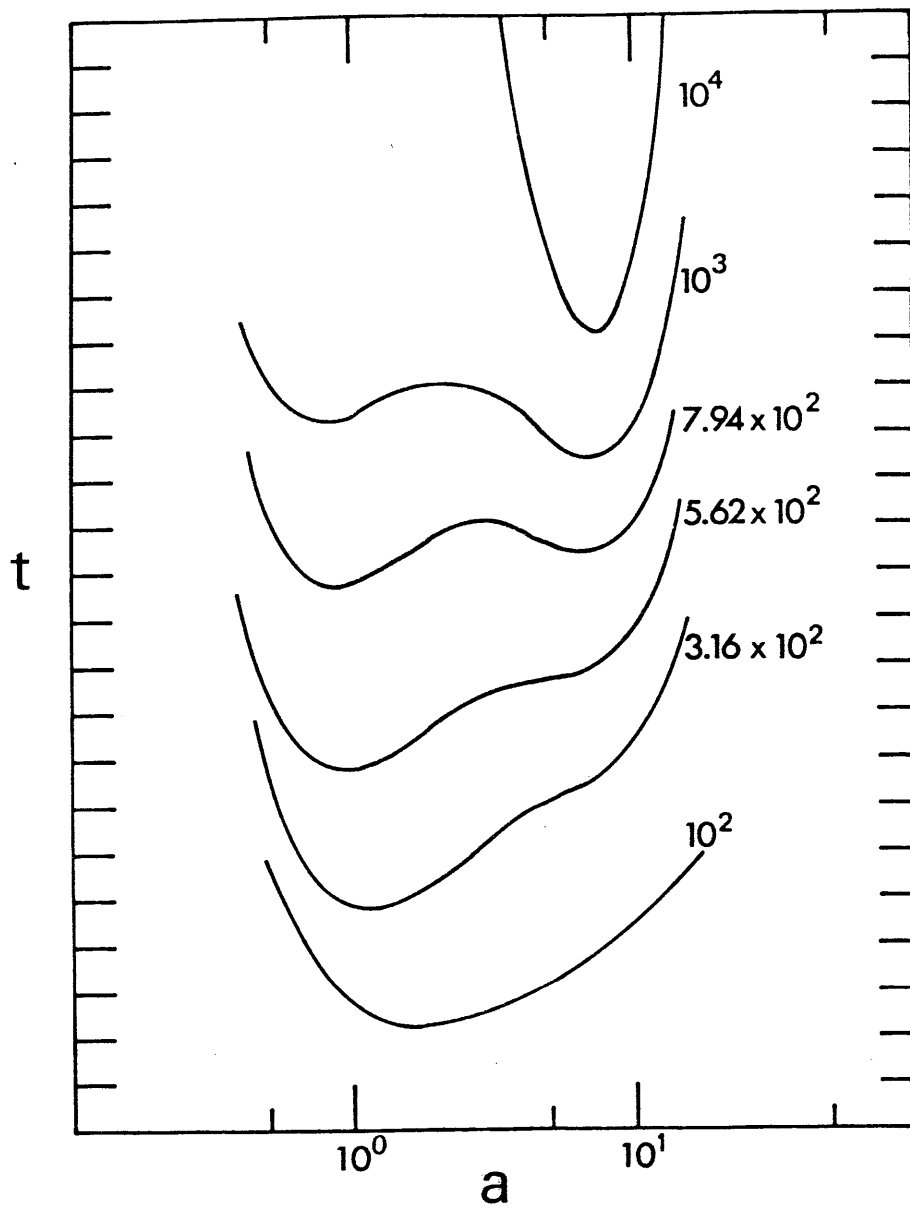


Fig. 4.10

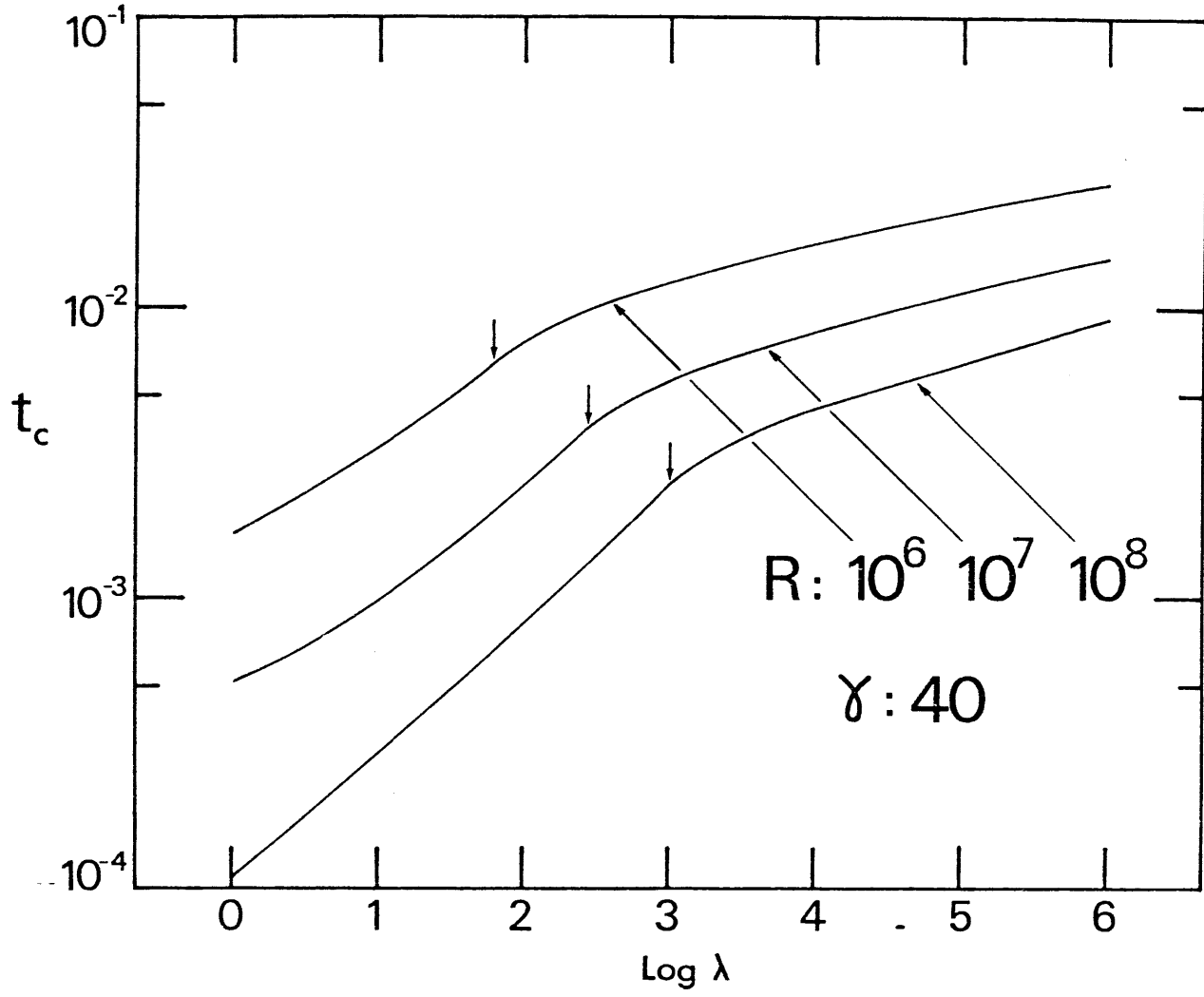


Fig. 4.11

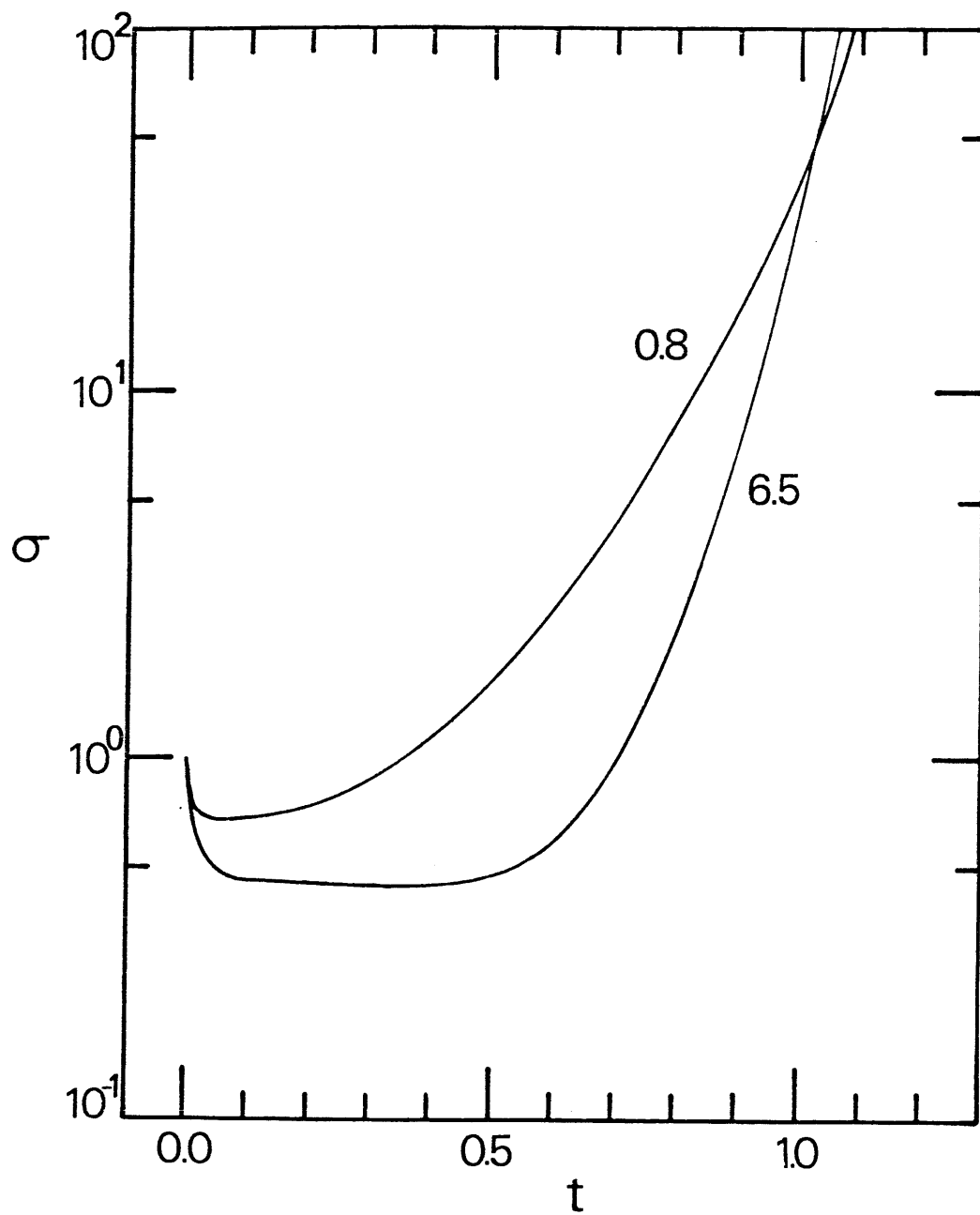


Fig. 4.12

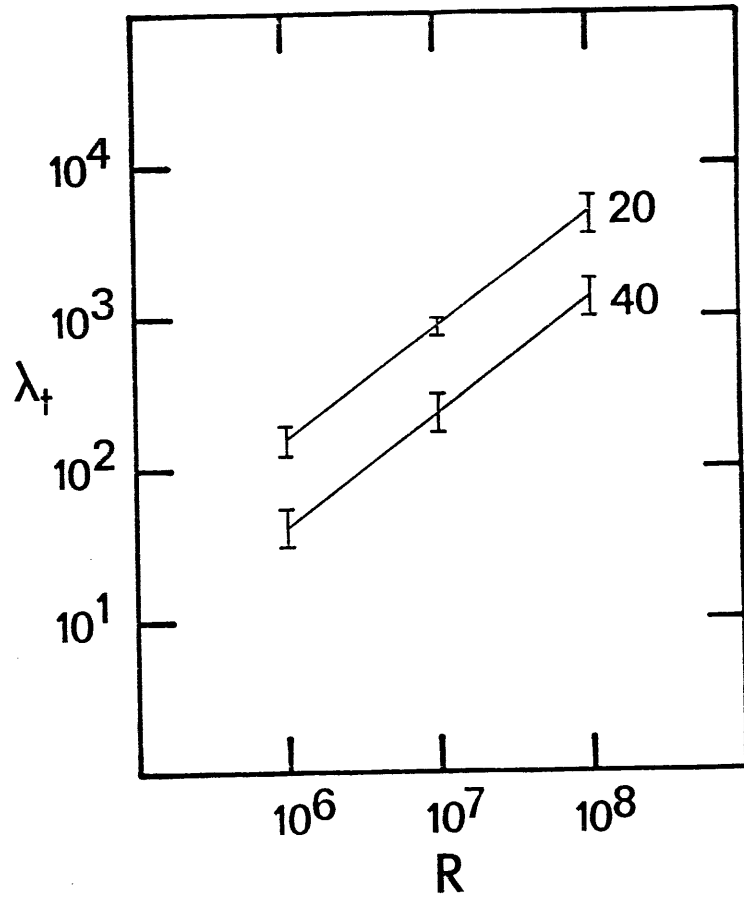


Fig. 4.13

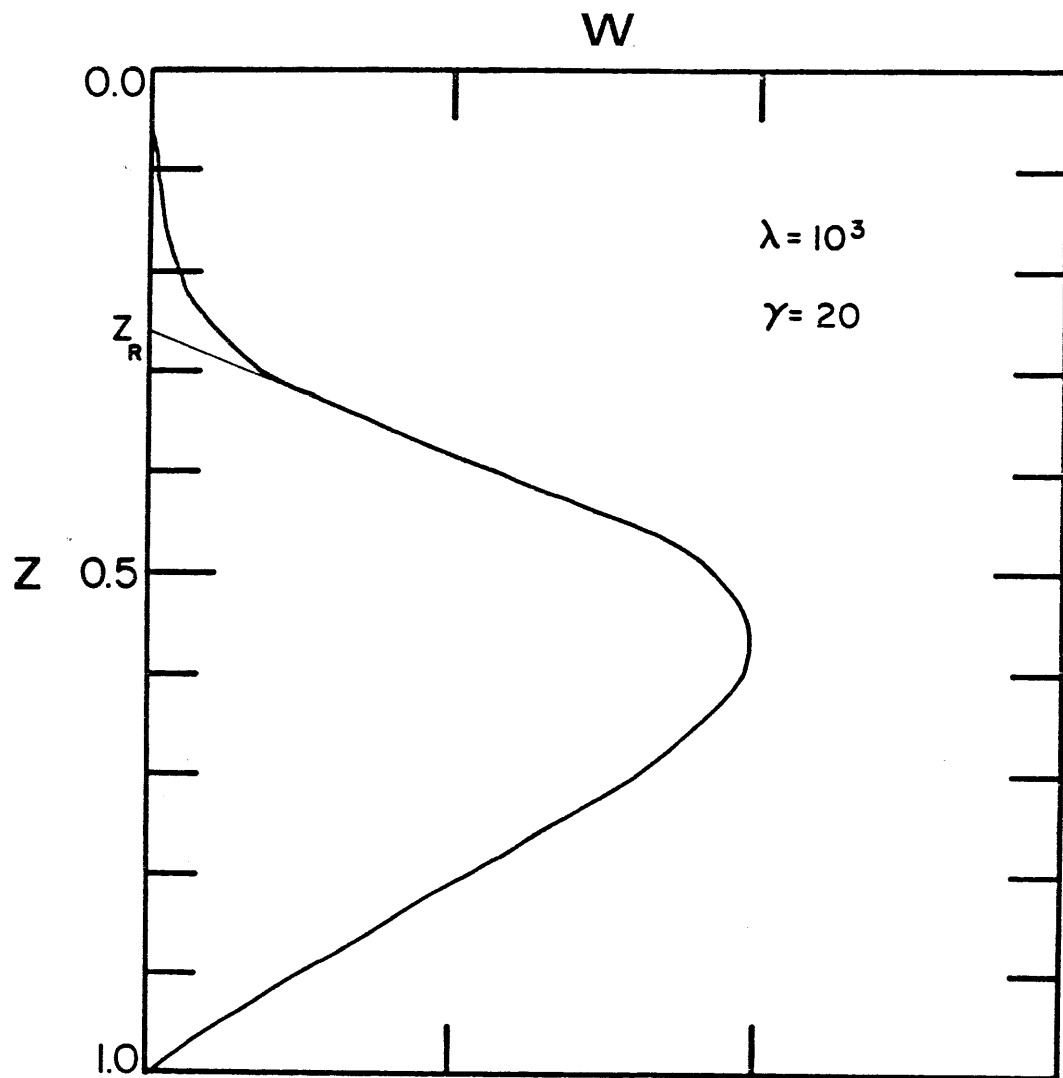


Fig. 4.14

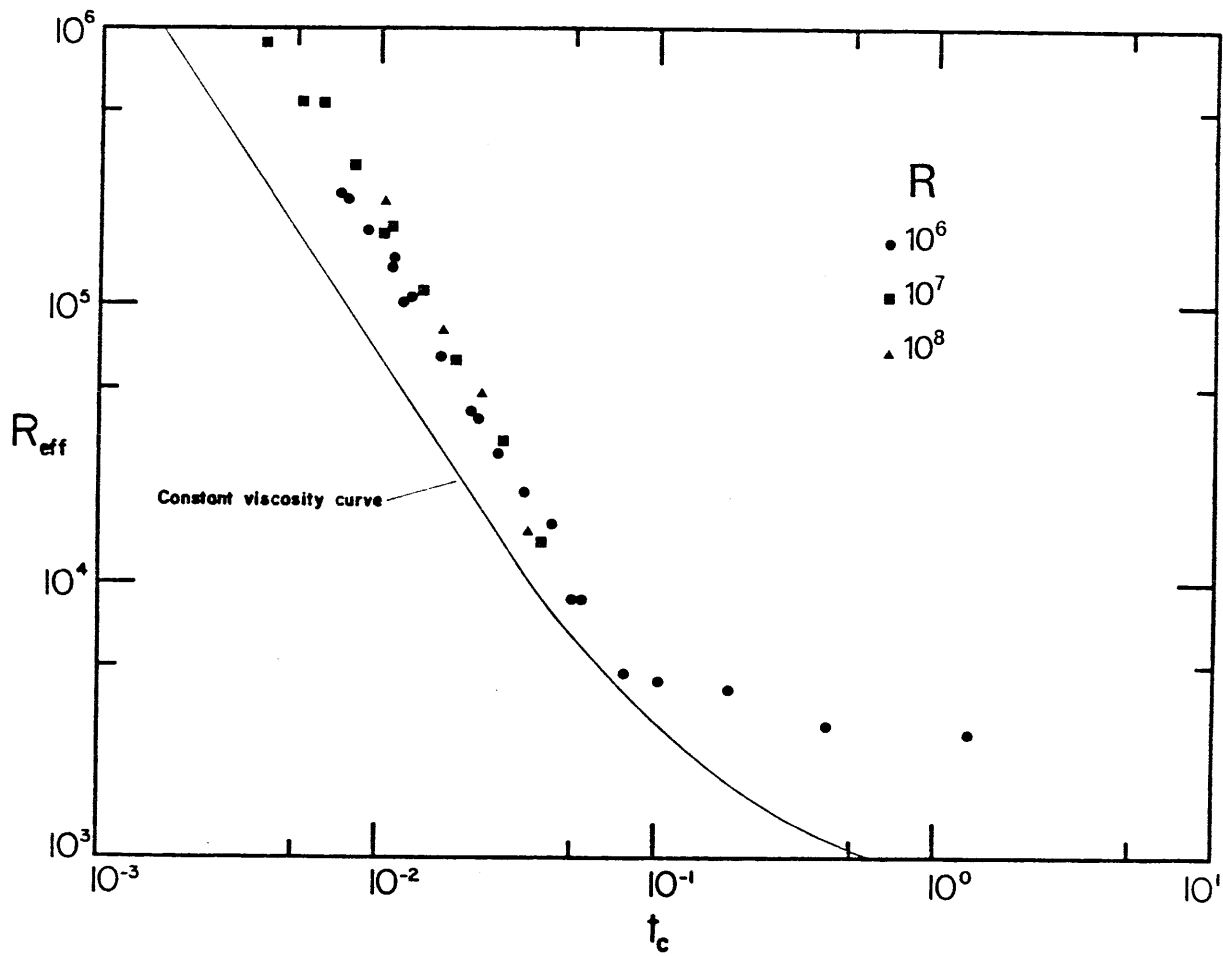


Fig. 4.15

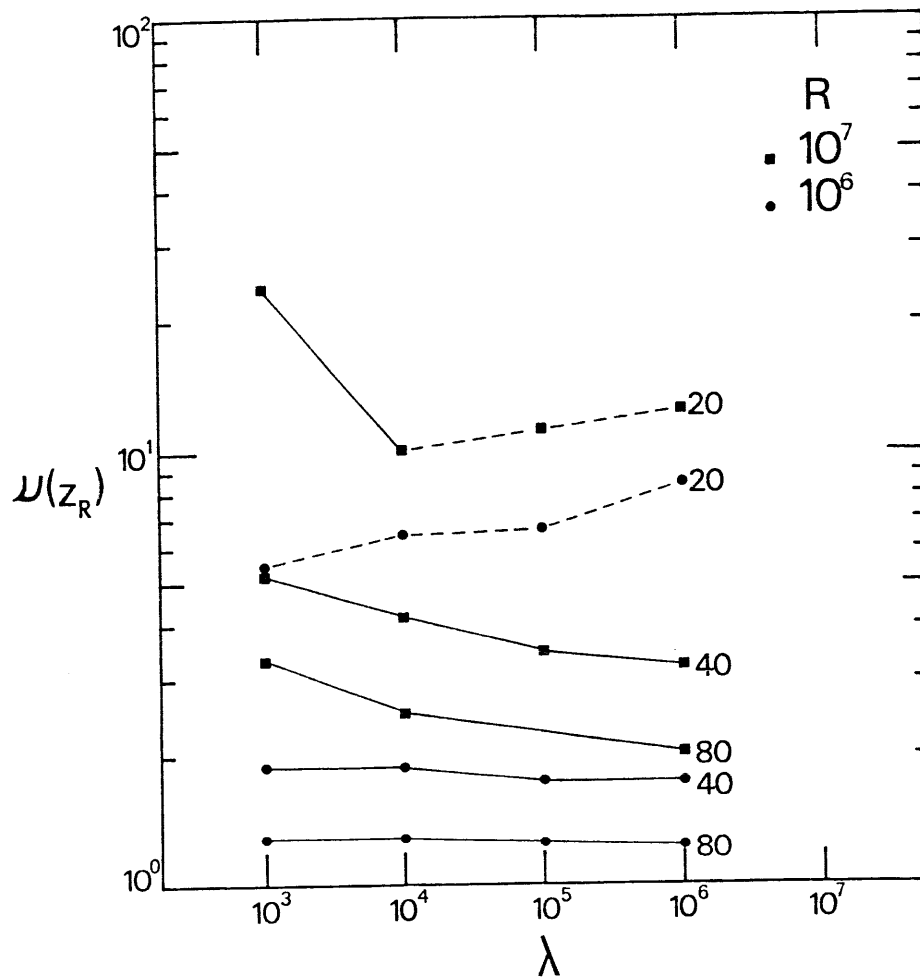


Fig. 4.16

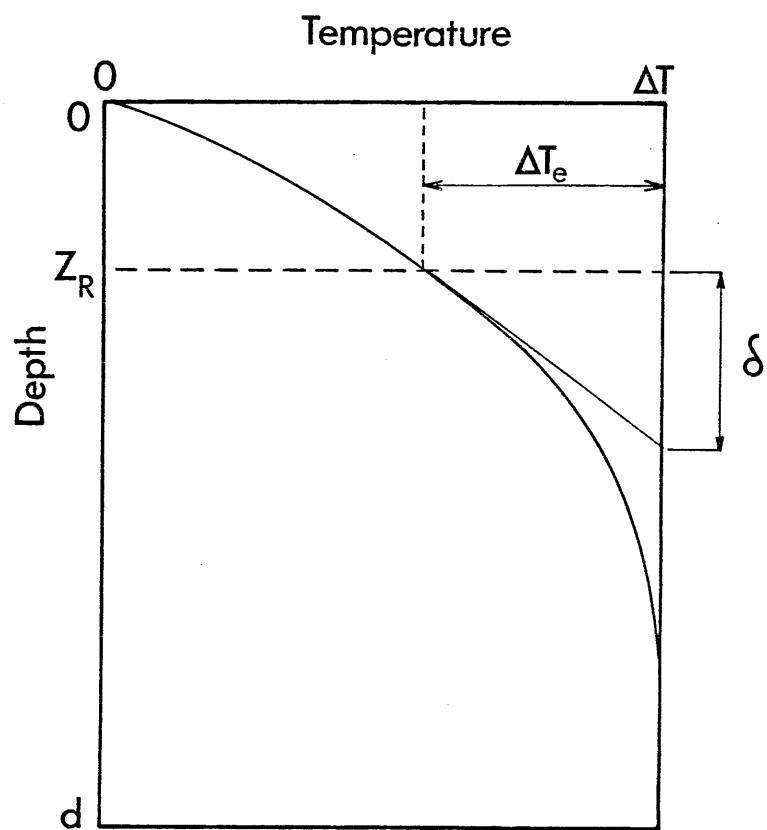


Fig. 4.17

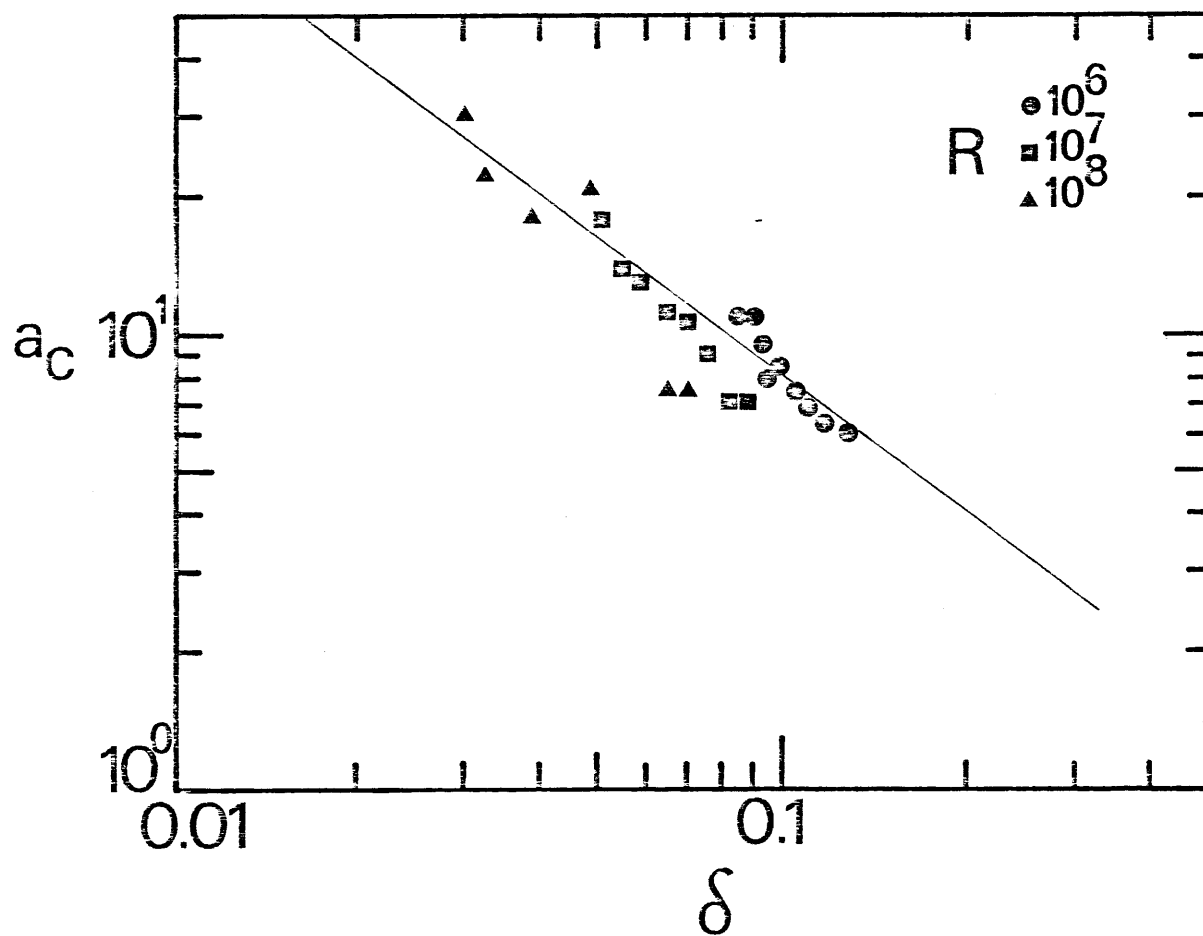


Fig. 4.18

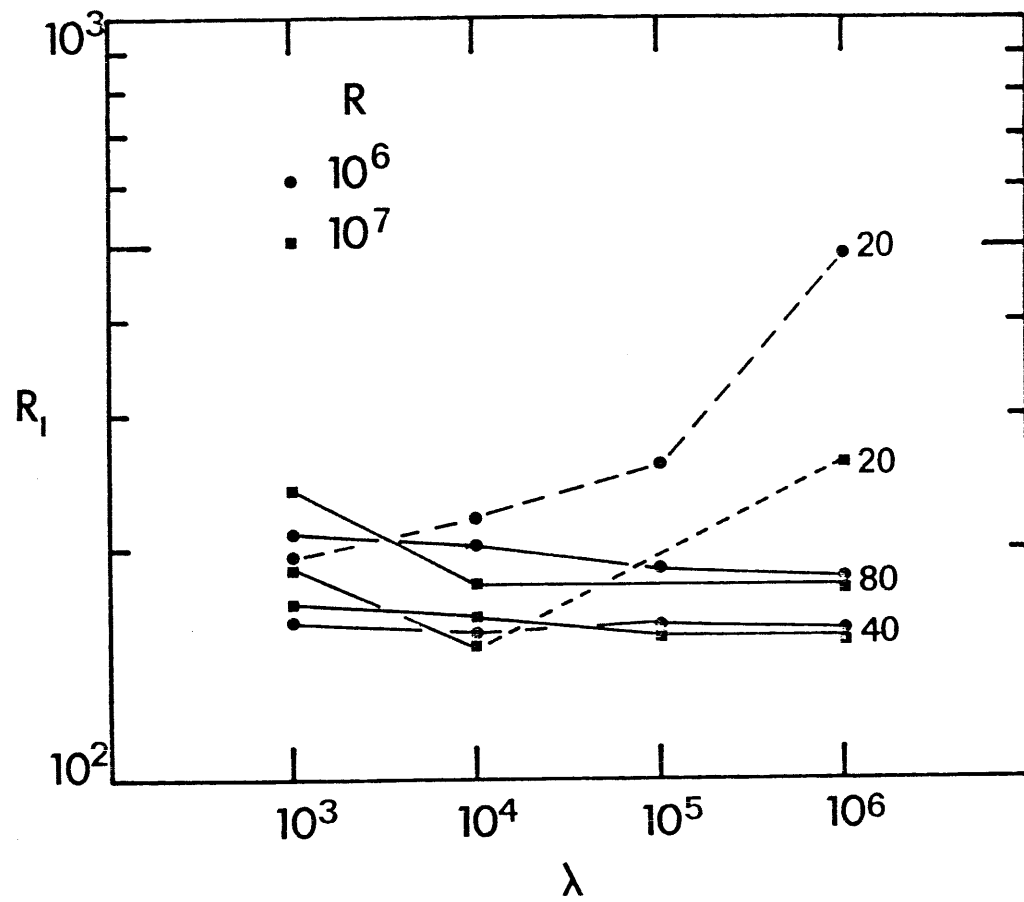


Fig. 4.19

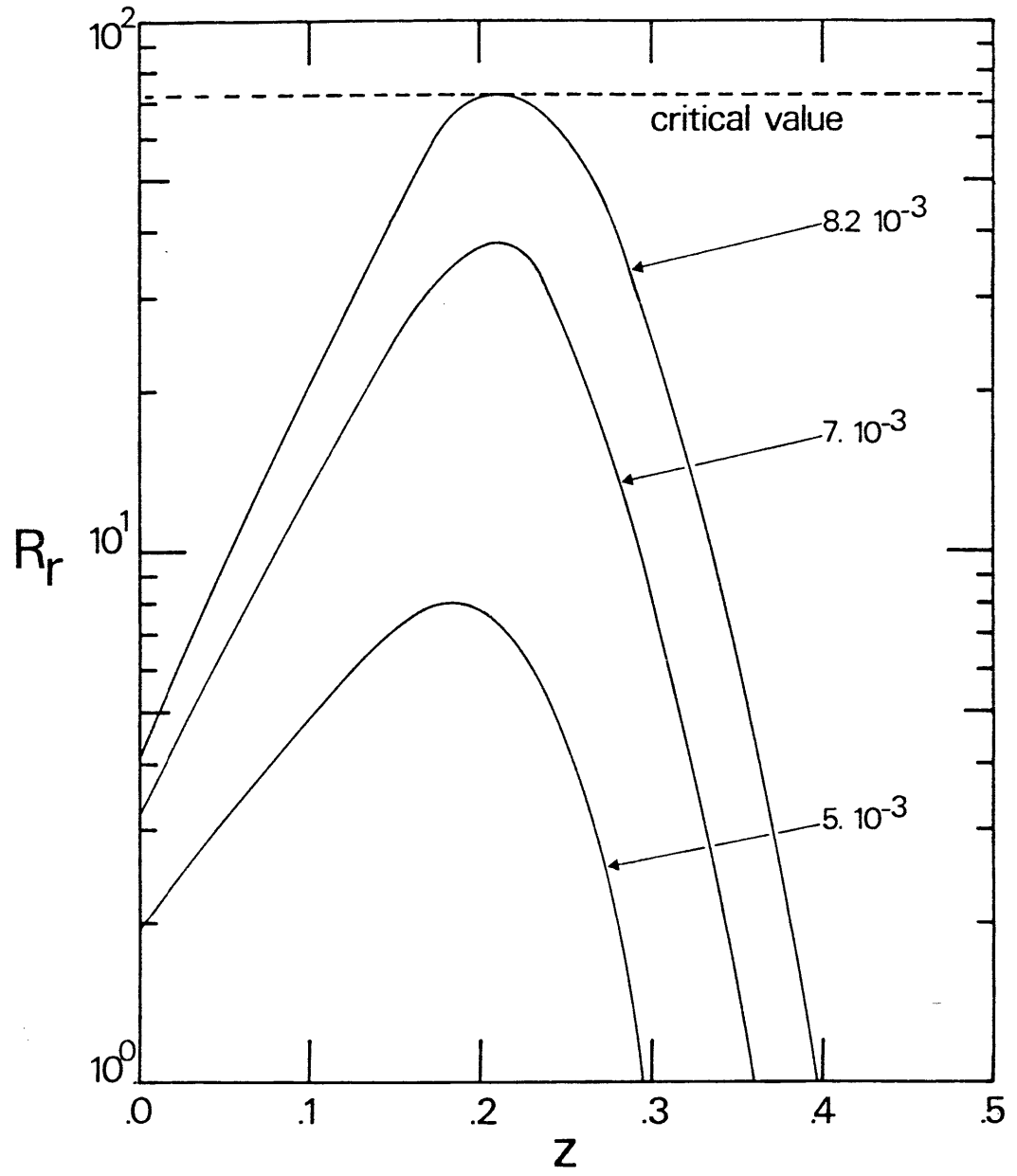


Fig. 4.20

APPENDIX 4.A. EXPRESSIONS FOR THE COUPLING COEFFICIENTS

The velocity and temperature perturbations are written as:

$$w = (\cos ax) \sum_n A_n \sin(n\pi z).$$

$$\theta = (\cos ax) \sum_n C_n \sin(n\pi z)$$

Coefficients A_n and C_n are coupled through equation (4.12). This is written in matrix form:

$$C_n = Q_{nm} A_m$$

with

$$\begin{aligned} -Ra^2 Q_{nm} = & \frac{\delta_{nm}}{2} \left[v_0 (a^2 + n^2 \pi^2)^2 + v_1 \frac{(e^\gamma - 1) \times 4n^2 \pi^2}{\gamma(\gamma^2 + 4n^2 \pi^2)} \right] \\ & + v_1 \gamma \frac{(a^2 + m^2 \pi^2)^2}{2} \left[\frac{e^\gamma \cos(m-n)\pi - 1}{\gamma^2 + (m-n)^2 \pi^2} - \frac{e^\gamma \cos(m+n)\pi - 1}{\gamma^2 + (m+n)^2 \pi^2} \right] \\ & - v_1 \gamma \times (m\pi) (a^2 + m^2 \pi^2) \left[(m^4 + n) \pi \frac{1 - e^\gamma \cos(m+n)\pi}{\gamma^2 + (m+n)^2 \pi^2} + (n-m) \pi \frac{1 - e^\gamma \cos(n-m)\pi}{\gamma^2 + (n-m)^2 \pi^2} \right] \\ & - v_1 \gamma^3 \frac{(m^2 \pi^2 - a^2)}{2} \left[\frac{e^\gamma \cos(m-n)\pi - 1}{\gamma^2 + (m-n)^2 \pi^2} - \frac{e^\gamma \cos(m+n)\pi - 1}{\gamma^2 + (m+n)^2 \pi^2} \right] \end{aligned}$$

APPENDIX 4.B. CONVERGENCE OF THE NUMERICAL SOLUTIONS

We checked the accuracy of our numerical scheme in several ways. We first wrote a program for a constant viscosity fluid having a finite Prandtl number and reproduced the results published by Foster (1965b) for a Prandtl number (Pr) equal to 7. The method was exactly the same as that outlined in the text. This was accomplished in order to understand how results converge as Pr goes to infinity. A limited set of computations may be found in Table 4.B1.

We then wrote the program for the infinite Prandtl number case, and compared its results with those of the previous one in the high Pr limit (Table 4.B1). Throughout the following, N will denote the number of Fourier components used to evaluate the series, and Δt the time-step used to integrate equation (4.9d).

In the constant viscosity limit, the equations have a straightforward analytical solution in the particular case $N=1$. A comparison of the numerical results with those of this expression was exact to the accuracy of the computations (9 places). To illustrate the convergence of the solutions of the numerical scheme, some computations are presented in Figure B1 for a Rayleigh number of 10^8 . The convergence in terms of the critical time t_c is quite rapid, both as a function of N and as a function of Δt (Figure 4.B1). We also checked the smoothness of the eigenfunctions, which is a more stringent constraint (Figure 4.B2).

The behavior of the variable viscosity scheme was asserted routinely by verifying that the eigenfunctions were smooth and by comparing results obtained with N and $(N+10)$ terms in the expansions. We kept the difference below 1%.

Several factors determine the number of Fourier components to be used, but the most important is the Rayleigh number or, more precisely, $\delta(t_c)$ the thickness of the thermal boundary layer at the onset of instability. As is shown by the analysis presented before, the critical wavenumber scales with $\delta(t_c)$, so that the minimum number of Fourier components needed also scales with a_c .

TABLE 4.B1

CRITICAL PARAMETERS AS A FUNCTION OF THE PRANDTL NUMBER Pr

(Calculations made with $R = 10^6$ and $N = 8$)

Pr	7	10^2	10^3	∞
$t(10)$	1.63×10^{-3}	1.09×10^{-3}	9.93×10^{-4}	9.74×10^{-4}
a_c	14	10	6	6

Figure 4.B1. Constant viscosity calculations for a Rayleigh number of 10^8 .

Convergence of the critical time as a function of N and $1/\Delta t$. (Δt is the time step used in the calculations). a is the wavenumber.

Upper curve: runs for $t=2.5 \times 10^{-6}$ ($1/\Delta t = 40 \times 10^4$).

Lower curve: runs for $N=60$.

Figure 4.B2. Constant viscosity calculations for a Rayleigh number of 10^8 .

Temperature perturbation profiles for $n=60$ and $N=100$. N is the number of Fourier components used in the scheme.

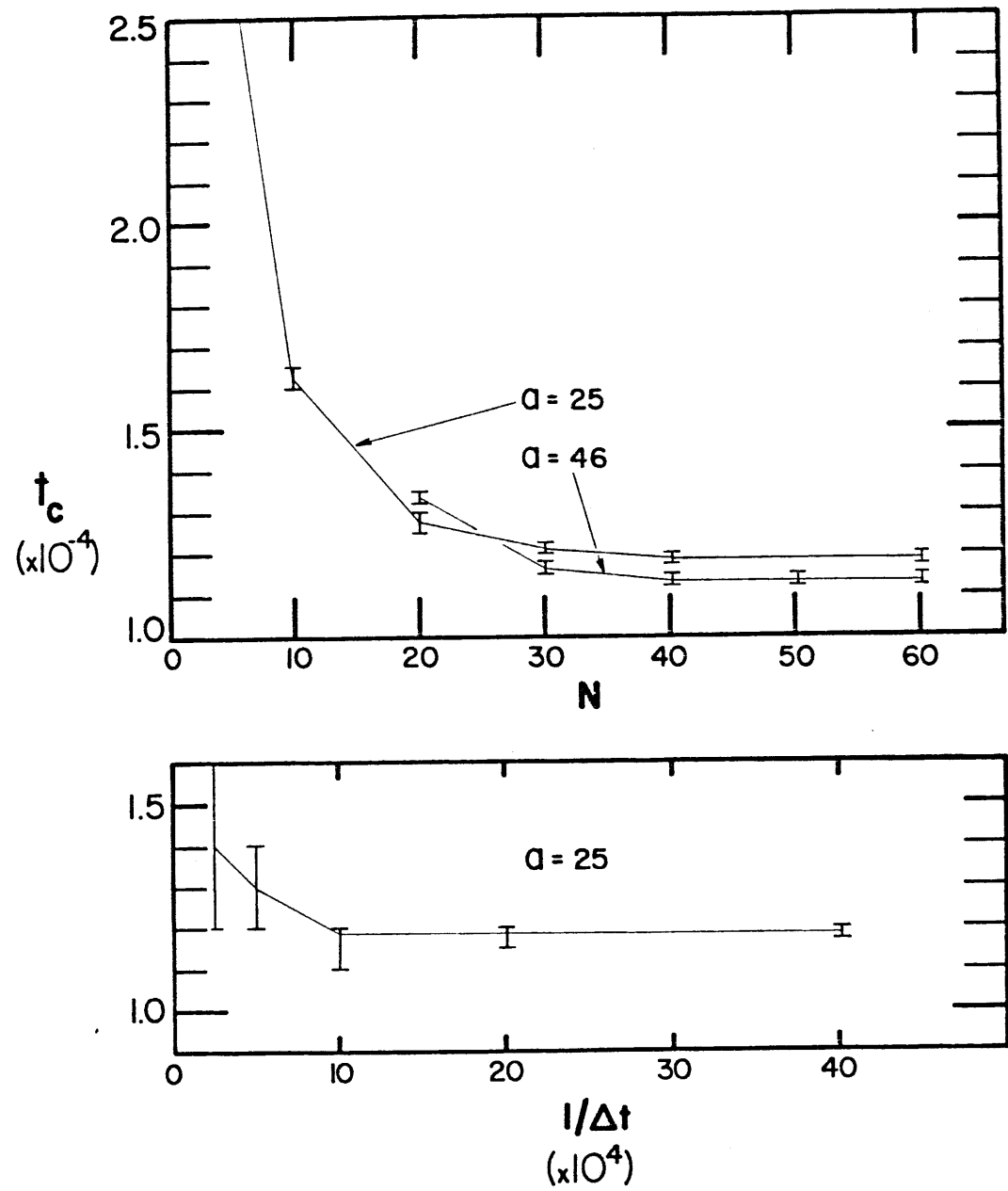


Fig. 4.B1

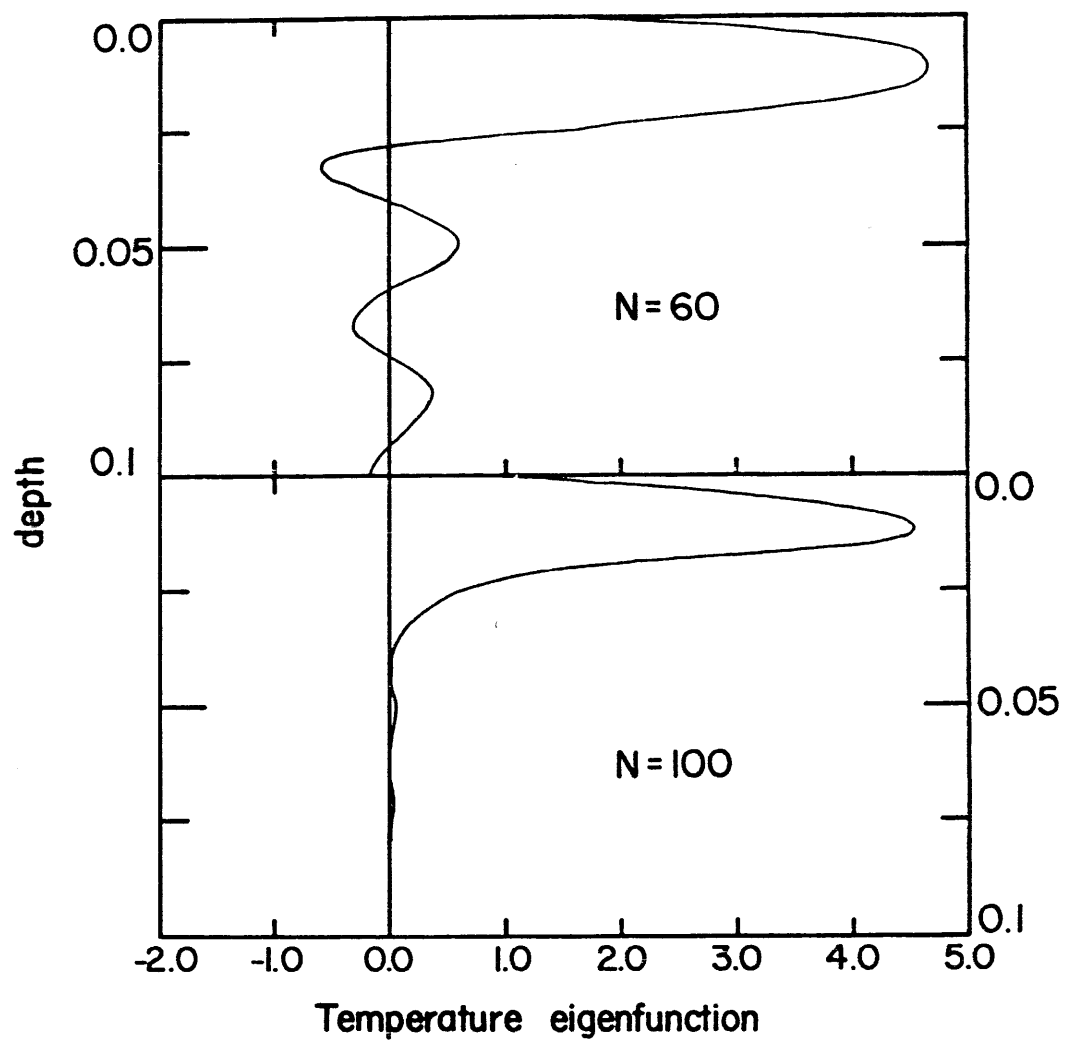


Fig. 4.B2

CHAPTER FIVE
SYNTHESIS AND CONCLUSION

We have shown clearly that the time-scale of the continental heat flow decay is smaller than the rough world-wide analysis indicates. In New Hampshire, there is no evidence for any thermal perturbation having detectable effects on the continental lithosphere over a time span greater than about 300 My. This figure may still be too high as the 200 My old thermal event which resulted in the generation of the huge masses of White Mountain granites has also left no imprint on the heat flow. The seemingly high heat flow which was presumed to characterize New England (see Diment et al., 1972) is the result of a bias in favor of radioactive plutons. The mean heat flow through metasedimentary formations which cover the largest area in New Hampshire is exactly equal to the mean heat flow for old continents determined by Sclater et al. (1980). This rather small time-scale is confirmed by the analysis of the variation of the reduced heat flow with age (Figure 5.1; data from chapter 3). The plot of Figure 5.1 indicates that values of the reduced heat flow are indistinguishable after about 300 My. The larger time-scale indicated by the world heat flow analysis of Sclater et al. (1980) may therefore be due simply to a bias in favor of radioactive terrains. Also, we have shown that the heat flow distribution in New England was more complicated than was suggested by the original investigation of Roy et al. (1968a). We detected two anomalies in the heat flow vs. radioactivity relationship and explained them by the presence at depth of radioactive plutons. This hypothesis is confirmed by gravity and geologic data. Thus local highs may be recorded in a region under equilibrium thermal conditions, and may augment the scatter in the heat flow distribution. The large time-scale may also result from the

effects of erosion (England and Richardson, 1980) and to recurring tectonic episodes at shorter time-scales which have no surface expression (Lachenbruch and Sass, 1977).

The global heat flow data between 0 and 800 My may be fitted to several different models and most probably are explained by some combination of them. We have shown on a typical portion of continental crust that the heat flow distribution is complex. This stresses that it is necessary to examine the measurements in their local geological context before attempting to integrate them in a global model. Given the present state of the art, only the asymptotic value of heat flow for large times is of any definitive value in the estimation of temperatures at depth beneath continents.

We have suggested that the observed correlation between heat flow and radioactivity could be the result of several processes which can be deciphered using heat flow and U, Th and K concentrations data. We have shown that most of the observed variations of the bulk parameter D may be due to superficial processes such as alteration. In young areas, the bulk of the radiogenic heat production is concentrated in a thin upper layer and the data can be explained by the existence of a uniform background heat flow below. In old cratons, the depth-scale D is large and so are the individual depth-scales for uranium and thorium. Thus the reduced heat flow is a reasonable estimate of the heat flow at great depths in the crust and may be considered as close to the mantle heat flow. This is consistent with the fact that the values of the reduced heat flow are remarkably constant in the old continents.

The reduced heat flow shows no variation after 300 My and remains at a value of $0.6 \pm 0.1 \mu\text{cal}/\text{cm}^2 \cdot \text{s}$ ($25 \pm 4 \text{ mW}/\text{m}^2$) (Table 3.1). The range

is not necessarily that large. Part of the scatter may result from the neglect of any correction for Pleistocene glaciation. The need for this correction is still the subject of controversy (Sass et al., 1971; Swanberg et al., 1974). However, all the global climate models of the last ice age, including those based on sea surface temperature data (CLIMAP, 1976) show large temperature decreases in the northern latitudes (Heath, 1979). The southern continents appear to be much less affected presumably because of the continued flow of the circumpolar current (Heath, 1979). The reduced heat flow values in the southern hemisphere are about $0.15 \mu\text{cal}/\text{cm}^2 \text{ s}$ ($6 \text{ mW}/\text{m}^2$) higher than those in the northern hemisphere (Table 5.1). The Pleistocene glaciation applied by Jessop and Lewis (1978) to the Canadian Shield heat flow data raises the reduced heat flow by almost exactly this amount. We conclude that our best estimate for the reduced heat flow on old continents lies between 0.6 and $0.7 \mu\text{cal}/\text{cm}^2 \text{ s}$ (25 and $29 \text{ mW}/\text{m}^2$). This estimate is close to the minimum heat flow observed on continents (Sclater et al., 1980) and is only slightly less than the predicted equilibrium heat flux through the base of the oceanic crust of 0.6 to $0.9 \mu\text{cal}/\text{cm}^2 \text{ s}$ (25 to $38 \text{ mW}/\text{m}^2$) estimated by Sclater et al. (1980).

The best estimate for the mantle heat flow beneath an old continent lies between 0.6 and $0.7 \mu\text{cal}/\text{cm}^2 \text{ s}$ (25 and $29 \text{ mW}/\text{m}^2$). Adding an error of $0.1 \mu\text{cal}/\text{cm}^2 \text{ s}$ ($4 \text{ mW}/\text{m}^2$), we arrive at a total range of 0.5 to $0.8 \mu\text{cal}/\text{cm}^2 \text{ s}$ (21 to $34 \text{ mW}/\text{m}^2$). To compute temperatures at depth beneath an old continent, we assume a value of D equal to 10 km because it is representative of old provinces. From this value and the range in the mantle heat flow estimates, we have calculated the distribution of radioactivity and temperatures corresponding to the mean heat flow on cratons: $1.1 \mu\text{cal}/\text{cm}^2 \text{ s}$ ($46 \text{ mW}/\text{m}^2$). We have selected thermal

conductivities of 6×10^{-3} and 8×10^{-3} cal/cm s°C for crustal and mantle rocks respectively. The mantle value is taken from Lister (1977). At a depth of 100 km, the temperatures range from 900 to 1400°C (Figure 5.2). The range could be narrowed down if the errors on the mantle heat flow values are reduced. Our present bias would favor the higher temperatures.

The oldest ocean floor is close to thermal equilibrium. Parsons and Sclater (1977) have estimated that the equilibrium heat flow was 0.9 ± 0.1 $\mu\text{cal/cm}^2 \text{ s}$ (38 ± 4 mW/m^2). We computed the heat flux at the base of an oceanic geotherm (Figure 5.2) by assuming a 10 km layer of heat generation between 1 and 2×10^{-13} cal/cm³ s (42 and 84 $\mu\text{W/m}^3$). These values yield a range of heat flow of 0.6 to 0.9 $\mu\text{cal/cm}^2 \text{ s}$ (25 to 38 mW/m^2) at the base of the oceanic crust and temperatures ranging from 1000°C to 1500°C at a depth of 125 km (Figure 5.2). Thus the oceanic and continental temperatures overlap significantly at depths greater than about 80 km. The thicker low conductivity continental crust compensates for the slightly higher oceanic geothermal gradient. We conclude that there is no evidence for significant differences between the thermal structures of the old oceanic and the old continental parts of a plate. Therefore the thicknesses of the corresponding lithospheres may also be similar. This conclusion is consistent with the relatively small time constant of the continental heat flow decay.

The thermal and mechanical definitions of a plate are distinct, as was emphasized by Parsons and McKenzie (1978) and Bottinga and Steinmetz (1979), although they are related through the thermal structure. We have shown in the fourth chapter of this thesis that the thickness of the layer which behaves rigidly beneath oceans is essentially a function of the viscosity structure. The viscosity structure of the upper mantle remains

poorly determined on the large scale required for our purposes and our analysis has placed constraints on it rather than yielding definitive conclusions. However, the observations on the similarity between the thermal structures at intermediate depths around 100 km for both oceans and continents (Figure 5.2) would suggest that this depth range marks the transition between the rigid upper layer where heat transfer is conductive and the lower mantle where heat transfer is convective. If the transition depth is significantly larger than 100-150 km under continents, then there would be differences between continents and oceans at great depths.

We conclude that heat flow data are easy to account for by a model of the oceanic and continental mantle where the lithosphere consists of a rigid mechanical layer underlain by a thermal convecting boundary layer. In such a model, the mechanical layer extends to a depth smaller than 125 km, i.e. the plate thickness determined from bathymetry and reliable heat flow data (Parsons and Sclater, 1977), but the convecting boundary layer to 100-200 km (see Parsons and McKenzie, 1978). The thickness of both layers is roughly inversely proportional to the equilibrium heat flux which is still approximate. Small long wavelengths variations in this heat flux would be associated with corresponding variations in the boundary layer thicknesses. We plot in Figure 5.2 the oceanic geotherm determined using the analysis of Parsons and McKenzie and a value of $0.75 \mu\text{cal}/\text{cm}^2 \text{ s}$ ($31 \text{ mW}/\text{m}^2$) for the background heat flow. In agreement with the preceding discussion, this geotherm is compatible with both continental and oceanic estimates.

TABLE 5.1

A COMPARISON OF THE REDUCED HEAT FLOW VALUES FOR OLD SHIELD
PROVINCES OF THE NORTHERN AND SOUTHERN HEMISPHERES

Northern Hemisphere		Southern Hemisphere	
Province	Q_r	Q_r	Province
Ukrainian Shield ⁺	0.60 (25)	0.67 (28)	Brazilian Shield
Baltic Shield	0.53 (22)	0.64 (27)	Central Australia
Canadian Shield	0.50 (21)	0.63 (26)	Western Australia

Q_r is the reduced heat flow in $\mu\text{cal}/\text{cm}^2 \text{ s}$ (mW/m^2).

⁺It is probable that the Ukrainian Shield was subjected to temperature changes significantly smaller than in the Baltic and Canadian Shields (Heath, 1979).

References are: Swanberg et al. (1974), Kutas (1977), Jessop and Lewis (1978), Sass and Lachenbruch (1979), Vitorello et al. (1980).

FIGURE CAPTIONS

Figure 5.1. Reduced heat flow as a function of age. The circles are unreliable estimates from the younger heat flow provinces. The theoretical heat flow (assuming the plate model) through ocean crust with the crustal contribution subtracted is presented as the dashed curve.

Figure 5.2. Predicted range in geotherms beneath oceans and continents. The heavy line is the presumed temperature structure beneath old oceans.

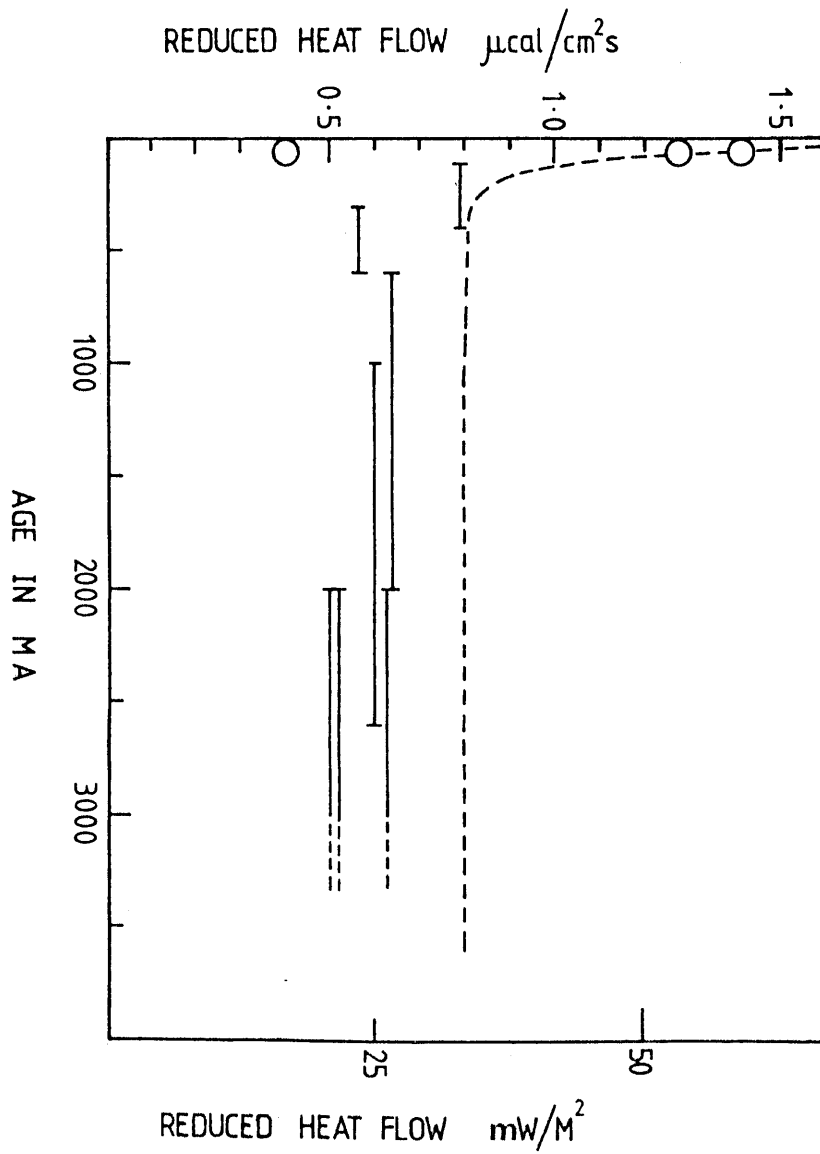


Fig. 5.1

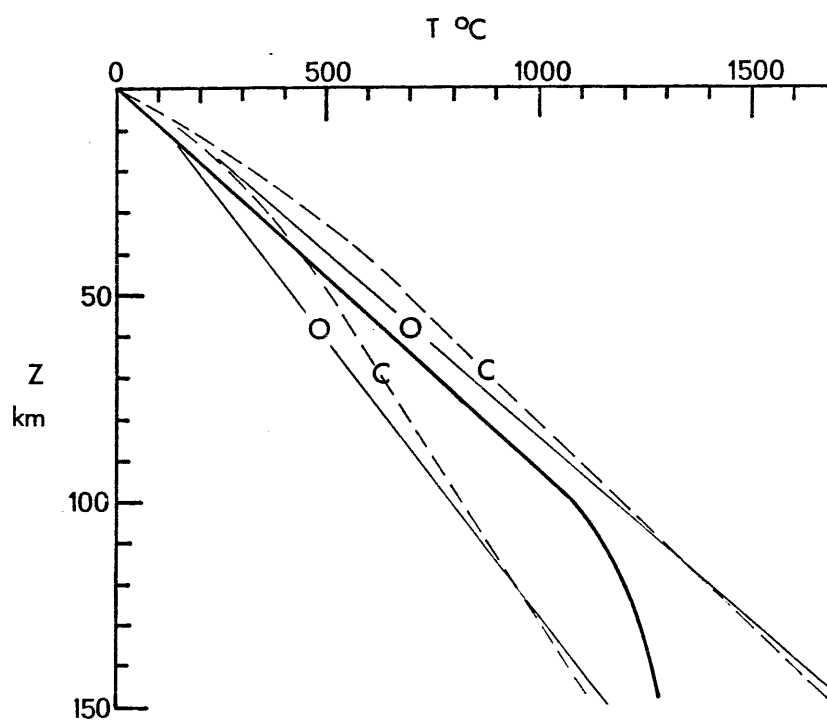


Fig. 5.2

REFERENCES

- Adams, J.A.S. and P. Gasparini, Gamma-ray spectrometry of rocks, Amsterdam, 295 pp., 1970.
- Albarede, F., The heat flow/heat generation relationship: an interaction model of fluids with cooling intrusions, *Earth Planet. Sci. Lett.* 27, 73-78, 1975
- Aleinikoff, J.N., Petrochemistry and tectonic origin of the Ammonoosuc volcanics, N.H.-Vermont, *Bull. Geol. Soc. Am.*, 88, 1546-1552, 1977
- Aleinikoff, J.N., R.E. Zartman and J.B. Lyons, U-Th-Pb geochronology of the Massabessic gneiss and the granite near Milford, South-Central New Hampshire. New evidence for Avalonian basement and Taconic and Alleghenian disturbances in Eastern New England, *Contrib. Mineral. Petrol.* 71, 1-11, 1979
- Allis, R.G., and G.D. Garland, Heat flow measurements under some lakes in the Superior Province of the Canadian Shield, *Can. J. Earth Sci.*, 16, 1951-1964, 1979
- Arth, G., and G. Hanson, Quartz diorites derived by partial melting of eclogite or amphibolite at mantle depths, *Contrib. Mineral. Petrol.*, 37, 161-174, 1972
- Ashby, M.F., and R.A. Verrall, Micromechanisms of flow and fracture and their relevance to the rheology of the upper mantle, *Phil. Trans. Roy. Soc. Lond.*, 288A, 59-95, 1978
- Ave Lallemand, H.G., J-C.C. Mercier, N.L. Carter and J.V. Ross, Rheology of the upper mantle: inferences from peridotite xenoliths, *Tectonophysics*, 70, 85-113, 1980

- Bailey, R.C., R.N. Edwards, G.D. Garland and J.P. Greenhouse, Geomagnetic sounding of eastern North America and the White Mountain heat flow anomaly, *Geophys. J. R. Astron. Soc.*, 55, 499-502, 1978
- Barbier, M.J., Continental weathering as a possible origin of vein-type uranium deposits, *Mineral. Deposita.*, 9, 271-288, 1974
- Billings, M.D., The geology of New Hampshire, Part II: bedrock geology, The New Hampshire Department of Resources and Economic Development, Concord, N.H., 1956
- Birch, F., R.F. Roy and E.R. Decker, Heat flow and thermal history in New England and New York, in: Studies of Appalachian Geology, E. An-Zen, ed., Interscience, New York, 437-451, 1968
- Blair, L.M., and J.A. Quinn, The onset of cellular convection in a fluid layer with time-dependent density gradients, *J. Fluid. Mech.*, 36, 385-400, 1969
- Bothner, W.A., Gravity study of the Exeter pluton, southeastern New Hampshire, *Geol. Soc. Am. Bull.*, 85, 51-56, 1974
- Bottinga, Y., and L. Steinmetz, A geophysical, geochemical, petrological model of the submarine lithosphere, *Tectonophysics*, 55, 311-347, 1979
- Brimhall, W.H., and J.A.S. Adams, Concentration changes in Th, U and other metals in hydrothermally altered Conway granite, New Hampshire, *Geochim. Cosmochim. Acta*, 33, 1308-1311, 1969
- Buchbinder, G., and G. Poupinet, P-wave residuals in Canada, *Can. J. Earth Sci.*, 14, 1292-1304, 1977
- Bunker, C.M., C.A. Bush, R.J. Munroe and J.H. Sass, Abundances of uranium, thorium and potassium for some Australian crystalline rocks, Open-File Rep. 75-393, U.S. Geol. Surv., 39 pp., Menlo Park, California, 1975

- Buntebarth., G., Distribution of uranium in intrusive bodies due to combined migration and diffusion, *Earth Planet. Sci. Lett.*, 32, 84-90, 1976
- Burwash, R.A., and P.A. Cavell, Uranium-thorium enrichment in alkali-olivine basalt magma, Simpson Islands Dyke, North-West Territories, Canada, *Contrib. Mineral. Petrol.*, 66, 243-250, 1978
- Cathles, L.M., The viscosity of the Earth's mantle, Princeton University Press, Princeton, N.J., 1975
- Chandrasekhar, S., Hydrodynamic and Hydromagnetic Stability, Oxford University Press, 1961
- Chapman, C.A., Structural evolution of the White Mountain Magma Series, *G.S.A. Memoir* 146, 281-300, 1976
- Chapman, C.J., and M.R.E. Proctor, Non-linear Rayleigh-Benard convection between poorly conducting boundaries, *J. Fluid. Mech.*, 101, 759-782, 1980
- Chapman, C.J., S. Childress and M.R.E. Proctor, Long wavelength thermal convection between non-conducting boundaries, *Earth Planet. Sci. Lett.* 51, 362-369, 1980
- Chopra, P.N., and M.S. Paterson, The experimental deformation of dunite, Submitted to *Tectonophysics*, 1980
- Clark, S.P. Jr, Comment on 'Erosion, uplift, exponential heat source distribution and transient heat flux' by T.C. Lee, *J. Geophys. Res.*, 85, 2694-2695, 1980
- CLIMAP, The surface of the ice-age earth, *Science*, 191, 1131-1137, 1976
- Combs, J., and G. Simmons, Terrestrial heat flow determinations in the North Central United States, *J. Geophys. Res.*, 78, 441-451, 1973

- Corbel, J., Vitesse de l'erosion, *Z. Geomorphol.*, 3, 1-28, 1959
- Costain, J.K., Relationship between surface heat generation and surface heat flow, in: Evaluating and targeting of geothermal energy sources in the southeastern United States, Progress Report, U.S. Department of Energy, C17-C22, 1977
- Currie, I.G., The effect of heating rate on the stability of stationary fluids, 29, 337-347, 1967
- Dewey, J.F. and W.S Kidd, Continental collisions in the Appalachian Orogenic belt. Variations related to complete and uncomplete suturing, *Geology*, 2, 5430-5461, 1974
- Diment, W.H., T.C. Urban and F.A Revetta, Some geophysical anomalies in the eastern United States, in: The Nature of the Solid Earth, Robertson E., ed., McGraw Hill, New York, 544-574, 1972
- Elder, J.W., The unstable thermal interface, *J. Fluid. Mech.*, 32, 69-96, 1968
- England, P.C., and S.W. Richardson, Erosion and the age dependence of continental heat flow, *Geophys. J. R. Astron. Soc.*, 62, 421-437, 1980
- England, P.C., E.R. Oxburgh and S.W. Richardson, Heat refraction and heat production in and around granite plutons in north-east England, *Geophys. J. R. Astron. Soc.*, 62, 439-455, 1980
- Feves, M., G. Simmons and R.W. Siegfried, Microcracks in crustal igneous rocks, in: The Earth's crust, *Geophys. Monogr.*, vol. 20, J.G. Heacock ed., A.G.U., Washington, D.C., 95-117, 1977
- Foland, K.A. and H. Faul, Ages of the White Mountain intrusives, New Hampshire, Vermont and Maine, U.S.A., *Am. J. Sci.*, 277, 888-904, 1977

- Foland, K.A., and I. Friedman, Application of Sr and O isotope relations to the petrogenesis of the alkaline rocks of the Red Hill complex, N.H., U.S.A., *Contrib. Mineral. Petrol.*, 65, 213-225, 1977
- Forsyth, D.W., The evolution of the upper mantle beneath mid-ocean ridges, *Tectonophysics*, 38, 89-118, 1977
- Foster, T.D., Onset of convection in a layer of fluid cooled from above, *Phys. Fluids*, 8, 1770-1774, 1965a
- Foster, T.D., Stability of a homogeneous fluid cooled uniformly from above, *Phys. Fluids*, 8, 1249-1257, 1965b
- Foster, T.D., Effect of boundary conditions on the onset of convection, *Phys. Fluids*, 11, 1257-, 1968
- Foster, T.D., Convection in a variable viscosity fluid heated from within, *J. Geophys. Res.*, 74, 685-693, 1969
- Gaudette, H.E., A.W. Fairbairn, A. Kovocho and A.M. Hussey, Preliminary Rb-Sr whole-rock age determinations of granitic rocks in southwestern Maine, *Geol. Soc. Am. Abs.*, 7, 62-63, 1975
- Glikson, A.Y., and I.B. Lambert, Vertical zonation and petrogenesis of the early Precambrian crust in Western Australia, *Tectonophysics*, 30, 55-89, 1976
- Goetze, C., The mechanisms of creep in olivine, *Phil. Trans. R. Soc. Lond.*, 288A, 99-119, 1978
- Goss, R.D., Empirical relationships between thermal conductivity and other physical parameters in rocks, unpublished Ph.D. thesis, University of California at Riverside, 1974
- Gresho, P.M., and R.L. Sani, The stability of a fluid layer subjected to a step change in temperature: transient vs. frozen time analyses, *Int. J. Heat Mass Transfer*, 14, 207-221, 1971

- Heath, G.R., Simulations of a glacial paleoclimate by three different atmospheric general circulation models, *Paleogeography, Paleoclimatology, Paleoecology*, 26, 291-303, 1979
- Heier, K.S., and G.K. Billings, Potassium, in: Handbook of Geochemistry, K.H. Wedepohl ed., Springer Verlag, Berlin, 19B-19N, 1970
- Hewitt, J.M., D.P. McKenzie and N.O. Weiss, Large aspect ratio cells in two-dimensional thermal convection, *Earth Planet. Sci. Lett.*, 51, 370-, 1980
- Horai K., and G. Simmons, Seismic travel-time anomalies due to anomalous heat flow and density, *J. Geophys. Res.*, 73, 7577-7588, 1968
- Horai, K., and S. Baldrige, Thermal conductivity of nineteen igneous rocks I. Application of the needle-probe method to the measurement of the thermal conductivity of rock, *Phys. Earth Planet. Inter.*, 5, 151-156, 1972
- Houseman, G., and D.P. McKenzie, Numerical experiments on the onset of convective instability in the Earth's mantle, Submitted to *Geophys. J. R. Astron. Soc.*, 1980
- Howard, L.N., Convection at high Rayleigh numbers, in: Proceedings of the 11th International Congress of Applied Mechanics, H. Gortler ed., Springer Verlag, New York, 1109-1115, 1966
- Hurle, D.T.J., E. Jakeman and E.R. Pike, On the solution of the Benard problem with boundaries of finite conductivity, *Proc. R. Soc. Lond.*, 296A, 469-475, 1967
- Hurley, P.M., Direct radiometric measurement, *Bull. Geol. Soc. Am.*, 67, 395-420, 1956

- Hyndman, R.D., I.B. Lambert, K.S. Heier, J.C. Jaeger and A.E. Ringwood,
Heat flow and surface radioactivity measurements in the Precambrian
Shield of Western Australia, *Phys. Earth Planet. Inter.*, 1,
129-135, 1968
- Jaeger, J.C., Heat flow and radioactivity in Australia, *Earth Planet. Sci.
Lett.*, 8, 285-292, 1970
- Jarvis, G.T., and W.R. Peltier, Oceanic bathymetry profiles flattened by
radiogenic heating in a convecting mantle, *Nature*, 285, 649-651, 1980
- Jessop, A.M., The distribution of glacial perturbation of heat flow in
Canada, *Can. J. Earth Sci.*, 8, 711-716, 1971
- Jessop, A.M., and T. Lewis, Heat flow and heat generation in the Superior
Province of the Canadian Shield, *Tectonophysics*, 50, 55-77, 1978
- Joyner, W.B., Gravity in North-Central New England, *Geol. Soc. Am. Bull.*,
74, 831-857, 1963
- Kane, M.F., G. Simmons, W.H. Diment, M.N. Fitzpatrick, W.B. Joyner and
R.W. Bromery, Bouguer gravity and generalized geologic map of New
England and adjoining areas, U.S.G.S. Geophys. Div., Map GP.839, 1972
- Kasameyer, P.W., Low-frequency magnetotelluric survey of New England,
unpublished Ph.D. thesis, Massachusetts Institute of Technology, 1974
- King, P.B., Tectonic map of North America, scale 1:5.000.000, U.S.G.S.,
Washington, D.C., 1969
- King, W. and G. Simmons, Heat flow near Orlando, Florida, and Uvalde, Texas
determined from well cuttings, *Geothermics*, 1, 133-139, 1972
- Kutas, R.I., Investigation of heat flow in the territory of the Ukraine,
Tectonophysics, 41, 139-145, 1977
- Lachenbruch, A.H., Preliminary geothermal model of the Sierra Nevada, J.
Geophys. Res., 73, 6977-6989, 1968

- Lachenbruch, A.H., The effect of 2-D topography on superficial thermal gradients, U.S.G.S. Bull. 1203-E, 86, 1969
- Lachenbruch, A.H., Crustal temperatures and heat production: implications of the linear heat flow relation, J. Geophys. Res., 75, 3291-3300, 1970
- Lachenbruch, A.H., and C.M. Bunker, Vertical gradients of heat production in the continental crust, 2, Some estimates from borehole data, J. Geophys. Res., 76, 3852-3860, 1971
- Lachenbruch, A.H., and J.H. Sass, Heat flow in the United States and the thermal regime of the crust, in: The Earth's crust, Geophys. Monogr., vol.20, J.G. Heacock ed., A.G.U., Washington, D.C., 626-675, 1977
- Lambert, I.B., and K.S. Heier, The vertical distribution of uranium, thorium and potassium in the continental crust, Geochim. Cosmochim. Acta, 31, 377-390, 1967
- Langmuir, D., and J.S. Herman, The mobility of thorium in natural waters at low temperatures, Geochim. Cosmochim. Acta, 44, 1753-1766, 1980
- Lee, T.C., Erosion, uplift, exponential heat source distribution and transient heat flux, J. Geophys. Res., 84, 585-590, 1979
- Lick, W., The instability of a fluid layer with time-dependent heating, J. Fluid Mech., 21, 265-276, 1965
- Lister, C.R.B., Estimators for heat flow and deep rock properties based on boundary layer theory, in: Heat Flow and Geodynamics, A.M. Jessop ed., Tectonophysics, 41, 157-171, 1977
- Loiselle, M., Geochemistry and petrogenesis of the Belknap Mountains Complex and Pliny Range, White Mountain Series, New Hampshire, unpublished Ph.D. thesis, Massachusetts Institute of Technology, 1978

- Lubimova, E.A., B.G. Polyak, Ya.B. Smirnov, R.I. Kutas, F.V. Firsov, S.I. Sergienko and L.N. Liusova, Heat flow in the USSR, in: Catalogue of data, 1964-1972, Soviet Geophysical Committee, Academy of Sciences of the USSR, Moscow, 1973
- Ludwig, K.R., and J.S. Stuckless, Uranium lead isotopes systematics and apparent ages of zircons and other minerals in Precambrian granitic rocks, Granite Mountains, Wyoming, Contrib. Mineral. Petrol., 65, 243-254, 1978
- Lyons, J.B., Distribution of thorium and uranium in three early Paleozoic plutonic series of New Hampshire, U.S.G.S. Bull., 1144-F, 43pp., 1964
- Lyons, J.B., Geological map of New Hampshire, unpublished map, 1978
- Lyons, J.B., and D.E. Livingston, Rb-Sr age of the New Hampshire plutonic series, Bull. Geol. Soc. Am., 88, 1808-1812, 1977
- McKenzie, D.P., J.M. Roberts and N.O. Weiss, Convection in the Earth's mantle: towards a numerical simulation, J. Fluid Mech., 62, 465-538, 1974
- Mahler, E.G., R.S. Schechter and E.H. Wissler, Stability of a fluid layer with time-dependent density gradients, Phys. Fluids, 11, 1901-1912, 1968
- Mercier, J-C. C., Magnitude of continental lithospheric stresses inferred from rheomorphic petrology, J. Geophys. Res., 85, 6293-6303, 1980
- Miller, W.R., and J.I. Drever, Chemical weathering and related controls on surface water chemistry, Geochim. Cosmochim. Acta, 41, 1693-1702, 1977
- Moench, R.H., and R.E. Zartman, Chronology and styles of multiple deformation, plutonism and polymetamorphism in the Merrimack Synclinorium of Western Maine, Geol. Soc. Am. Bull. mem. 146, 203-238, 1976

- Morton, B.R., On the equilibrium of a stratified layer of fluid, *Quart. J. Mech. Appl. Math.*, 10, 433-447, 1957
- Naylor, R.S., Acadian orogeny: an abrupt and brief event, *Science*, 172, 558-560, 1971
- Nield, D.A., The onset of transient convective instability, *J. Fluid. Mech.* 71, 441-454, 1975
- Nielson, D.L., R.G. Clark, J.B. Lyons, E.J. Englund and D.J. Borns, Gravity models and mode of emplacement of the New Hampshire plutonic series, *Geol. Soc. Am. Mem.* 146, 301-318, 1976
- Ollier, C., *Weathering*, Elsevier Pub. Co., New York, 304pp., 1969
- Oversby, V.M., Lead isotopic systematics and ages of Archean acid intrusives in the Kalgoorlie-Norseman area, Western Australia, *Geochim. Cosmochim. Acta*, 39, 1107-, 1975
- Oversby, V.M., Isotopic ages and geochemistry of Archean acid igneous rocks from the Pilbara, Western Australia, *Geochim. Cosmochim. Acta*, 40, 817-829, 1976
- Parmentier, E.M., D.L. Turcotte and K.E. Torrance, Studies of finite amplitude non-Newtonian thermal convection with application to convection in the Earth's mantle, *J. Geophys. Res.*, 81, 1839-1846, 1976
- Parsons, B., and J.G. Sclater, An analysis of the variation of ocean floor bathymetry and heat flow with age, *J. Geophys. Res.*, 82, 803-827, 1977
- Parsons, B., and D.P. McKenzie, Mantle convection and the thermal structure of the plates, *J. Geophys. Res.*, 83, 4485-4496, 1978
- Peltier, W.R., and J.T. Andrews, Glacial-isostatic adjustment, I, The forward problem, *Geophys. J. R. Astron. Soc.*, 46, 605-646, 1976

- Poupinet, G., On the relation between P-wave travel-time residuals and the age of the continental plates, *Earth Planet. Sci. Lett.*, 43, 149-161, 1979
- Ragland, P.C., G.K. Billings and J.A.S. Adams, Chemical fractionation and its relationship to the distribution of thorium and uranium in a zoned granite batholith, *Geochim. Cosmochim. Acta*, 31, 17-33, 1967
- Ranchin, G., Contribution a l'etude de la repartition de l'uranium a l'etat de traces dans les roches granitiques saines, *Sciences de la Terre*, 13, 163-205, 1968
- Rankin, D.W., Appalachian salients and recesses: Late Precambrian continental breakup and the opening of the Iapetus Ocean, *J. Geophys. Res.*, 81, 5605-5619, 1976
- Reid, D.L., Total rock Rb-Sr and U-Th-Pb isotopic study of Precambrian metavolcanic rocks in the lower Orange River Region, Southern Africa, *Earth Planet. Sci. Lett.*, 42, 368-378, 1979
- Relandeau, C., High temperature creep of Forsterite polycrystalline aggregates, in preparation, 1981
- Rich, R.A., H.D. Holland and U. Petersen, Vein-type uranium deposits, ERDA Report GJO-1640, 383pp., 1975
- Richardson, S.W., and E.R. Oxburgh, Heat flow, radiogenic heat production and crustal temperatures in England and Wales, *J. Geol. Soc. Lond.*, 135, 323-337, 1978
- Richardson, S.W., and E.R. Oxburgh, The heat flow field in mainland U.K., *Nature*, 282, 565-567, 1979
- Richter, F.M., and D.P. McKenzie, Simple plate models of mantle convection, *J. Geophys.*, 44, 441-471, 1978

- Robinson, J.L., A note on the stability of an infinite fluid heated from below, *J. Fluid Mech.*, 29, 461-464, 1967
- Rodgers, J., The Tectonics of the Appalachians, Wiley-Interscience, New York, 271 pp., 1970
- Rogers, J.J.W., and J.A.S. Adams, Thorium, in: Handbook of Geochemistry, K.H. Wedepohl ed., Springer Verlag, Berlin, 90B-900, 1969
- Rosholt, J.N., and A.J. Bartel, U, Th and lead systematics in Granite Mountains, Wyoming, *Earth Planet. Sci. Lett.*, 7, 141-147, 1969
- Rosholt, J.N., R.E. Zartman and I.T. Nkomo, Lead isotope systematics and uranium depletion in the Granite Mountains, Wyoming, *Geol. Soc. Am. Bull.*, 84, 989-1002, 1973
- Roy, R.F., D.D. Blackwell and F. Birch, Heat generation of plutonic rocks and continental heat flow provinces, *Earth Planet. Sci. Lett.*, 5, 1-12, 1968a
- Roy, R.F., E.R. Decker, D.D. Blackwell and F. Birch, Heat flow in the United States, *J. Geophys. Res.*, 73, 5207-5221, 1968b
- Rumble, D., Mineralogy, petrology and oxygen isotopic geochemistry of the Clough formation, Black Mountain, Western New Hampshire, USA, *J. Petrol.*, 19, 317-340, 1978
- Sass, J.H., A.H. Lachenbruch and R.J. Munroe, Thermal conductivity of rocks from measurements on fragments and its application to heat flow determinations, *J. Geophys. Res.*, 76, 3391-3401, 1971a
- Sass, J.H., A.H. Lachenbruch and A.M. Jessop, Uniform heat flow in a deep hole in the Canadian Shield and its paleoclimatic implications, *J. Geophys. Res.*, 76, 8586-8596, 1971b

- Sass, J.H. and A.H. Lachenbruch, Thermal regime of the Australian continental crust, in: The Earth, M. McElhinny ed., Academic Press, New York, 301-351, 1979
- Schubert, G., C. Froidevaux and D.A. Yuen, Oceanic lithosphere and asthenosphere: thermal and mechanical structure, *J. Geophys. Res.*, 81, 3525-3540, 1976
- Schwenn, M.B. and C. Goetze, Creep of olivine during hot-pressing, *Tectonophysics*, 48, 41-60, 1978
- Sclater, J.G., C. Jaupart and D. Galson, The heat flow through oceanic and continental crust and the heat loss of the Earth, *Rev. Geophys. Space Phys.*, 18, 269-311, 1980
- Sharp, J.A. and G. Simmons, Geologic/geophysical models of intrusives of the White Mountain Series, *USGS Abstracts with Programs*, 10, (no.2), 85, 1978
- Singh, R.N. and J.G. Negi, Comment on 'Erosion, uplift, exponential heat source distribution and transient heat flux' by T.C. Lee, *J. Geophys. Res.*, 85, 2696-2697, 1980
- Sinha, A.K., Tectonic significance of Th/U ratios from Archean basalts, *Chem. Geol.*, 215-225, 1976
- Smithson, S.B. and E.R. Decker, A continental crustal model and its geothermal applications, *Earth Planet. Sci. Lett.*, 22, 215-225, 1974
- Smithson, S.B., Modeling continental crust : structural and chemical constraints, *Geophys. Res. Lett.*, 5, 749-752, 1978
- Soberman, R.K., Onset of convection in liquids subject to transient heating from below, *Phys. Fluids*, 2, 131-138, 1959
- Spangenberg, W.G. and W.R. Rowland, Convective circulation in water induced by evaporative cooling, *Phys. Fluids*, 4, 743-750, 1961

- Sparrow, E.M., R.J. Goldstein and V.K. Jonsson, Thermal instability in a horizontal fluid layer: effect of boundary conditions and non-linear temperature profile, *J. Fluid. Mech.*, 18, 513-528, 1964
- Sparrow, E.M., R.B. Husar and R.J. Goldstein, Observations and other characteristics of thermals, *J. Fluid Mech.*, 41, 793-800, 1970
- Stuckless, J.S., C.M. Bunker, C.A. Bush, W.P. Doering and J.H. Scott, Geochemical and petrological studies of a uraniferous granite from the Granite Mountains, Wyoming, *J. Res. U.S.G.S.*, 5, 61-81, 1977
- Swanberg, C.A., Vertical distribution of heat production in the Idaho batholith, *J. Geophys. Res.*, 77, 2508-2513, 1972
- Swanberg, C.A., M.D. Chessman, G. Simmons, S.B. Smithson, G. Gronlie and K.S. Heier, Heat flow-heat generation studies in Norway, *Tectonophysics*, 23, 31-48, 1974
- Szalay, A., and Z. Samsoni, Investigations on the leaching of uranium from crushed magmatic rocks, in: *Proceedings of Symposium on hydrogeochemistry and biogeochemistry*, vol. 1, Tokyo, 261-272, 1970
- Tammemagi, H.Y. and J. Wheildon, Terrestrial heat flow and heat generation in south-west England, *Geophys. J. R. Astron. Soc.*, 38, 83-94, 1974
- Tammemagi, H.Y. and N.L. Smith, A radiogenic study of the granites of S.W. England, *J. Geol. Soc. Lond.*, 131, 415-427, 1975
- Taylor, S.R. and M.N. Toksoz, Three-dimensional crust and upper-mantle structure of the northeastern United States, *J. Geophys. Res.*, 84, 7627-7644, 1979
- Taylor, S.R., Crust and upper mantle structure of the northeastern United States, unpublished Ph.D. thesis, Massachusetts Institute of Technology, 1980

- Thomson, J., On a changing tessellated structure in certain fluids, Proc. Phil. Soc. Glasgow, 13, 464-469, 1882
- Tilling, R.I., D., Gottfried and F.C.W. Dodge, Radiogenic heat production of contrasting magma series : bearing on the interpretation of heat flow, Geol. Soc. Am. Bull., 81, 1447-1467, 1970
- Thompson, J.B., P. Robinson, T.N. Clifford and N.J. Trask, Nappes and gneiss domes in West-Central New England, in: Studies of Appalachian Geology, E. An-Zen ed., Interscience, New York, 203-218, 1968
- Vitarello, I. and H.N. Pollack, On the variation of continental heat flow with age and the thermal evolution of continents, J. Geophys. Res., 85, 983-995, 1980
- Vitarello, I., V.M. Hamza and H.N. Pollack, Terrestrial heat flow in the Brazilian Highlands, J. Geophys. Res., 85, 3778-3788, 1980
- Von Herzen, R.P., and A.E. Maxwell, Measurements of thermal conductivity of deep-sea sediments by a needle-probe method, J. Geophys. Res., 64, 1557-1563, 1961
- Ward, P.L., Microearthquakes: prospecting tool and possible hazard in the development of geothermal resources, Geothermics, 1, 3-12, 1972
- Watts, A.B., An analysis of isostasy in the world's oceans, 1. Hawaiian-Emperor seamount chain, J. Geophys. Res., 83, 5989-, 1978
- Weston Geophysical Research Inc., Aeromagnetic map of southeastern New England and the western gulf of Maine, Pl. 2c-1, 1976
- Wetterauer, R., and W.A. Bothner, Gravity investigations of the geothermal potential of the Conway granite, New Hampshire, EOS Trans., Am. Geophys. Union, 58, 542, 1977

- Whitehead, J.A., and M.M. Chen, Thermal instability and convection of a thin fluid layer bounded by a stably stratified region, *J. Fluid Mech.* 40, 549-576, 1970
- Wilson, C.J.L., Combined diffusion-infiltration of uranium in micaceous schists, *Contrib. Mineral. Petrol.*, 65, 171-181, 1977
- Woodhouse, J.H., and F. Birch, Comment on 'Erosion, uplift, exponential heat source distribution and transient heat flux' by T.C. Lee, *J. Geophys. Res.*, 85, 2691-2693, 1980
- Woodside, W., and J.H. Messmer, Thermal conductivity of porous media, *J. Appl. Phys.*, 32, 1688-1699, 1961
- Yuen, D.A., W.R. Peltier and G. Schubert, On the existence of a second scale of convection in the upper mantle, *Geophys. J. R. Astron. Soc.*, 65, 171-190, 1981
- Zielinski, Z.A., Uranium abundances and distribution in associated glassy and crystalline rhyolites of the western U.S., *Geol. Soc. Am. Bull.*, 89, 409-414, 1978
- Zielinski, R.A., and J.N. Rosholt, Uranium in waters and aquifer rocks at the Nevada test site, Nye County, Nevada, *J. Res. U.S.G.S.*, 6, 489-498, 1978